WSRC-TR-2007-00440, REVISION 0

Keywords: **Hydrogen Kinetics,**
Hydrogen Storage Vessel
Metal Hydride

Retention: Permanent

Integrated Hydrogen Storage System Model

Bruce J. Hardy

November 16, 2007

Washington Savannah River Company
Savannah River Site
Aiken, SC 29808

Prepared for the U.S. Department of Energy
Under Contract Number DEAC09-96-SR18500

Printed in the United States of America

Prepared For the
U.S. Department of Energy

WSRC-TR-2007-00440, REVISION 0

Keywords: **Hydrogen Kinetics,**
Hydrogen Storage Vessel
Metal Hydride

Retention: Permanent

Integrated Hydrogen Storage System Model

Bruce J. Hardy

November 16, 2007

Washington Savannah River Company
Savannah River Site
Aiken, SC 29808

Prepared for the U.S. Department of Energy
Under Contract Number DEAC09-96-SR18500

SRNL
SAVANNAH RIVER NATIONAL LABORATORY

TABLE OF CONTENTS

1.0 EXECUTIVE SUMMARY 1

2.0 INTRODUCTION 2

3.0 LITERATURE REVIEW 3

4.0 MODEL DESCRIPTION 6

4.1 Model Geometry 6

4.2 Model Dimensions 9

4.3 Heat Removal Parameters 12

4.4 Governing Equations and Boundary Conditions 13
4.4.1 Hydrogen Mass Balance 13
4.4.2 Hydrogen Momentum Balance 14
4.4.3 Bed Energy Balance 15
4.4.4 Energy Balance for the Tubes and Fins 16
4.4.5 Reaction Kinetics 16
4.4.6 Equation of State 19

4.4 Model Input Parameters 19

4.5 Mesh Used in 2 and 3-Dimensional Models 24

5.0 RESULTS 25

5.1 Bed Capacity 26

5.2 Loading Rate 27

5.3 Bed Temperatures 30

5.4 Bed Gas Flow 32

5.5 Hydride Concentration Profiles 34

6.0 CONCLUSIONS 37

7.0 FUTURE WORK 39

8.0 REFERENCES 40

APPENDIX 43

A.1 GOVERNING EQUATIONS 43

A.1.1 Mass Balance 43

A.1.2 Momentum Balance 44

A.1.3 Energy Balance 45

A.1.4 Reaction Kinetics 49
A.1.4.1 United Technologies Sodium Alanate Model 49

A.2 SYSTEM SCALING AND KINETICS 53

A.2.1 System Dimensions 53

A.2.2 Heat Transfer Requirements For the $NaAlH_4$ System 54

A.2.3 $NaAlH_4$ Reaction Kinetics 55

ATTACHMENTS 60

Attachment 1 60

Attachment 2 66

Attachment 3 82

LIST OF FIGURES

Figure 4.1-1 Illustration of a shell, tube and fin hydride bed configuration developed by the United Technologies Research Center™, East Hartford, Connecticut. 7

Figure 4.1-2 Schematic of cross-section for hydride bed. 8

Figure 4.1-3 Geometry used for computations in 2-dimensional COMSOL® model. 8

Figure 4.1-4 Geometry used for computations in 3-dimensional COMSOL® model. 9

Figure 4.5-1 Two-dimensional mesh. 24

Figure 4.5-2 Three-dimensional mesh. 25

Figure 5.2-1 Comparison of the weight fraction of stored hydrogen for the kinetics scoping model and the 2 and 3-dimensional finite element bed models. 29

Figure 5.2-2 Comparison of weight fraction of stored hydrogen relative to the theoretical gravimetric capacity of the bed, $wf(t)/0.056$, for the kinetics scoping model and the 2 and 3-dimensional finite element bed models. 29

Figure 5.3-1 Isometric and plan views of temperature profile for 3-dimensional model at 40 seconds. 30

Figure 5.3-2 Comparison between 2-dimensional and 3-dimensional midplane temperature profiles at 30 seconds. 31

Figure 5.3-3 Comparison between 2-dimensional and 3-dimensional midplane temperature profiles at 60 seconds. 31

Figure 5.3-4 Comparison between 2-dimensional and 3-dimensional midplane temperature profiles at 120 seconds. 32

Figure 5.3-5 Comparison between 2-dimensional and 3-dimensional midplane temperature profiles at 720 seconds. 32

Figure 5.4-1 Hydrogen velocity profile at 10 seconds. 33

Figure 5.4-2 Hydrogen velocity profile at 40 seconds. 33

Figure 5.5-1 Comparison of 2-dimensional and 3-dimensional bed midplane hydride concentrations at 40 seconds. 34

Figure 5.5-2 Comparison of 2-dimensional and 3-dimensional bed midplane hydride concentrations at 60 seconds. 35

Figure 5.5-3 Comparison of 2-dimensional and 3-dimensional bed midplane hydride concentrations at 120 seconds. 36

Figure 5.5-4 Comparison of 2-dimensional and 3-dimensional bed midplane hydride concentrations at 720 seconds. 37

Figure A.2.1 System dimensions calculated with the scaling tool. 53

Figure A.2.2 System heat transfer parameters estimated with the scaling tool. 54

LIST OF TABLES

Table 4.2-1	Input to the Geometry Scoping Model	10
Table 4.2-2	Bed Dimensions and Characteristics	11
Table 4.3-1	Input to Heat Removal Scoping Model	12
Table 4.3-2	Parameters From Heat Removal Scoping Model	12
Table 4.4.5-1	Values for $wf_{iso}^{sat}(T)$	18
Table 4.4-1	Values of Constants Used in the $NaAlH_4$ Model	20
Table 4.4-1	Values of Constants Used in the $NaAlH_4$ Model (Continued)	21
Table 4.4-2	Global Expressions Used in the $NaAlH_4$ Model	22
Table 4.4-3	Subdomain Expressions Used in the $NaAlH_4$ Model	23
Table 4.5-1	Two-Dimensional Mesh Statistics	24
Table 4.5-2	Three-Dimensional Mesh Statistics	25
Table A.1.4.1-1	Constants for the Rate and Equilibrium Expressions	50
Table A.1.4.1-2	Values for $wf_{iso}^{sat}(T)$	51

LIST OF ACRONYMS

DAE	Differential Algebraic Equation
DOE	Department of Energy
UTRC™	United Technologies Research Center™

NOMENCLATURE

C = Concentration of H_2 [mole H_2/m^3 of interparticle void]

C_{eqv} = Equivalent concentration of $NaAlH_4$ [mole/m^3] based on the initial concentrations of all metal species

= $C_{10} + 3C_{20} + C_{30}$

C_{NaH} = The bulk concentration of NaH [mole NaH/m^3]

C_{NaAlH_4} = The bulk concentration of $NaAlH_4$ [mole $NaAlH_4/m^3$]

C_{nd} = The non-dimensionalized concentration of $H_2 = \frac{C}{C_{ref}}$

$C_{p\,metal}$ = Specific heat of the metal [J/(kg-K)]

C_1 = Concentration of $NaAlH_4$ [mole/m^3]

C_2 = Concentration of Na_3AlH_6 [mole/m^3]

C_3 = Concentration of NaH [mole/m^3]

$C_{1\,0}$ = Initial concentration of $NaAlH_4$ [mole/m^3]

$C_{2\,0}$ = Initial concentration of Na_3AlH_6 [mole/m^3]

$C_{3\,0}$ = Initial concentration of NaH [mole/m^3]

D_p = Mean diameter of particles in bed [m]

$\vec{g}$ = Gravitational acceleration vector [m/s^2]

h = Specific enthalpy [J/kg]

$h_{conv\ cool}$ = Convection heat transfer coefficient for heat transfer fluid [W/m^2-°C]

$h_{H_2\ cool}$ = Convection heat transfer coefficient for H_2 in the feed tube [W/m^2-°C]

ι = Specific internal energy [J/kg]

k = Bed thermal conductivity

k_{metal} = Thermal conductivity of the metal [W/(m-s)].

P = Pressure [Pa]

M_i = Molecular weight of species i per mole [kg/g-mole]

M_{H_2} = Gram molecular weight of H_2

M_{NaH} = Gram molecular weight of NaH [kg/g-mole]

M_{NaAlH_4} = Gram molecular weight of $NaAlH_4$ [kg/g-mole]

$M_{Na_3AlH_6}$ = Gram molecular weight of Na_3AlH_6

M_{H_2} = Gram molecular weight of H_2 [kg/g-mole]

$\hat{n}$ = Outward normal to surface

n_{NaH} = Number of moles of NaH

n_{NaAlH_4} = Number of moles of $NaAlH_4$

$n_{Na_3AlH_6}$ = Number of moles of Na_3AlH_6

P = Pressure [Pa]

P_{nd} = $\frac{P}{P_{ref}}$ = Non-dimensional pressure

P_{ref} = Reference pressure [Pa]

$\vec{q}''$ = Heat flux vector [W/m^2]

R = Gas constant

S = Surface area [m^2]

S_{H_2} = Rate of H_2 generation per volume of bed from all chemical reactions [mol $H_2/(m^3 - s)$],

$S_{H_2} > 0$ if H_2 is produced

$S_{H_2} < 0$ if H_2 is removed

$T_{coolant\ bulk}$ = Bulk temperature of the heat transfer fluid [K]

T_{nd} = $\frac{T}{T_{ref}}$ = Non-dimensional temperature

$T_{H_2\ bulk}$ = Bulk temperature of the H_2 in the feed tube [K]

T_{ref} = Reference temperature [K]

T_{wall} = Tube wall temperature [K]

V = Volume [m^3]

$\vec{v}$ = H_2 velocity [m/s]

u = x component of the velocity, $\vec{v}$ [m/s]

u_{nd} = $\frac{u}{U_{ref}}$ = Non-dimensional x-component of velocity

U_{ref} = Reference velocity [m/s]

v = y component of the velocity, $\vec{v}$ [m/s]

v_{nd} = $\frac{v}{U_{ref}}$ = Non-dimensional y-component of velocity

w = z component of the velocity, $\vec{v}$ [m/s]

w_{nd} = $\frac{w}{U_{ref}}$ = Non-dimensional z-component of velocity

Greek

ΔH_i = Enthalpy of reaction on a molar basis of species i [J/(mole of i)]

$\Delta H_{rxn\ 1}$ = Heat of per mole of H_2 consumed going to left for reaction 1

= -37 kJ/(mole H_2)

$\Delta H_{rxn\ 2}$ = Heat of per mole of H_2 consumed going to left for reaction 2

= -47 kJ/(mole H_2)

ρ_i = Mass density of species i [kg/m^3]

ρ_{metal} = Density of the metal [kg/m^3].

ε = Void between particles in bed

μ = Viscosity of H_2 [Pa-s]

ρ = Mass density [kg/m^3]

$\underline{\underline{\tau}}$ = Stress tensor, having components τ_{ij} [N/m^2]

Symbols and Operators

$\left.\frac{\nu_{H_2}}{\nu_{NaH}}\right|_{Rxn2}$ = Ratio of the stoichiometric coefficient of H_2 to NaH in reaction 2 = 0.5

$\left.\frac{\nu_{H_2}}{\nu_{NaAlH_4}}\right|_{Rxn1}$ = Ratio of the stoichiometric coefficient of H_2 to $NaAlH_4$ in reaction 1 = 1

$()_{H_2}$ = For H_2 gas

$()_R$ = For solid phase reactants

$()_P$ = For solid phase products

$()_I$ = For inert (non-reacting) material, such as metal foam

1.0 EXECUTIVE SUMMARY

Hydrogen storage is recognized as a key technical hurdle that must be overcome for the realization of hydrogen powered vehicles. Metal hydrides and their doped variants have shown great promise as a storage material and significant advances have been made with this technology. In any practical storage system the rate of H_2 uptake will be governed by all processes that affect the rate of mass transport through the bed and into the particles. These coupled processes include heat and mass transfer as well as chemical kinetics and equilibrium. However, with few exceptions, studies of metal hydrides have focused primarily on fundamental properties associated with hydrogen storage capacity and kinetics.

A full understanding of the complex interplay of physical processes that occur during the charging and discharging of a practical storage system requires models that integrate the salient phenomena. For example, in the case of sodium alanate, the size of $NaAlH_4$ crystals is on the order of 300nm and the size of polycrystalline particles may be approximately 10 times larger (~3,000nm). For the bed volume to be as small as possible, it is necessary to densely pack the hydride particles. Even so, in packed beds composed of $NaAlH_4$ particles alone, it has been observed that the void fraction is still approximately 50-60%. Because of the large void fraction and particle to particle thermal contact resistance, the thermal conductivity of the hydride is very low, on the order of 0.2 W/m-°C, Gross, Majzoub, Thomas and Sandrock [2002]. The chemical reaction for hydrogen loading is exothermic. Based on the data in Gross [2003], on the order of 10^8 J of heat of is released for the uptake of 5 kg of H_2 and complete conversion of NaH to $NaAlH_4$. Since the hydride reaction transitions from hydrogen loading to discharge at elevated temperatures, it is essential to control the temperature of the bed. However, the low thermal conductivity of the hydride makes it difficult to remove the heat of reaction, especially in the relatively short target refueling times, see Attachment 3.

This document describes a detailed numerical model for general metal hydride beds that couples reaction kinetics with heat and mass transfer, for both hydriding and dehydriding of the bed. The detailed model is part of a comprehensive methodology for the design, evaluation and modification of hydrogen storage systems. In Hardy [2007], scoping models for reaction kinetics, bed geometry and heat removal parameters are discussed. The scoping models are used to perform a quick assessment of storage systems and identify those which have the potential to meet DOE performance targets. The operational characteristics of successful candidate systems are then evaluated with the more detailed models discussed in this document.

The detailed analysis for hydrogen storage systems is modeled in either 2 or 3-dimensions, via the general purpose finite element solver COMSOL Multiphysics®. The two-dimensional model serves to provide rapid evaluation of bed configurations and physical processes, while the three-dimensional model, which requires a much longer run time, is used to investigate detailed effects that do not readily lend themselves to two-dimensional representations. The model is general and can be adapted to any geometry or storage media. In this document, the model is applied to a modified cylindrical shell and tube geometry with radial fins perpendicular to the axis, see Figures 4.1-1 and 4.1-2. Sodium alanate, $NaAlH_4$, is used as the hydrogen storage medium. The model can be run on any DOS, LINUX or Unix based system.

2.0 INTRODUCTION

It is acknowledged that a critical function of a hydrogen storage system is meeting the DOE refueling goal of three minutes, see Attachment 3. The rapid fueling rate, coupled with the high heat of reaction on uptake, requires a heat dissipation rate on the order of 111 kW per kilogram of stored H_2 in sodium aluminum hydride, $NaAlH_4$. Metal hydride (and other) hydrogen storage systems have a number of physical phenomena that work against one another. For example, the rate of hydrogen uptake for hydrides decreases exponentially, and reverses, as temperatures increase beyond a particular value (e.g. 390K for $NaAlH_4$). In view of the target charging time and the very large quantity of heat released during the uptake process (on the order of 10^8 J for conversion of NaH to $NaAlH_4$ for the uptake of 5 kg of H_2), a high rate of heat transfer must be maintained for the uptake reaction to proceed at an acceptable rate. However, most hydrides also possess low material, and even lower, bulk thermal conductivities. Bed thermal conductivities have been enhanced by embedding the hydride into metal foam, but this reduces the volumetric and gravimetric capacities of the system, as defined in Attachment 3. The goals for volumetric and gravimetric capacity, as well as for the refueling rate, adds additional constraints to the design of the system. To ensure adequate mass transfer rates within the hydride crystals, the polycrystalline particles must have small transport length scales, yielding high surface area to volume ratios. But, in a practical bed the particle size must be sufficiently large to permit an adequate flowrate of hydrogen to supply the demand during the loading and discharge phases. For example, individual $NaAlH_4$ crystals have a length scale of approximately 300nm and the polycrystalline particles comprising the bed have length scales of approximately 3000nm. Particles in this size range meet both the requirements for rapid transport within the hydride and flow through the bed.

It is difficult and expensive to design experiments that fully measure the complex processes occurring during the loading and discharge of hydrogen from a storage media, let alone perform sensitivity studies for a complete system. Moreover, any such experiments would be limited to a particular hydride and system design. A much more efficient approach is to evaluate proposed designs for hydrogen storage systems through the use of numerical models that couple heat and mass transport with the reaction kinetics occurring in the bed. By systematically combining scoping models that quickly evaluate whether a storage system has the potential to meet DOE performance targets with more sophisticated models that provide more detailed predictions of operational performance, the most promising designs can be efficiently identified. The scoping models not only eliminate designs that perform poorly relative to target criteria, but also can be used to identify design improvements and provide input to the more time consuming sophisticated models. The detailed models can be used to perform sensitivity studies and to identify design improvements. Those systems that appear most likely to approach the performance objectives can then be tested as prototypes, greatly reducing the number of necessary experiments. It is perhaps inevitable that deficiencies in available data, required as input to the models, will be discovered. In these instances, experiments can be performed to specifically obtain the necessary data.

Scoping models for hydriding/dehydriding reaction kinetics, bed geometry and heat removal parameters, for generalized storage systems are discussed in Hardy [2007]. This document describes a detailed numerical model for general metal hydride beds that couples reaction kinetics with heat and mass transfer, for both hydriding and dehydriding of the bed. The detailed model is part of a comprehensive methodology for the design, evaluation and modification of hydrogen storage systems. The detailed analysis for hydrogen storage systems is conducted in either 2 or 3-

dimensions, via the general purpose finite element solver COMSOL Multiphysics®. The two-dimensional model serves to provide rapid evaluation of bed configurations and physical processes, while the three-dimensional model, which requires a much longer run time, is used to investigate effects that do not readily lend themselves to two-dimensional representations. The model is general and can be adapted to any geometry or storage media. In this document, however, the model is applied to sodium alanate, $NaAlH_4$, with its associated kinetics and equilibrium equations, and to a particular bed geometry.

3.0 LITERATURE REVIEW

In the past, a number of numerical models have been developed for metal hydride beds. These models have attempted to address, at least in part, the coupled phenomena occurring as the bed is charged with or discharges hydrogen. The models, however, tended to be either of limited scope, addressing either a limited number of physical phenomena, simplifying the phenomena or simplifying the bed geometry. A survey of these models is presented in this section.

El-Osery [1984a] developed a one-dimensional transient model for a granular Ti-Fe bed, which approximated the system as an azimuthally symmetric cell in cylindrical geometry, having only radial dependence. The model considered heat conduction in the portion of the cell comprising the bed and convection from the bed surface. It was applied to heat removal during the exothermic chemical reaction that occurred during the charging process and to heating by convection at the external surface to discharge the stored hydrogen. In El-Osery [1984b] this simple model was extended to a variety of geometric configurations represented as one-dimensional cells in their respective coordinate geometries. An elaboration of the model was presented in El-Osery [1986].

A model for the discharging reaction in a $LaNi_5H_6$ bed was developed in El-Osairy, et. al. [1992a]. The bed was in the form of a 1-dimensional porous channel with hydrogen introduced at one end. The bed was adiabatic along its sides, with a specified solid phase temperature at the inlet and with a temperature gradient of zero at the exit. Further, it was assumed that the bed was subject to fixed uniform H_2 pressure. This one-dimensional, transient model considered the bed to be composed of gas and solid phases, each having separate energy and mass balances that were coupled through convection heat transfer and interphase mass conservation. Temperature-dependent reaction rates for H_2 uptake, and the subsequent heat of reaction, were used in the model. El-Osairy, et. al. [1992b] applied the model to a variety of channel configurations, some of which replaced the adiabatic conditions on the sides for the channel with forced convection cooling. The model was applied to $FeTiH_{1.6}$ and Mg_2NiH_4 beds in El-Osairy, et. al. [1993]. By modifying the reaction rate to apply to H_2 discharge, El-Osery, et. al. [1993] applied the model to the discharge of the bed. In this model, dehydriding was effected by circulating heated H_2 through the bed. Heat transfer from the gas to the solid phase was used to control the endothermic chemical reaction. El-Gammal, et. al. [1993] applied the model to dehydriding annular cylinders composed of $LaNi_5H_6$, where heated gas is passed through the porous media and over its exterior surfaces.

Aldas, et. al. [2002] developed a model based on the PHOENICS® general purpose finite volume Computational Fluid Dynamics (CFD) software to investigate heat and mass transfer in porous metal hydride bed. The transient spatial dependence for hydride formation was predicted by the model. They found that coolant flowrate affected the temperature distribution in the system but did not significantly change the amount of hydrogen absorbed. PHOENICS® was also used by

Biligi and Ataer [1996] to model the transient temperature and H_2 uptake by a porous $LaNi_5$ bed. The bed was an annulus having a length of 30mm, and inner and outer radii of 10mm and 20mm, respectively. Because of the bed geometry, the model was axisymmetric. Bed porosity was fixed at 50.5%. The model was used to calculate the transient temperature and hydrogen content for the annular configuration. The model addressed the mass and energy balance within the bed. The momentum balance was given by Darcy's law. Cooling by the heat transfer fluid was invoked as a boundary condition. The energy balance assumed the solid and H_2 phases to have the same local temperature. It appears that the convection terms in mass balance equation should have been multiplied by the porosity; however, this might have been a typographical error. The rate of H_2 uptake by the metal was determined from a reaction kinetics equation and the equilibrium Van't Hoff equation. The model had the potential for generalization to other geometries and metals.

Gopal and Murthy [1992] developed a one-dimensional model for heat and mass transfer in an annular bed, which was charged with hydrogen on its inner surface and cooled at its outer surface. The model was used to obtain correlations for a range of bed alloys and operating conditions. The correlations were then demonstrated for a lanthanum-rich mischmetal (Lm) bed alloyed with nickel and aluminum, $LmNi_{4.7}Al_{0.3}$. The authors later conducted experiments on a cylindrical metal bed using porous $MnNi_{4.5}Al_{0.5,}$ Gopal and Murthy [1995]. In the experiments, hydrogen uptake and release was measured for various coolant temperatures. Although good agreement was obtained between their measured heat and mass transfer rates, and those predicted by their 1992 model, there was a discrepancy between measured and predicted bed temperatures.

Mat and Kaplan [2001] and Aldas and Mat [2002] conducted a numerical analysis of hydride formation in a porous metal bed of $LaNi_5Sn_{0.2}$, having the shape of a finite length cylinder. The model addressed heat, mass and chemical reactions in the bed. Predictions made by Mat and Kaplan's model agreed well with the experimental data of Mayer, et. al. [1987].

A numerical model that calculated the pressure and temperature histories associated with H_2 desorption from a lanthanum-rich mischmetal (Lm) hydride bed alloyed with nickel and aluminum, $Lm_{1.06}Ni_{4.96}Al_{0.04}$, was developed by Gadre, Ebner, Al-Muhtaseb and J. Ritter [2003]. The models were able to predict the P-T behavior of the hydride bed at low discharge rates. However, at higher discharge rates none of the modeling scenarios were able to properly predict the behavior of the bed. The authors postulated that this was the result of a more complex the heat transfer process at higher discharge rates, and that the simplified assumptions employed by the model were insufficient for this regime.

Askri, Jemini and Nasrallah [2004] developed a transient model for a $LiNi_5$ bed in a closed vessel. The governing equations included those for mass, momentum and energy. $LiNi_5$ kinetics and equilibrium equations were used to determine the rate and extent of the reaction. The system of equations was solved numerically using the Control Volume based Finite Element Method (CVFEM) in a computer program developed by the authors. The vessel had the form of a vertical cylinder in which the metal hydride occupied the lower part of the vessel, with a gas space present above the bed. A heat transfer fluid, in contact with the external walls of the vessel, was used to control the temperature of the bed and gas space. The effect of the ratio of the bed height to radius on the rate of hydrogen desorption was investigated. In a comparison with experimental results, the model slightly under-predicted the transient hydrogen pressure during desorption.

Ha, et. al [2004] developed a two dimensional mathematical model for transient heat and mass transfer within a metal hydride bed using the finite volume method. In this analysis, the relation between hydrogen uptake and the bed thermal conductivity, diameter, and heat transfer fins was

investigated. Darcy's Law was used to relate the pressure gradient to the superficial velocity in the bed. The equation of state was the ideal gas law. Uptake kinetics were modeled via an Arrhenius-type expression, for which a two-step absorption mechanism was postulated. The first step of the uptake reaction was a nucleation and growth process. The second step was diffusion through a hydrogen layer that formed on the hydride. The results of the model indicated that the fractional hydrogen uptake during the first nucleation step is quite rapid and rather invariant with temperature, but is strongly affected by the difference between the actual gas pressure and the hydrogen equilibrium pressure. The second step, however, was found to be strongly affected by temperature, implying that the overall system performance can be greatly improved by the implementation of thermal management and heat transfer controls.

Mazumdar, Gopal and Bhattacharyya [2005] used a steady-state thermodynamic model to predict the performance of a metal hydride refrigeration system. Four metal hydrides were considered: $MnNi_{4.5}Al_{0.5}$, $LaNi_5$, $TiFe_{0.85}Mn_{0.15}$, $Zr_{0.9}Ti_{0.1}Cr_{0.55}Fe_{1.45}$. The thermodynamic model utilized the basic thermo-physical properties of the metal hydride including the density, thermal conductivity, specific heat, the equilibrium pressure of H_2 for a given hydride, as well as, the material composition and geometry of the bed and heat transfer fins (via standard heat transfer relationships). The objective of the model was to determine the effect that these properties had on the performance of the compressor and its ability to cool the system. Heat and mass transfer were not solved for within the physical domain of the hydride bed.

Kikkinides, Georgiadis and Stubos [2006] modeled a $LaNi_5$ bed using the equations for heat and mass transfer in two-dimensional axisymmetric cylindrical geometry. Predicitions of the model were compared with data taken by Jemini and Nasrallah [1995], Nasrallah and Jemini [1997], and Jemini, Nasrallah and Lamloumi [1999]. In the model, it was assumed that the velocity of hydrogen was constant within the bed, and the hydrogen temperature and density were dependent on time. The resulting system of differential algebraic equations (DAE's) was solved using the commercial software package gPROMS®. The model was used to evaluate the time required for the system to reach 99% of its hydrogen capacity for several heat exchange configurations. Model assumptions included: ideal gas behavior for hydrogen and equal solid and gas phase temperatures in the bed. The hydrogen mass balance included radial dispersion, with the relation between the gas velocity and pressure gradient in the bed given by the Blake-Kozeny equation. It was found that H_2 absorption time could be minimized through the use of a cooling ring that split the bed, radially, into two approximately, equal portions. By using this configuration the model indicated that the time required for absorption could be reduced to approximately 60% of that when only an outer cooling jacket was used.

Transient, two dimensional models for the loading of hydrogen into a sodium alanate bed having a shell, tube and fin configuration, see Figure 4.1-1, were developed by Mosher, et.al [2007]. The models coupled heat transfer and reaction kinetics, including heat of reaction, but did not include mass transfer of the hydrogen through the bed. To accommodate the effect of the fin, which is an axial layer, in the two-dimensional (radial and azimuthal) heat transfer model, the bed thermal conductivity was modified. The model compared reasonably well with data obtained from a scaled experiment.

4.0 MODEL DESCRIPTION

The model developed in this document applies to a general metal hydride bed, which is governed by the physical processes occurring as hydrogen is loaded into or discharged from the hydride. The model includes:

1. Gas flow within the bed (interstitial flow), which depends on:
    a. The pressure gradient (or gas phase H_2 concentration gradient) in the bed.
    b. The void fraction and effective particle diameter.
2. Heat transfer, essential to control the bed temperature, which is governed by:
    a. Exothermic and endothermic reactions occurring during uptake and release of H_2, respectively.
    b. The effective bed thermal conductivity.
    c. Convection heat transfer within the bed.
    d. System boundary conditions and geometry.
    e. Thermal contact for various components of the bed.
3. Reaction kinetics for hydriding and dehydriding reactions.
    a. Dependence of reaction rates on temperature, H_2 pressure and composition of the solid phase.
    b. Dependence of reaction equilibrium on the state of the system.

A model that captures the physical phenomena listed above was built using the COMSOL Multiphysics®, version 3.3.0.405, finite element software, COMSOL [2006].

Assumptions made in the model are:

1 Only hydrogen is allowed to flow in the system.
2 The bed does not expand or contract. This assumption is especially significant because all materials proposed for hydrogen storage undergo significant expansion during hydrogen loading.
3 The thermal properties of the bed do not change with the amount of hydrogen loading.
4 The thermal properties of the bed do not vary with temperature.
5 The characteristics of the bed are unaffected by the number of loading-unloading cycles. That is, bed aging is neglected.
6 Heat transfer from the bed occurs only via the heat transfer fluid (in the cooling tubes), by convection to the hydrogen in the feed tubes, and by homogeneous heat exchange with the hydrogen flowing through the bed.
7 The solid material and hydrogen have the same instantaneous temperature at all locations within the bed.
8 The thermal conductivity, specific heat and viscosity of hydrogen do not vary with pressure over the operational regime of the storage system.
9 The tubes and fins are composed of 6063 T83 aluminum.
10 Thermal contact between the bed and the cooling tubes, the bed and the fin, and the fin and the cooling tubes is good, i.e. neglect thermal contact resistance.
11 The bed void fraction remains constant and uniform throughout.
12 The bed fills the entire volume of the space between the fins and tubes.
13 The bulk temperature of the heat exchange fluid and the hydrogen supplied to the bed is constant and uniform.
14 The hydrogen flows (circulates) through the feed tubes.
15 For this system, the equation of state for hydrogen is given by the ideal gas law.
16 Axial end effects have negligible impact on the performance of the storage system.

4.1 Model Geometry

In this work, the detailed 2 and 3-dimensional finite element models are applied to the analysis of sodium alanate, $NaAlH_4$, bed. The storage system has the configuration of a cylindrical shell, tube and fin heat exchange. The bed is divided by an array of fins that are normal to the axis and extend in the radial direction. The fins are press-fit to coolant tubes that are parallel to the axis. Figure 4.1-1 shows a storage system developed and tested by the United Technologies Research Center™ (UTRC™), Mosher, et al. [2007]. The system in this figure has a geometric configuration that is similar to the system modeled in this document. However, the system modeled in the current analysis does not possess the same dimensions as the bed displayed in the Figure 4.1-1.

The bed modeled in this document has 9 coolant tubes and 8 tubes used for the injection of hydrogen, see Figure 4.1-2. The model focuses on a layer of hydride material located at sufficient distance from the axial ends of the bed, that the axial boundary conditions are periodic from the midplane of one fin to the midplane of the next adjacent fin. Therefore, axial symmetry conditions can be applied to the midplane of the hydride layer and the midplane of the fin. Further, there are planes of azimuthal symmetry , as shown in Figure 4.1-2. The geometry used for the 2-dimensional COMSOL® model is shown in Figure 4.1-3 and the geometry used in the 3-dimensional model is shown in Figure 4.1-4.

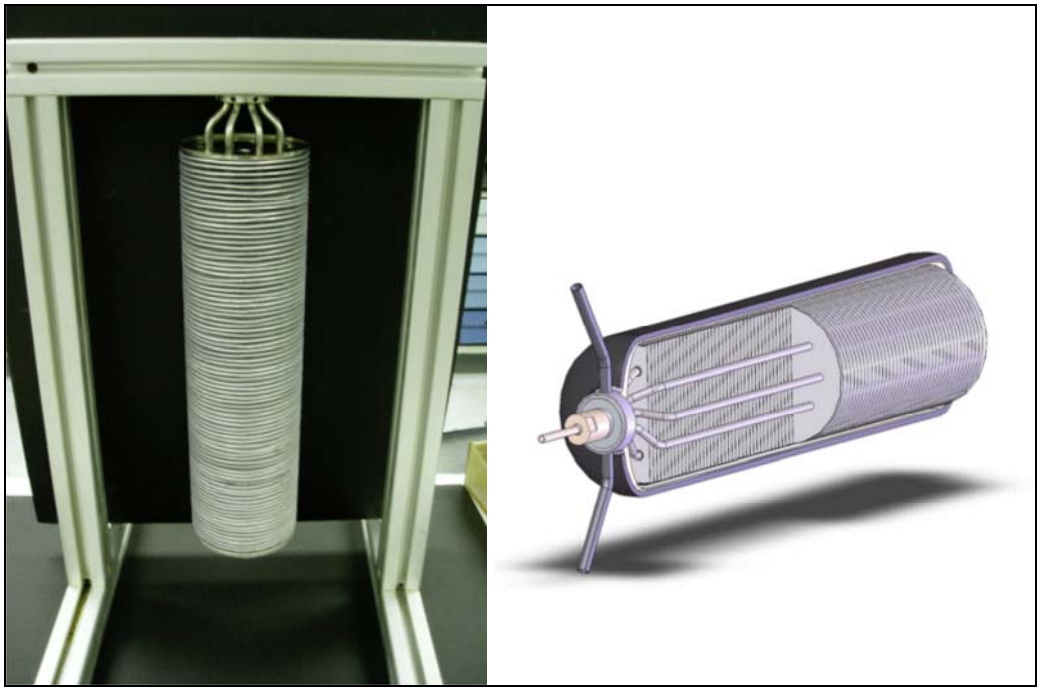

Figure 4.1-1 Illustration of a shell, tube and fin hydride bed configuration developed by the United Technologies Research Center™, East Hartford, Connecticut.

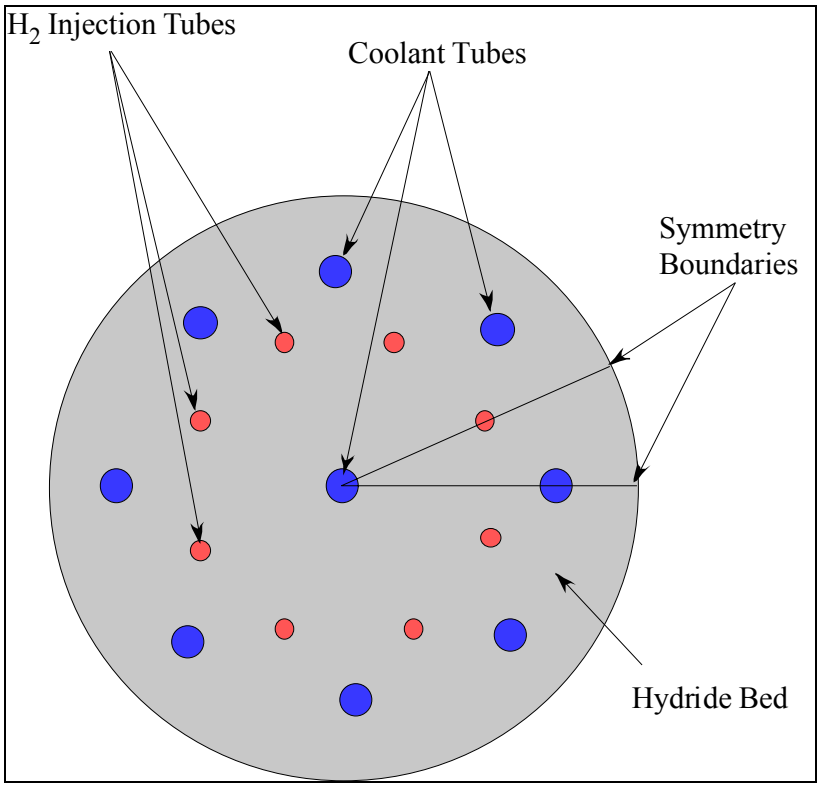

Figure 4.1-2 Schematic of cross-section for hydride bed.

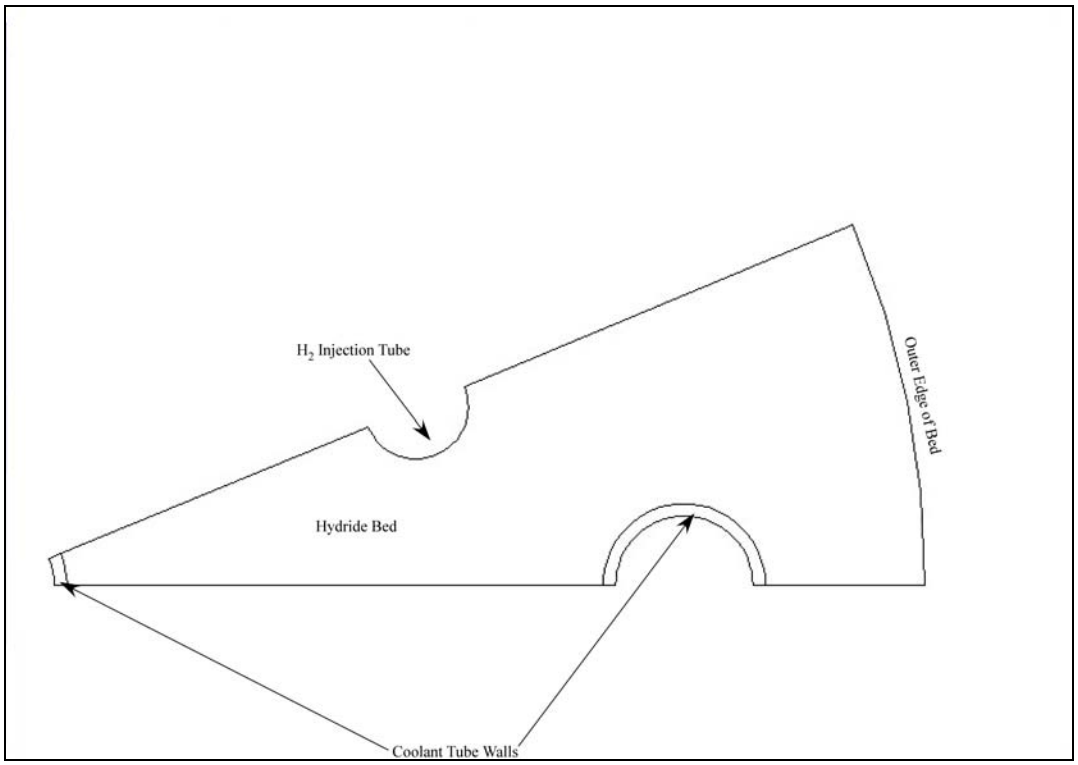

Figure 4.1-3 Geometry used for computations in 2-dimensional COMSOL® model.

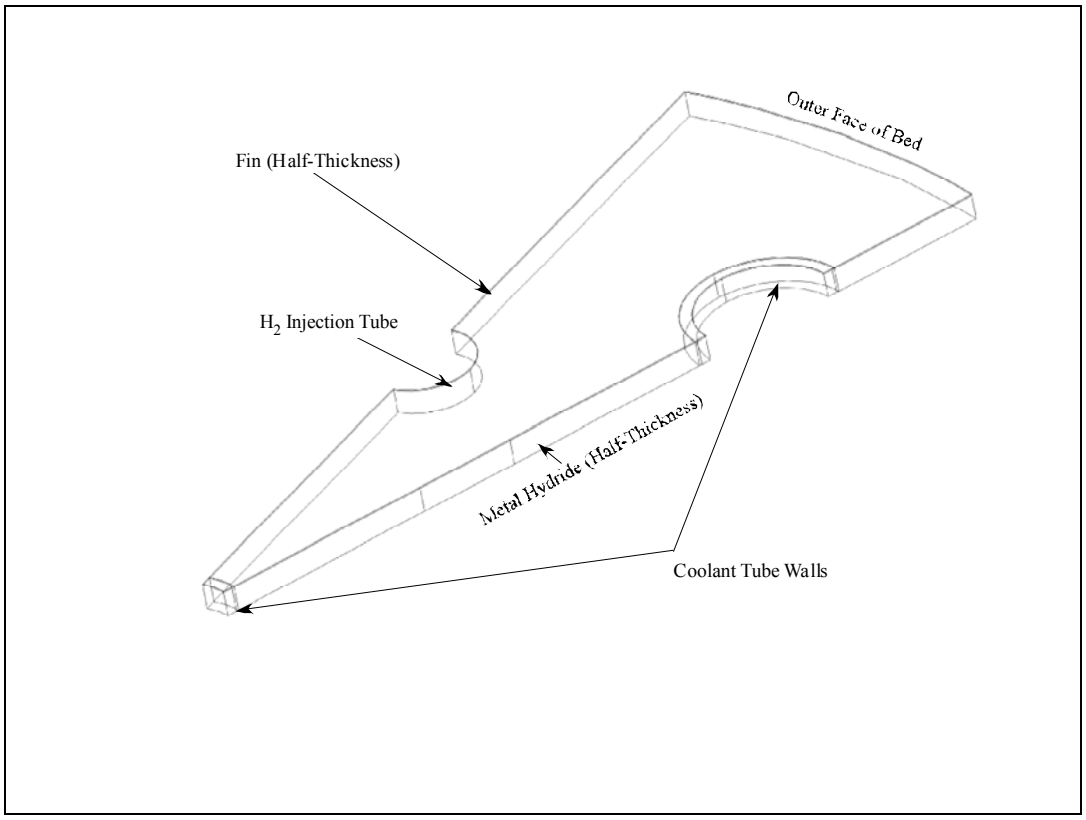

Figure 4.1-4 Geometry used for computations in 3-dimensional COMSOL® model.

4.2 Model Dimensions

The dimensions (length scales) of the storage system were calculated with the geometry scoping model described in Hardy [2007]. Input to the scoping model, for application to the finned shell and tube heat exchanger, is listed in Table 4.2-1 and the calculated dimensions are listed in Table 4.2-2.

Table 4.2-1 Input to the Geometry Scoping Model

Parameter	Value
Mass of recoverable H_2 to be stored in vessel	1000.00 g
Practical ratio of moles H_2 to moles $NaAlH_4$ that can be stored in 12 minutes	1.5
Bulk density of $NaAlH_4$ powder	0.72 g/ cm^3
Hydride bed diameter, no walls	23.00 cm
Concentration of $NaAlH_4$	13,333.33 mole/m^3
Diameter of coolant tubes	1.91 cm
Diameter of H_2 injection tubes	1.27 cm
Number of coolant tubes	9
Number of H_2 injection tubes	8
Thickness of fin plates	0.0313 cm
Approximate spacing between fin plates	0.64 cm
Tube wall thickness	0.12 cm
Density of tube material (6061-T6 Al from table on pg 6-11 of Avallone and Baumeister [1987])	2.70 g/ cm^3
Density of fin material (6061-T6 Al from table on pg 6-11 of Avallone and Baumeister [1987])	2.70 g/ cm^3
Material density of porous insert for H_2 delivery (6061-T6 Al from table on pg 6-11 of Avallone and Baumeister [1987])	2.70 g/ cm^3
Void fraction of porous insert for H_2 delivery	0.70
Density of tank material (Composite @ 0.05419lbm/in^3)	1.50 g/ cm^3
Density of liner material (6061-T6 Al from table on pg 6-11 of Avallone and Baumeister [1987])	2.70 g/cm^3
Assume 1/16 in gap between bed & liner	0.159 cm
Assume 1/32 in thick liner	0.079 cm
Tank wall thickness at 50 bar w/ safety factor	0.132 cm

Table 4.2-2 Bed Dimensions and Characteristics

Feature	Value
Required length of hydride only	65.62 cm
Total number of fin plates, including end plates	105
Total length of bed, no vessel	68.90 cm
Actual spacing of plates	0.63 cm
Mass of bed; including fins, tubes & $NaAlH_4$	24642.84 g
Volume of bed without vessel & liner	36237.36 cm^3
Overall length of vessel	92.64 cm^3
Total volume of coolant tubes	431.70 cm^3
Total volume of plate fins, including part of fin extruded over the outside of the coolant tubes	1358.11 cm^3
Total volume of gap including semi-spherical ends	6899.97 cm^3
Total volume of liner	266.38 cm^3
Total volume of tank material	445.52 cm^3
Total volume of H_2 injection tubes	698.22 cm^3
Moles of H_2 to be stored in vessel	496.03 mols
Moles of $NaAlH_4$ required for vessel	330.69 mols
Mass of $NaAlH_4$ required for vessel	17857.28 g
Volume of NaAlH4 required to store hydrogen	24801.77 cm^3
Total area of coolant tube holes	27.36 cm^2
Total area of H_2 injection tube holes	10.13 cm^2
With Outer Vessel & Liner	0.041 kg H_2/Kg Total
With Outer Vessel & Liner	0.028 kg H_2/L Total
Radial location of center of coolant tube. optimized for hydride area to cooling surface ratio.	8.55 cm
Angle at center of coolant tube formed by intersection of tube center radius and tube inner wall	3.04 radians
Arc length along inner wall of coolant tube from intersections of tube center radius and tube inner wall	2.52 cm
Cross-sectional area of bed, inside the radius to the center of the coolant tubes, less interior of coolant tubes	209.13 cm^2
Cross-sectional area of bed, outside the radius to the center of the coolant tubes, less interior of coolant tubes	176.82 cm^2
Sum of arc lengths of inner wall of all coolant tubes inside the radius to the center of the cooling tubes	25.37 cm
Sum of arc lengths of inner wall of all coolant tubes outside the radius to the center of the cooling tubes	21.45 cm
Gravimetric Capacity of the System	0.041 kg H_2/kg
Volumetric Capacity of the System	0.028 kg H_2/L

4.3 Heat Removal Parameters

Typical coolant flow velocities, convection heat transfer coefficients, pressure drops over the length of the coolant channels and the change in coolant temperature over the length of the coolant channels were estimated with the system heat removal scoping model described in Hardy [2007]. The hydrogen storage material was $TiCl_3$ catalyzed $NaAlH_4$, which followed the reaction in Equation 4.4.5-1. The dimensions (length scales) of the coolant tubes, mass of $NaAlH_4$, mass of stored H_2, number of coolant tubes, etc., were passed directly from the geometry scoping model. The remaining input to the heat removal scoping model is listed in Table 4.3-1 and calculated parameters are listed in Table 4.3-2. The coolant used in the model was Dowtherm T®, see Attachment 1 of Hardy [2007]; the thermal properties of this heat transfer fluid are listed in Table 4.3-1.

Table 4.3-1 Input to Heat Removal Scoping Model

Parameter	Value
ΔH_{Rxn1} (Enthalpy of Reaction 1, see Eq. 4.4.5-1) Ref. Gross, et. al. [2002]	37.00 kJ/mol H_2
ΔH_{Rxn2} (Enthalpy of Reaction 2, see Eq. 4.4.5-1) Ref. Gross, et. al. [2002]	47.00 kJ/mol H_2
Charging Time	180.00 sec
Wall Temperature	90.00 °C
Coolant Liquid Density	0.82 g/cm^3
Coolant Liquid Themal Conductivity	1.04E-03 W/(cm °C)
Coolant Viscosity	3.00E-02 g/(cm s)
Coolant Specific Heat	2.30 J/(g °C)
Coolant Prandtl Number	66.52

Table 4.3-2 Parameters From Heat Removal Scoping Model

Parameter	Value
$\Delta H_{overall}$ (Overall Enthalpy of Reaction, see Eq. 4.4.5-1)	40.33 kJ/mol H_2
Total Amount of Heat to be Removed for Mass of Stored Hydrogen in Table 4.2-1	20,006.61 kJ
Heat Removal Rate Based on Total Heat to be Removed and the Charging Time in Table 4.3-1	111,147.85 W
Wall Heat Flux on Coolant Tube	3.45E+01 W/cm^2
Convection Heat Transfer Coefficient by Diitus-Boelter Correlation, Ref Holman [1976]	0.4922 W/(cm^2 °C)
Coolant Mass Flux, Per Tube	1030.04 g/(cm^2 s)
Coolant Velocity	1260.73 cm/s
Re_D	56861.02
Pressure Drop Over Length of Coolant Tube	1.18E+01 psi
Bulk Coolant Temperature Increase Over Length of Coolant Tube	2.42 °C

4.4 Governing Equations and Boundary Conditions

Both the 2 and 3-dimensional models consist of a set of governing equations together with their input parameters and a mesh for the section of the hydride bed. Details of all equations used in the model are discussed in Appendix A.1.

4.4.1 Hydrogen Mass Balance

The mass (mole) balance for hydrogen flowing through the bed is given by

$$\frac{\partial C_{nd}}{\partial t} + \nabla \cdot \left(C_{nd} \vec{v} \right) = \frac{1}{C_{ref}} \left(\frac{S_{H_2}}{\varepsilon} \right) \qquad 4.4.1\text{-}1$$

where: S_{H_2} = Rate of H_2 generation per volume of bed [mole H_2/(m^3 - s)]

ε = Void fraction (porosity) of particle bed

$\vec{v}$ = Mean interstitial H_2 velocity [m/s]

C_{nd} = The non-dimensionalized concentration of H_2 = $\frac{C}{C_{ref}}$

C= Concentration of H_2 in the void space of the bed [mole/m^3].

C_{ref} = The reference H_2 concentration in the void space, C_{ref} [mole/m^3]

∇ = Gradient [1/m].

For example, in a sodium alanate bed the H_2 uptake/discharge reaction occurs via a two-step reaction given by the chemical balance equation

$$\underbrace{NaAlH_4}_{\text{Species 1}} \underbrace{\leftrightarrow}_{\text{Reaction 1}} \underbrace{\frac{1}{3}Na_3AlH_6}_{\text{Species 2}} + \frac{2}{3}Al + H_2 \underbrace{\leftrightarrow}_{\text{Reaction 2}} \underbrace{NaH}_{\text{Species 3}} + Al + \frac{3}{2}H_2 \qquad A.4.1\text{-}2$$

In this case, the source rate for hydrogen is

$$S_{H_2} = \left. \frac{\nu_{H_2}}{\nu_{NaH}} \right|_{Rxn2} \frac{\partial C_{NaH}}{\partial t} - \left. \frac{\nu_{H_2}}{\nu_{NaAlH_4}} \right|_{Rxn1} \frac{\partial C_{NaAlH_4}}{\partial t} \qquad 4.4.1\text{-}3$$

where: $\left. \frac{\nu_{H_2}}{\nu_{NaH}} \right|_{Rxn2}$ = Ratio of the stoichiometric coefficient of H_2 to NaH in reaction 2 = 0.5

$\left. \frac{\nu_{H_2}}{\nu_{NaAlH_4}} \right|_{Rxn1}$ = Ratio of the stoichiometric coefficient of H_2 to $NaAlH_4$ in reaction 1 = 1

C_{NaH} = The bulk concentration of NaH [mole/m^3]

C_{NaAlH_4} = The bulk concentration of $NaAlH_4$ [mole/m^3].

Mass balance boundary conditions applied to the model are:

$\nabla \cdot \left(C_{nd} \vec{v} \right) = 0$ (on all walls and surfaces of symmetry) 4.4.1-4

and

$$C_{nd} = \frac{P_{inj} T_{ref}}{P_{ref} T_{wall}} \quad \text{(where the } H_2 \text{ feed tube wall joins the bed)} \qquad 4.4.1\text{-}5$$

where: P_{inj} = H_2 pressure in the feed tube [Pa]
T_{ref} = Reference temperature [K]
P_{ref} = Reference pressure [Pa]
T_{wall} = Feed tube wall temperature [K].

4.4.2 Hydrogen Momentum Balance

The components of velocity, effectively the momentum balance, are obtained from the Blake-Kozeny equation, see Bird, Stewart and Lightfoot [1960]. Modifying the Blake-Kozeny equation to give the mean interstitial velocity, rather than the superficial velocity, gives:

$$u = -\frac{D_p^{\,2}}{150\mu}\left(\frac{\varepsilon}{1-\varepsilon}\right)^2 \frac{\partial P}{\partial x}$$
$$v = -\frac{D_p^{\,2}}{150\mu}\left(\frac{\varepsilon}{1-\varepsilon}\right)^2 \frac{\partial P}{\partial y} \qquad 4.4.2\text{-}1$$
$$w = -\frac{D_p^{\,2}}{150\mu}\left(\frac{\varepsilon}{1-\varepsilon}\right)^2 \frac{\partial P}{\partial z}$$

where u, v, w = x, y and z components of the mean interstitial velocity, $\vec{v}$, respectively [m/s]
D_p = Mean diameter of particles in bed [m]
μ = Viscosity of H_2 [Pa-s]
P = Pressure [Pa]

Divide by U_{ref} to non-dimensionalize the components of velocity in Eqs. 4.4.1-1 to get the non-dimensionalized velocities

$$u_{nd} = -\frac{D_p^{\,2}}{150\mu}\left(\frac{\varepsilon}{1-\varepsilon}\right)^2 \frac{P_{ref}}{U_{ref}} \frac{\partial P_{nd}}{\partial x}$$
$$v_{nd} = -\frac{D_p^{\,2}}{150\mu}\left(\frac{\varepsilon}{1-\varepsilon}\right)^2 \frac{P_{ref}}{U_{ref}} \frac{\partial P_{nd}}{\partial y} \qquad 4.4.2\text{-}2$$
$$w_{nd} = -\frac{D_p^{\,2}}{150\mu}\left(\frac{\varepsilon}{1-\varepsilon}\right)^2 \frac{P_{ref}}{U_{ref}} \frac{\partial P_{nd}}{\partial z}$$

where: U_{ref} = Reference velocity [m/s].
$u_{nd} = \frac{u}{U_{ref}}$ = Non-dimensional x-component of the mean interstitial velocity.
$v_{nd} = \frac{v}{U_{ref}}$ = Non-dimensional y-component of the mean interstitial velocity.

$w_{nd} = \dfrac{w}{U_{ref}}$ = Non-dimensional z-component of the mean interstitial velocity.

P_{ref} = Reference pressure [Pa].

$P_{nd} = \dfrac{P}{P_{ref}}$ = Non-dimensional pressure.

Since the velocities are given explicitly in terms of the pressure gradient, there is no need to apply boundary conditions to the momentum balance.

4.4.3 Bed Energy Balance

It is assumed that, at a given location, both the hydrogen contained within the voids of the bed, and the solid material comprising the bed, have the same instantaneous temperature. Thus, in the sense of temperature, the solid and gas phases of the bed are assumed homogeneous. Because hydrogen flows through the bed, it transports thermal energy by convection. The enthalpies of reaction occurring during the uptake and release of hydrogen constitute a heat source that is assumed to be uniformly distributed over the volume occupied by the bed. The bed energy balance treats both the solid and gas phases as a homogeneous region, and is given by

$$\rho_{bed} C_{p\ bed} \frac{\partial T_{nd}}{\partial t} - \nabla \cdot k \nabla T_{nd} = -\varepsilon \rho_{H_2} C_{p\ H_2} \left(\frac{\partial T_{nd}}{\partial t} + \vec{v} \cdot \nabla T_{nd} \right) + \frac{1}{T_{ref}} \left(\frac{\partial P}{\partial t} + \varepsilon \vec{v} \cdot \nabla P \right) + \frac{1}{T_{ref}} \text{Source} \qquad 4.4.3\text{-}1$$

where: Source = Heat of reaction [W/m^3] $= -\left(\sum_i \left[\dfrac{1}{M_i} \dfrac{\partial \rho_i}{\partial t} \Delta H_i \right] \right)$

M_i = Molecular weight of species i per mole [kg/g-mole]

ρ_i = Bulk mass density of species i [kg/m^3]

$C_{p\ i}$ = Specific heat of species i [J/kg]

ΔH_i = Enthalpy of reaction on a molar basis of species i [J/(mol of i)]

$\rho_{bed} C_{p\ bed} = \rho_{Solid\ Reactants} C_{p\ Solid\ Reactants} + \rho_{Solid\ Products} C_{p\ Solid\ Products}$

T_{ref} = Reference temperature [K]

$T_{nd} = \dfrac{T}{T_{ref}}$ = Non-dimensional temperature

k = Bed thermal conductivity

P = Pressure [Pa]

The boundary conditions for the energy balance are:

$\hat{n} \cdot \nabla \cdot \left(k \nabla T_{nd} \right) = 0$ (thermal insulation, on all exterior boundaries and surfaces of symmetry) 4.4.3-2

$$\hat{n} \cdot \nabla \cdot \left(k \nabla T_{nd} \right) = -h_{H_2\ cool} \left(\frac{T_{wall} - T_{H_2\ bulk}}{T_{Ref}} \right) \quad \text{(on the walls of the } H_2 \text{ feed tubes)} \qquad 4.4.3\text{-}3$$

where: $\hat{n}$ = Outward normal to surface
$h_{H_2\ cool}$ = Convection heat transfer coefficient for H_2 in the feed tube [W/m^2-°C]
T_{wall} = Tube wall temperature [K]
$T_{H_2\ bulk}$ = Bulk temperature of the H_2 in the feed tube [K].

4.4.4 Energy Balance for the Tubes and Fins

The energy balance within the metal composing the fins and tubes is

$$k_{metal}\nabla^2 T = \rho_{metal} C_{p\,metal}\frac{\partial T}{\partial t} \qquad 4.4.4\text{-}1$$

where: k_{metal} = Thermal conductivity of the metal [W/(m-s)].
ρ_{metal} = Density of the metal [kg/m^3].
$C_{p\,metal}$ = Specific heat of the metal [J/(kg-K)]

The boundary conditions applied to the metal tube and fins are:

$$\nabla\cdot\left(k_{metal\ 1}\nabla T_{metal\ 1}\right) = \nabla\cdot\left(k_{metal\ 2}\nabla T_{metal\ 2}\right) \quad \text{(at the interfaces between the fins and tubes)} \qquad 4.4.4\text{-}2$$

$$\nabla\cdot\left(k_{metal}\nabla T_{metal}\right) = \nabla\cdot\left(k_{bed}\nabla T_{bed}\right) \quad \text{(at the interface between the bed and the metal)} \qquad 4.4.4\text{-}3$$

$$\hat{n}\cdot\nabla\cdot\left(k_{metal}\nabla T_{metal}\right) = -h_{conv\ cool}\left(T_{wall} - T_{coolant\ bulk}\right) \quad \text{(on the walls of the cooling tubes)} \qquad 4.4.4\text{-}3$$

where: $\hat{n}$ = Outward normal to surface
$h_{conv\ cool}$ = Convection heat transfer coefficient for heat transfer fluid [W/m^2-°C]
T_{wall} = Tube wall temperature [K]
$T_{coolant\ bulk}$ = Bulk temperature of the heat transfer fluid [K]

4.4.5 Reaction Kinetics

Chemical kinetics depend on the material used as a storage media. Thus, to permit the kinetics equations to be easily modified, they are cast as a separate module within the set of governing equations defined in COMSOL Multiphysics®. At present, the model can accept kinetics models in the form of differential-algebraic equations or as tabulated data (which can be fit using a cubic spline).

The particular storage system examined in this report consisted of a bed that was converted from NaH to sodium aluminum hydride, $NaAlH_4$, as given by Equation 4.4.5-1, when loaded with hydrogen. Specifically, the hydride used in the bed is $TiCl_3$ catalyzed $NaAlH_4$. As discussed in Appendx A.2, the United Technologies Research Center™ (UTRC) developed an empirical kinetics model for this material.

$$\underbrace{NaAlH_4}_{\text{Species 1}} \underbrace{\leftrightarrow}_{\text{Reaction 1}} \underbrace{\frac{1}{3}Na_3AlH_6}_{\text{Species 2}} + \frac{2}{3}Al + H_2 \underbrace{\leftrightarrow}_{\text{Reaction 2}} \underbrace{NaH}_{\text{Species 3}} + Al + \frac{3}{2}H_2 \qquad 4.4.5\text{-}1$$

Forward and reverse reaction rates for each reaction were fit to data using the following expressions:

$$r_{1F} \equiv C_{eqv} A_{1F} \exp\left[-\frac{E_{1F}}{RT}\right]\left[\frac{P(C,T)-P_{eq1}(T)}{P_{eq1}(T)}\right]$$

$$r_{1B} \equiv -C_{eqv} A_{1B} \exp\left[-\frac{E_{1B}}{RT}\right]\left[\frac{P_{eq1}(T)-P(C,T)}{P_{eq1}(T)}\right]$$

$$r_{2F} \equiv -C_{eqv} A_{2F} \exp\left[-\frac{E_{2F}}{RT}\right]\left[\frac{P(C,T)-P_{eq2}(T)}{P_{eq2}(T)}\right] \qquad 4.4.5\text{-}2$$

$$r_{2B} \equiv C_{eqv} A_{2B} \exp\left[-\frac{E_{2B}}{RT}\right]\left[\frac{P_{eq2}(T)-P(C,T)}{P_{eq2}(T)}\right]$$

where: C = Concentration of H_2 [mole H_2/m^3 of interparticle void]

C_{eqv} = Equivalent concentration of $NaAlH_4$ [mole/m^3] based on the initial concentrations of all metal species (concentration of bed fully converted to tetrahydride form)

= $C_{10} + 3C_{20} + C_{30}$

$C_{1\,0}$ = Initial concentration of $NaAlH_4$ [mole/m^3]

$C_{2\,0}$ = Initial concentration of Na_3AlH_6 [mole/m^3]

$C_{3\,0}$ = Initial concentration of NaH [mole/m^3].

$P_{eq1}(T)$ and $P_{eq2}(T)$ are the H_2 pressures, in Pa, in equilibrium with the $NaAlH_4$ and the Na_3AlH_6 metal hydrides, respectively, at temperature T, in [K]. These relations are given by the van't Hoff equations:

$$P_{eq1}(T) = 10^5 \exp\left[\frac{\Delta H_4}{RT} - \frac{\Delta S_4}{R}\right]$$

$$P_{eq2}(T) = 10^5 \exp\left[\frac{\Delta H_2}{RT} - \frac{\Delta S_2}{R}\right] \qquad 4.4.5\text{-}2$$

The reference for this model, contained in Appendix A.2, proposes the kinetics equations

$$\frac{dC_1}{dt} = \begin{cases} r_{1F}\left[\dfrac{3C_2(t)}{C_{eqv}} - C_{2sat}(T)\right]^{\chi_{1F}} & \text{if} \quad P \geq P_{eq1}(T) \\ r_{1B}\left[\dfrac{C_1(t)}{C_{eqv}}\right]^{\chi_{1B}} & \text{if} \quad P < P_{eq1}(T) \text{ and } C_1(t) \geq 0 \end{cases} \qquad 4.4.5\text{-}3a$$

and

$$\frac{dC_3}{dt} = \begin{cases} r_{2F}\left[\frac{C_3(t)}{C_{eqv}} - C_{3sat}(T)\right]^{\chi_{2F}} & \text{if} \quad P \geq P_{eq2}(T) \\ r_{2B}\left[\frac{3C_2(t)}{C_{eqv}}\right]^{\chi_{2B}} & \text{if} \quad P < P_{eq2}(T) \text{ and } C_2(t) \geq 0 \end{cases} \qquad 4.4.5\text{-}3b$$

By Eq. 4.4.5-1

$$\frac{dC_2}{dt} = -\frac{1}{3}\left(\frac{dC_1}{dt} + \frac{dC_3}{dt}\right) \text{ or } C_2 = C_{2\,0} - \frac{1}{3}\left[\left(C_1 - C_{1\,0}\right) + \left(C_3 - C_{3\,0}\right)\right] \qquad 4.4.5\text{-}3c$$

where: C_1 = Concentration of $NaAlH_4$ [mole/m^3]
C_2 = Concentration of Na_3AlH_6 [mole/m^3]
C_3 = Concentration of NaH [mole/m^3]

$C_{2\,sat}(T)$ and $C_{3\,sat}(T)$, in [mole/m^3], were estimated by UTRC in Appendix A.2 as

$$C_{2\,sat}(T) = 0$$

$$C_{3\,sat}(T) = r_{sat}\left(1 - \frac{wf_{iso}^{sat}(T)}{0.056}\right) \qquad 4.4.5\text{-}4a$$

where: $$r_{sat} = \text{Max}\left[1, \left(1 - \frac{0.0373}{0.056 - wf_{iso}^{sat}(T)}\right)\right] \qquad 4.4.5\text{-}4b$$

The values for $wf_{iso}^{sat}(T)$, the saturation hydrogen weight fraction for loading at a fixed temperature T, are listed in Table 4.4.5-1. The COMSOL® fits this data via a cubic spline, with extrapolated values fixed at the endpoints.

Table 4.4.5-1
Values for $wf_{iso}^{sat}(T)$

T (K)	$wf_{iso}^{sat}(T)$
353.15	0.021
363.15	0.023
373.15	0.029
393.15	0.022
413.15	0.018

The weight fraction of H_2 contained in the sodium alanate metal, based on Eq. 4.4.5-1, is defined as

$$wf = \frac{\text{Mass of } H_2 \text{ contained in the metal hydride at time t (kg } H_2)}{\text{Mass of the bed fully converted to tetrahydride form (kg } NaAlH_4)} = \frac{1.5C_1 + 0.5C_2}{C_{eqv}} \frac{M_{H_2}}{M_{NaAlH_4}} \quad 4.4.5\text{-}5$$

where: $M_{Na_3AlH_6}$ = Gram molecular weight of Na_3AlH_6 [kg/g-mole]
M_{H_2} = Gram molecular weight of H_2 [kg/g-mole].

For sodium alanate, the reaction heat term for the energy balance, Eq. 4.4.3-1 is

$$\text{Source} = \frac{dC_1}{dt}\Delta H_{rxn\ 1} - 0.5\frac{dC_3}{dt}\Delta H_{rxn\ 2} \quad 4.4.5\text{-}6$$

where by Gross [2003]:

$\Delta H_{rxn\ 1}$ = Heat of per mole of H_2 consumed going to left for reaction 1
= -37 kJ/(mole H_2)
$\Delta H_{rxn\ 2}$ = Heat of per mole of H_2 consumed going to left for reaction 2
= -47 kJ/(mole H_2)

4.4.6 Equation of State

Over the range of operating temperatures and pressures for the storage system, hydrogen behaves as an ideal gas. Hence, the ideal gas law, in the form of Eq. 4.4.6-1, constitutes the equation of state for the gas phase.

$$P = C_{H_2}RT \quad 4.4.6\text{-}1$$

where: C_{H_2} = Concentration of H_2 gas (mole/m^3).
R = Gas constant

4.4 Model Input Parameters

Table 4.4-1 contains the constant values or expressions used in the COMSOL® model for the $NaAlH_4$ bed. Global expressions used by COMSOL® are listed in Table 4.4-2. Finally, subdomain expressions, applied only to the metal hydride bed, are listed in Table 4.4-3

Table 4.4-1 Values of Constants Used in the $NaAlH_4$ Model

Description of Parameter	Expression or Value	Variable Notation Used in COMSOL®
Reference Pressure [Pa], Atmospheric Pressure	101325	Pref
Reference Speed [m/s]	0.1	Uref
Reference Length [m] ~ Bed Radius	0.1	Lref
Reference Concentration [mol/m^3]	Pref/(R*Tref)	Cref
Reference Temperature [K]	300	Tref
Reference H_2 Density [kg/m^3]	M_H2*Cref	rho_ref
Initial H_2 Concentration [mol/m^3]	P0/(R*T0)	C0
Bed Particle Diameter [m]	3E-7	Dp
Bed Void Fraction	0.5	epsilon
g-molecular weight of $NaAlH_4$ [kg/mol]	54/1000	M_NaAlH4
g-molecular weight of H_2 [kg/mol]	2.016/1000	M_H2
Gas Constant [J/mol-K]	8.314	R
Initial Pressure [Pa]	101325	P0
Initial Bed Temperature [K]	373	T0
Temperature of Injected H_2 [K]	373	Tinj
Velocity of Injected H_2 in Feed Tube [m/s]	14	Vinj
Inner Diameter of H_2 Injection Tube [m]	0.0127	Dinj
Concentration for Exit Pressure [Pa]	C0	Cout
Coolant Density [kg/m^3]; For DowTherm T®	820.0	rho_cool
Coolant Thermal Conductivity [W/m °C]; For DowTherm T®	0.325	k_cool
Coolant Specific Heat [J/kg K]; For DowTherm T®	820.0	Cp_cool
Coolant Viscosity [Pa-s]; For DowTherm T®	3.0e-3	mu_cool
Coolant Tube Diameter [m]	0.0168	D_cool
Coolant Velocity [m/s]	13.0	Vcool
Coolant Temperature [K]	373	T_cool
Fin-Tube Contact Conductance [W/m^2 °C]; From Holman [1976]	5.56e-4	h_contact_tube
Bed-Tube Contact Conductance [W/m^2 °C]; Estimated	1e-6	h_contact_bed
Bulk Density of Hydride Bed [kg/m^3], Mosher, et. el. [2007]	720.0	rho_bed
Thermal Cond of Hydride Bed [W/m K]; used sand from Avallone and Baumeister [1987], Table 4.4.4	0.325	k_bed
Specific Heat of Hydride Bed [J/kg K]; for sand from Avallone and Baumeister [1987], Table 4.2.25	820.0	Cp_bed
Density of 6063-T83 Aluminum (Tubes & Fins) [kg/m^3]; from Avallone and Baumeister [1987], and COMSOL® material data	2700	
Thermal conductivity of 6063-T83 Aluminum (Tubes & Fins) [W/(m-K)]; from COMSOL® material data	201	
Heat capacity of 6063-T83 Aluminum (Tubes & Fins) [J/(kg-K)]; from COMSOL® material data	900	
Test Source [W/m^3]	4.48e6	S0

Table 4.4-1 Values of Constants Used in the $NaAlH_4$ Model (Continued)

Description of Parameter	Expression or Value	Variable Notation Used in COMSOL®
Time [s] to Reach 90% of Full Heat Source Strength (S0)	60	tau
Constant in Time-Dependent Heat Source Expression, Source	-log(0.1)/tau	a
Forward Rate Constant for Reaction 1	1e8	A1F
Forward Activation Energy for Reaction 1 [kJ/mol]	80	E1F
Backward Rate Constant for Reaction 1	4e12	A1B
Backward Activation Energy for Reaction 1 [kJ/mol]	110	E1B
Exponent for Reaction 1	2	Chi1
Forward Rate Constant for Reaction 2	1.5e5	A2F
Forward Activation Energy for Reaction 2 [kJ/mol]	70	E2F
Backward Rate Constant for Reaction 2	6e12	A2B
Backward Activation Energy for Reaction 2 [kJ/mol]	110	E2B
Exponent for Reaction 2	1	Chi2
(Δ Enthalpy for Reaction 1)/R	-4475	DHR1
(Δ Entropy for Reaction 1)/R	-14.83	DSR1
(Δ Enthalpy for Reaction 2)/R	-6150	DHR2
(Δ Entropy for Reaction 2)/R	-16.22	DSR2
Heat of Reaction for Reaction 1 [J/mol H_2]	37000	DH_rx1
Heat of Reaction for Reaction 2 [J/mol H_2]	47000	DH_rx2
Initial Concentration of $NaAlH_4$ [mol/m^3]	0	C10
Initial Concentration of Na_3AlH_6 [mol/ m^3]	0	C20
Initial Concentration of NaH [mol/ m^3]	13,333.33	C30

Table 4.4-2 Global Expressions Used in the $NaAlH_4$ Model

Description of Expression	Expression	Expression Identifier Used in COMSOL®
H_2 Viscosity [Pa-s]; [TK]=K; Lide and Kehiaian [1994]	5.1899*10^-8*TK-1.23594*10^-10*TK^2+2.06597*10^-13*TK^3 -1.30208*10^-16*TK^4	mu_H2
Density of H_2 [kg/m^3]	C*M_H2	rho_H2
	rho_H2/rho_ref	rho_H2_nd
Thermal Cond for H_2 [W/m K]; [TK]=K; Lide and Kehiaian [1994]	(0.7042* TK -1.470*10^-4* TK ^2-3.652*10^-7* TK ^3 -1.738*10^-10* TK ^4)/1000	k_H2
Specific Heat for H_2 [J/kg K]; [TK]=K; Lide and Kehiaian [1994]	5.1899*10^-8* TK -1.23594*10^-10* TK ^2+2.06597*10^-13* TK ^3 -1.30208*10^-16* TK ^4	Cp_H2
Time Dependent Pressure in H_2 Feed Tubes [Pa]	49*P0*(1-exp(-.456*t))+P0	Pinj
Mass Flux of Injected H_2 [kg/m^2 s]	(Cinj*M_H2)*Vinj	G_H2_inj
Mass Flux of Coolant [kg/m^2 s]	rho_cool*Vcool	G_cool
Prandtl No for Injected H_2	visc_H2(Tinj)*spec_heat_H2(Tinj)/therm_cond_H2(Tinj)	Pr_H2
Prandtl No for Coolant, DowTherm T®	mu_cool*Cp_cool/k_cool	Pr_cool
Convection Heat transfer Coefficient for Injected H_2 [W/m^2 K]; Holman [1976]	0.023*therm_cond_H2(Tinj)/Dinj*(G_H2_inj*Dinj/visc_H2(Tinj))^0.8 *Pr_H2^0.4	h_conv_H2
Convection Heat Transfer Coefficient for Coolant [W/m^2 K] ; Holman [1976]	0.023*k_cool/D_cool*(G_cool*D_cool/mu_cool)^0.8*Pr_cool^0.4	h_conv_cool
Temperature [K] for use in Functions	T_nd*Tref	TK
Temperature [K]	TK	T

Table 4.4-3 Subdomain Expressions Used in the $NaAlH_4$ Model

Description of Expression	Expression	Expression Identifier Used in COMSOL®
Pressure [Pa]	C*R*TK	P
Non-Dimensionalized x-Component of Velocity	-Dp^2*Pref*(epsilon/(1-epsilon))^2*diff(P_nd,x)/(150*mu_H2*Uref)	u_nd
Non-Dimensionalized y-Component of Velocity	-Dp^2*Pref*(epsilon/(1-epsilon))^2*diff(P_nd,y)/(150*mu_H2*Uref)	v_nd
Non-Dimensionalized z-Component of Velocity	-Dp^2*Pref*(epsilon/(1-epsilon))^2*diff(P_nd,z)/(150*mu_H2*Uref)	w_nd
Heat Source Due to Chemical Reactions	C1t*DH_rx1-0.5*C3t*DH_rx2	Source
Non-Dimensionalized Pressure	P/Pref	P_nd
x-Component of Velocity [m/s]	u_nd*Uref	u
y-Component of Velocity [m/s]	v_nd*Uref	v
z-Component of Velocity [m/s]	w_nd*Uref	w
H_2 Equilibrium Pressure for Reaction 1 [Pa]	100000*exp(DHR1/TK-DSR1)	Peq1
H_2 Equilibrium Pressure for Reaction 2 [Pa]	100000*exp(DHR2/TK-DSR2)	Peq2
"Saturation Concentration" for Na_3AlH_6 [equiv units]	0	C2sat
"Saturation Concentration" for NaH [equiv units]	1-125*wf(TK)/7	C3sat
Concentration of Na_3AlH_6 [mol/m^3]	C20-(C11-C10+C3-C30)/3	C2
Basis for Equivalent Units [mol/m^3]	C10+3*C20+C30	Ceqv
Forward Rate for Reaction 1	A1F*Ceqv*exp(-1000*E1F/(R*TK))*(P-Peq1)*(3*C2/Ceqv-C2sat)^Chi1/Peq1	r1F
Backward Rate for Reaction 1	-A1B*Ceqv*exp(-1000*E1B/(R*TK))*(Peq1-P)*(C11/Ceqv)^Chi1/Peq1	r1B
Forward Rate for Reaction 2	-A2F*Ceqv*exp(-1000*E2F/(R*TK))*(P-Peq2)*(C3/Ceqv-C3sat)^Chi2/Peq2	r2F
Backward Rate for Reaction 2	A2B*Ceqv*exp(-1000*E2B/(R*TK))*(Peq2-P)*(3*C2/Ceqv)^Chi2/Peq2	r2B
H2 Concentration [mol/m^3]	C_nd*Cref	C
NaALH4 Concentration [mol/m^3]	C1*(C1>0)	C11

4.5 Mesh Used in 2 and 3-Dimensional Models

The mesh used in the 2-dimensional model is shown in Figure 4.5-1 and the mesh statistics are listed in Table 4.5-1. Similarly, Figure 4.5-2 shows the mesh used in the 3-dimensional model, and its mesh statistics are listed in Table 4.5-2

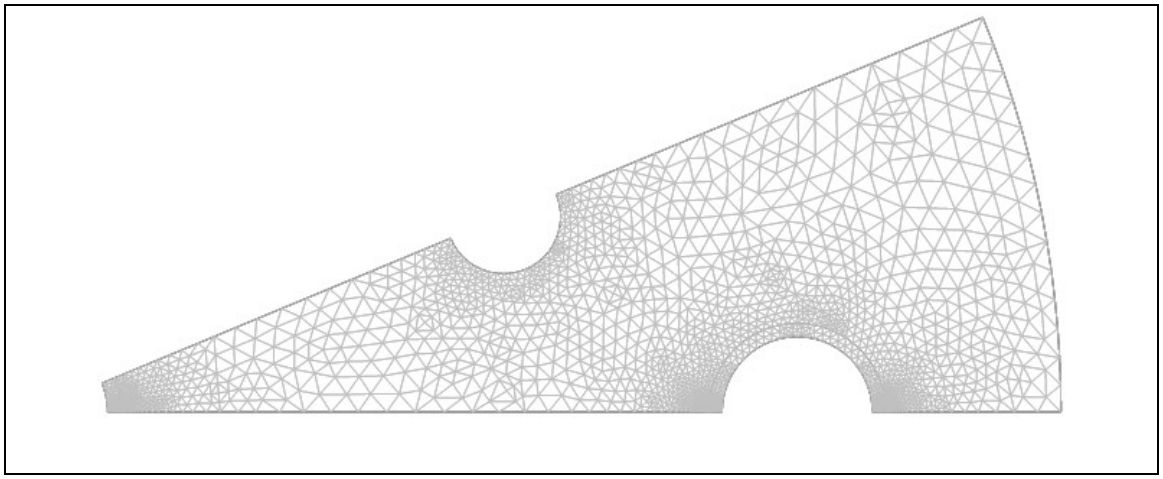

Figure 4.5-1 Two-dimensional mesh.

Table 4.5-1 Two-Dimensional Mesh Statistics

Number of degrees of freedom	106,697
Number of mesh points	7,793
Number of elements	15,136
Triangular	15,136
Quadrilateral	0
Number of boundary elements	568
Number of vertex elements	20
Minimum element quality	0.6474
Element area ratio	8.09E-4

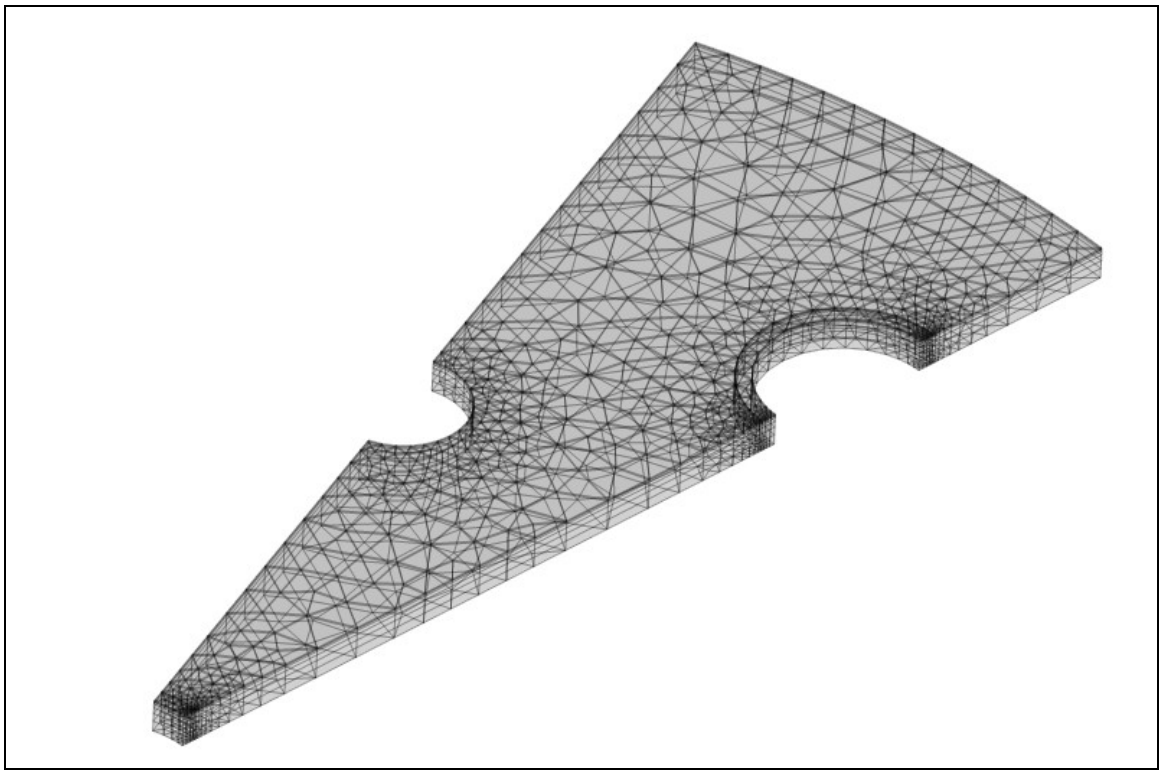

Figure 4.5-2 Three-dimensional mesh.

Table 4.5-2 Three-Dimensional Mesh Statistics

Number of degrees of freedom	98,454
Number of mesh points	4,382
Number of elements	6,696
Tetrahedral	0
Prism	6,696
Hexahedral	0
Number of boundary elements	4,332
Triangular	3,348
Quadrilateral	984
Number of edge elements	612
Number of vertex elements	60
Minimum element quality	0.055
Element volume ratio	0

5.0 RESULTS

Transient calculations were performed for the loading phase of the sodium alanate bed. Although the state of the bed was conducive to loading, the kinetics equations used in the model were capable of modeling forward and reverse hydriding reactions. Thus, if the exothermic hydriding reactions caused the local temperature to rise sufficiently, dehydriding could be predicted by the model.

Variables predicted by the model included spatially and time dependent temperature, pressure, molar concentrations of $NaAlH_4$, Na_3AlH_6, and NaH, the three components of gas velocity, gas concentration and/or density, and any parameter that could be computed from the aforementioned variables. The coolant was assumed to be DowTherm T®, which was at a constant temperature of 373K and flowed at a velocity of 13m/s. Hydrogen was introduced to the bed through injection tubes that allowed the gas to flow freely into the porous bed. Initially the gas pressure in the tubes and the bed was 1 bar. The pressure in the tubes exponentially approached 50 bar, reaching 99% of the final value in 10 seconds. As the gas pressure increased, the resulting pressure gradient caused the gas to flow from the interface between the tube and bed into the bed, according to the Blake-Kozeny equations. The gas temperature in the tube was fixed at 373K.

5.1 Bed Capacity

Both the two and three-dimensional COMSOL® models were applied to a sodium aluminum hydride bed having dimensions derived from the Microsoft Excel® based geometry scoping tool, as discussed in Section 4.2. Underlying the calculations for the bed dimensions was the requirement that the hydride contain 1000 g of H_2, and the assumption that all the hydride was converted from NaH to $NaAlH_4$ in 3 minutes. However, later investigation with the Mathcad® kinetics scoping model, which utilized the equations in Attachments 1 and 2 for $TiCl_3$ catalyzed $NaAlH_4$, showed that the uptake rate for hydrogen was slow. Even for near optimal loading conditions, with a temperature of 100°C and a pressure of 50 bar, a bed starting with pure NaH only achieved a hydrogen weight fraction (defined in Equation 4.4.5-5) of 0.00238 after 3 minutes, far lower than the theoretical value of 0.056. For this reason, the run time in the finite element models was increased to 12 minutes, while keeping the heat transfer parameters the same as for the 3 minute charging time. Even with the charging time increased to 12 minutes, the weight fraction of H_2 stored in the bed was approximately 0.00794. This value implies that to store 1000g of hydrogen in 12 minutes, the mass of hydride would need to be increased by more than 7 times.

Based on the UTRC™ kinetics equations for $TiCl_3$ catalyzed $NaAlH_4$ in Attachments 1 and 2, the maximum weight fraction of stored hydrogen (the bed gravimetric capacity defined in Equation 5.1.2) loaded at 100°C and 50 bar, was approximately 0.029, rather than the theoretical value of 0.056 discussed in Section 5.2. This difference may, in part, be because the UTRC™ kinetics equations were fit to data taken over less than 15,000 seconds. At longer periods of time the actual hydrogen weight fraction may be greater than that predicted by the correlations derived by UTRC™.

From Figure 5.1-1, it can be seen that, according to the UTRC™ kinetics equations, the weight fraction asymptotically approaches 0.029 as the charging time increases. This applies to a charging temperature of 100°C and pressure of 50 bar. The limiting conversion is due to the terms $C_{sat\ i}(T)$ in the kinetics equations, see Appendix A.1.4. These terms were introduced to improve the comparison of the kinetics model with data over less than 15,000 seconds. However, at very long times the $C_{sat\ i}(T)$ terms prevent full conversion to the tetrahydride, and perhaps limit the validity of the kinetics model at very long charging times. Because the saturation terms depend on temperature, the fraction of monohydride that can be converted to tetrahydride for long times varies with the system temperature during loading. The weight fraction depends on both the temperature and pressure during the charging process.

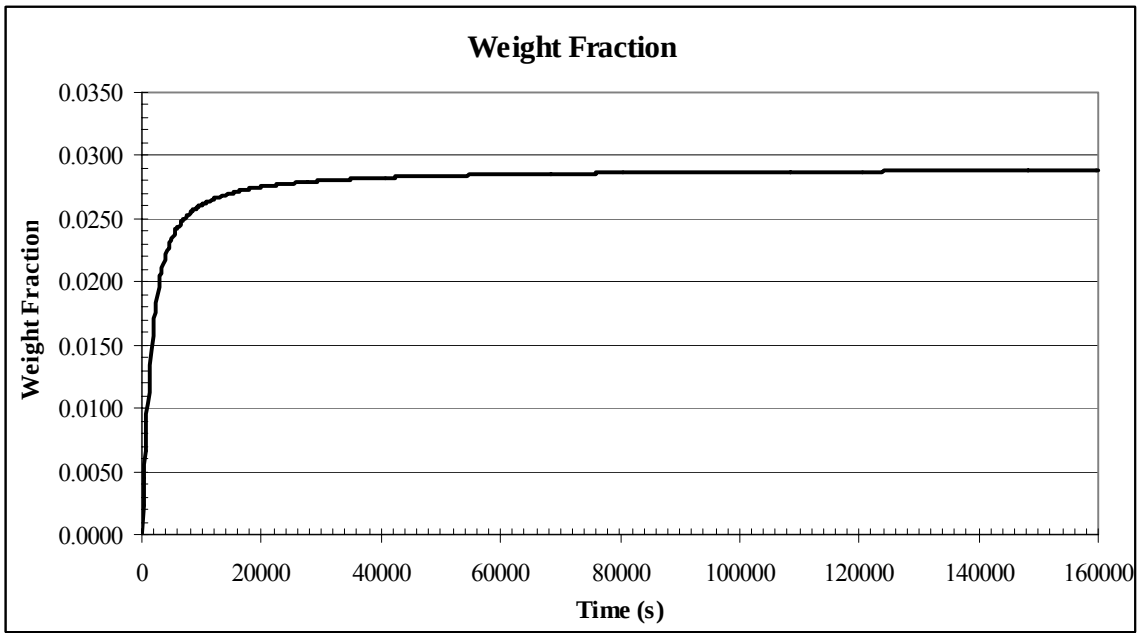

Figure 5.1-1 Bed weight fraction of stored hydrogen, loaded at 100°C and 50 bar. Storage in both $NaAlH_4$ and Na_3AlH_6 are included.

5.2 Loading Rate

Loading rates for the bed are given in terms of the weight fraction of stored hydrogen, $\mathrm{wf}(t)$, as opposed to the bed and system gravimetric capacities, G_{Bed} and G_{System}, respectively. These terms are defined as

$$\mathrm{wf}(t) = \frac{\text{Mass of } H_2 \text{ contained in the metal hydride at time t (kg } H_2)}{\text{Mass of the bed fully converted to tetrahydride form (kg } NaAlH_4)} \qquad 4.4.5\text{-}5$$

$$G_{Bed}(t) = \frac{\text{Stoichiometric mass of } H_2 \text{ used to produce } NaAlH_4 \text{ from NaH (kg } H_2)}{\text{Mass of the bed fully converted to tetrahydride form (kg } NaAlH_4)} \qquad 5.1\text{-}2$$

$$G_{System} = \frac{\text{Stoichiometric mass of } H_2 \text{ used to produce } NaAlH_4 \text{ from NaH (kg } H_2)}{\text{Mass of the system with the bed in tetrahydride form (kg system)}} \qquad 5.2\text{-}3$$

By Equation 4.4.5-1, the theoretical value of G_{Bed} is

$$G_{Bed} = \frac{\text{Stoichiometric mass of } H_2 \text{ used to produce 1 mole of } NaAlH_4 \text{ from NaH}}{\text{Mass of 1 mole of } NaAlH_4} = \frac{1.5M_{H_2}}{M_{NaAlH_4}} = 0.0560 \qquad 5.3\text{-}4$$

where: M_{H_2} = Molecular weight of H_2 (kg/g-mole) = 2.016×10^{-3} kg/g-mole

M_{NaAlH_4} = Molecular weight of $NaAlH_4$ (kg/g-mole) = 5.40×10^{-2} kg/g-mole

In the system model, it was assumed that the bed was initially all NaH, with sufficient Al to complete the reaction to $NaAlH_4$. The initial bed temperature was assumed to be 100°C. Three

models were used to estimate the loading rate for the bed. These were the kinetics scoping model and the 2 and 3-dimensional finite element models.

The 0-dimensional Matlab® based kinetics scoping model predicted the transient weight fraction of stored hydrogen for a bed being loaded at a fixed temperature and pressure; in this case 100°C and 50 bar. This model considered only the chemical kinetics of the loading process.

Both the 2 and 3-dimensional finite element COMSOL® based models also predict the transient bed weight fraction of stored hydrogen. For these models, heat transfer from the bed occurred via conduction through the bed, fins and tube walls, as well as by convection from hydrogen flowing through the porous bed. The bulk coolant temperature was fixed at 100°C, as was the bulk temperature of hydrogen in the injection tubes.

In the finite element models, the penetration of hydrogen into the bed was driven by an increase in gas pressure in the injection tubes. Within the tubes the hydrogen pressure underwent an asymptotic increase from 1 to 50 bar, rising to within 99% of 50 bar in 10 seconds. The porous wall of the injection tube allowed hydrogen to penetrate into the hydride bed, which was initially at a pressure of 1 bar. As the pressure in the injection tube increased, the resulting pressure gradient within the packed hydride bed resulted in gas flow, which experienced viscous resistance as it passed into the bed. Hence, at the beginning of the loading phase, the local gas pressure within the bed varied over time. Heat generated by the chemical reactions was transferred to the cooling and gas injection tubes by conduction and to much lesser extent by forced convection as the gas flowed through the bed. Therefore, the local bed temperature varied with time and position. Heat transfer in the 3-dimensional model also consisted of conduction to the axially spaced fins. Of course, this effect was not treated in the 2-dimensional model. Initial bed temperatures, coolant and gas temperatures in the 2 and 3-dimensional models were chosen to optimize the uptake kinetics. It was attempted to select temperatures that were sufficiently high to provide the most rapid uptake reaction rate, but not so high that exothermic reactions would yield bed temperatures that reversed the hydriding reaction.

A comparison of loading rates for the 0-dimensional kinetics model, and the 2 and 3-dimensional finite element models, in terms of the weight fraction of stored hydrogen, is shown in Figure 5.2-1. For the 0-dimensional kinetics model, the weight fraction of stored hydrogen was point dependent, however, for the 2 and 3-dimensional finite element models, the weight fraction of stored hydrogen depended on location and time. Therefore, for the 2 and 3-dimensional models, the weight fraction of stored hydrogen was expressed as an areal or volume average, respectively. To demonstrate capability, the 2 and 3 dimensional finite element models were run for initial NaH concentrations of 330.69 and 13,333.33 mole/m^3. Because these models included an energy balance that addressed the heat of reaction, increased initial NaH concentration resulted in increase transient temperatures, which impacted the rate of hydrogen uptake.

Loading rates predicted by 3-dimensional finite element models, which allowed for the presence of the axially located fins, were essentially identical to those for the 0-dimensional kinetics model. The higher loading rates for the 2-dimensional finite element model, with an initial NaH concentration of 330.69 mole/m^3, resulted from higher predicted bed temperatures due to the absence of fins. However, for the larger initial NaH concentration of 13,333.33 mole/m^3, temperatures in the 2-dimensional model were sufficiently high to reduce, and in some locations reverse, the hydriding reactions. This led to the lower loading rate shown in Figure 5.2-1

Figure 5.2-2 shows the transient weight fraction of stored hydrogen relative to bed gravimetric capacity, which had a theoretical value of 0.056.

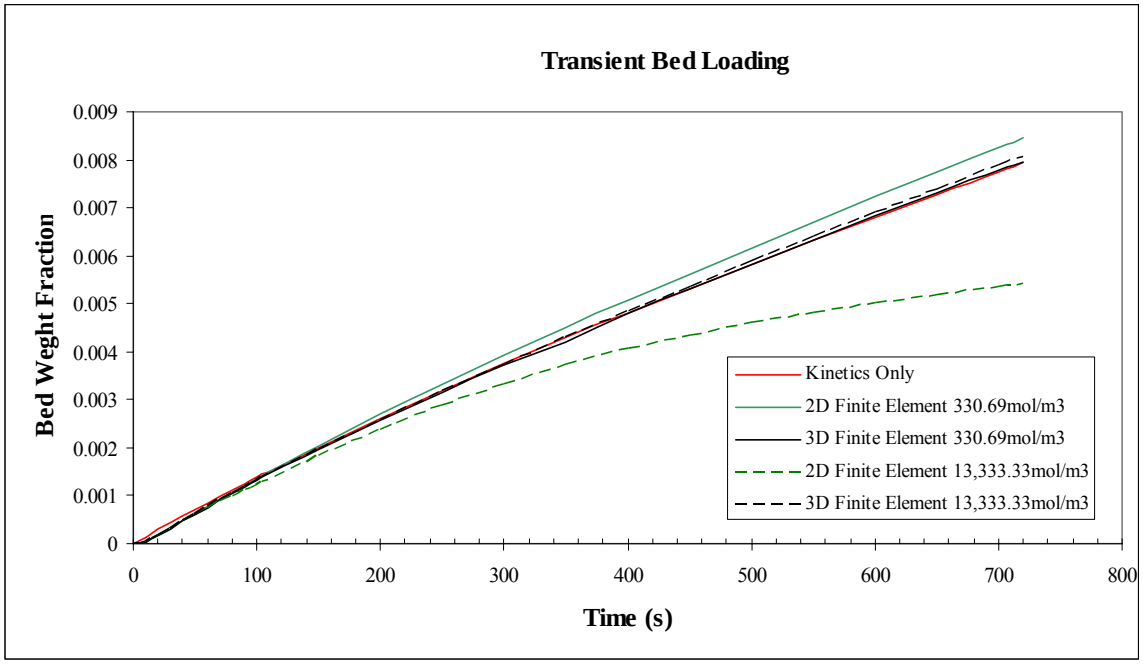

Figure 5.2-1 Comparison of the weight fraction of stored hydrogen for the kinetics scoping model and the 2 and 3-dimensional finite element bed models.

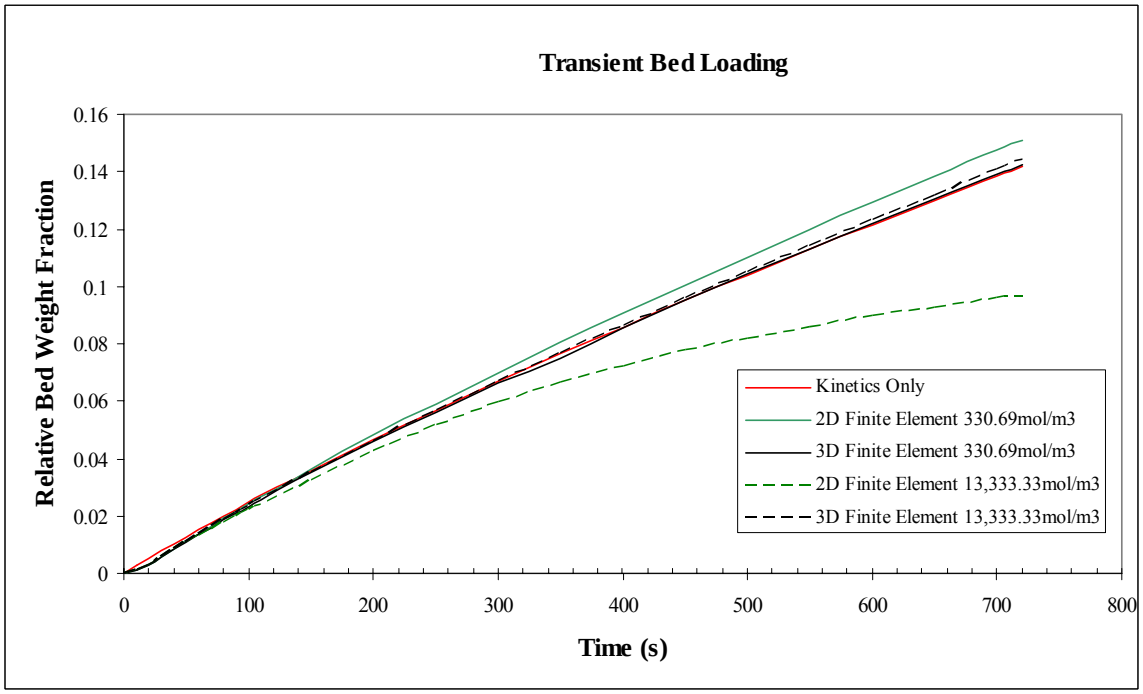

Figure 5.2-2 Comparison of weight fraction of stored hydrogen relative to the theoretical gravimetric capacity of the bed, $^{wf(t)}/_{0.056}$, for the kinetics scoping model and the 2 and 3-dimensional finite element bed models.

5.3 Bed Temperatures

Heat generated during the loading of the bed results in a temperature transient that impacts the reaction rates. The low thermal conductivity of the alanate necessitates design features that maintain a relatively short length scale for heat transfer within the bed. The models in this document were developed for shell and tube (the 2-dimensional finite element model) and shell, tube and fin (the 3-dimensional finite element model) configurations.

Figure 5.3-1 shows plan and isometric views of the temperature profile in the 3-dimensional model at 40 second into the loading transient. The image on the left shows the reduction in temperature from the mid-plane of the hydride layer to the midplane of the fin. The plan view, on the right, shows the temperature profile over the midplane of the hydride layer.

Figures 5.3-2 through 5.3-5 compare the transient temperature profile for the 2-dimensional model, which does not have fins, to the temperature profile at the midplane of the hydride layer for the 3-dimensional model. Comparisons were made at 30, 60, 120 and 720 seconds. In these figures, it can be seen that the fins result in a much more uniform temperature profile.

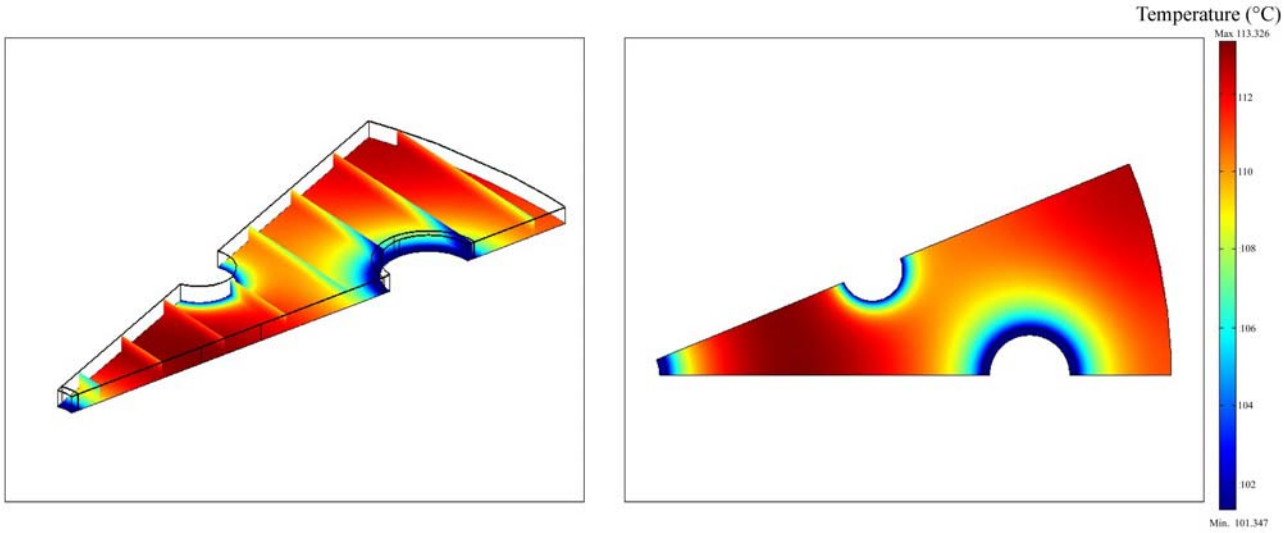

Figure 5.3-1 Isometric and plan views of temperature profile for 3-dimensional model at 40 seconds.

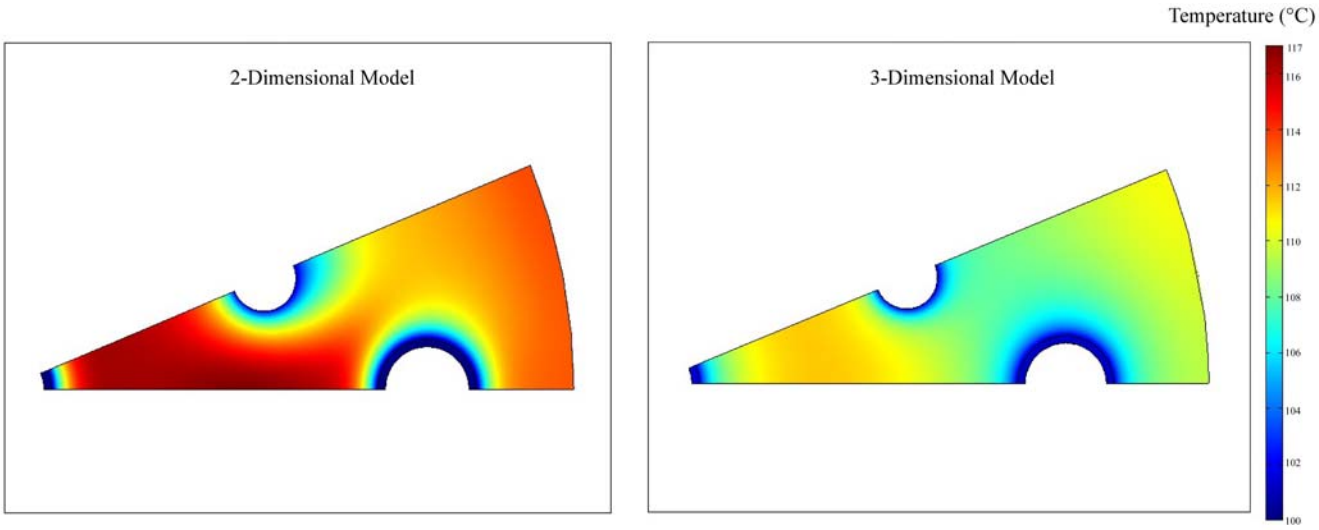

Figure 5.3-2 Comparison between 2-dimensional and 3-dimensional midplane temperature profiles at 30 seconds.

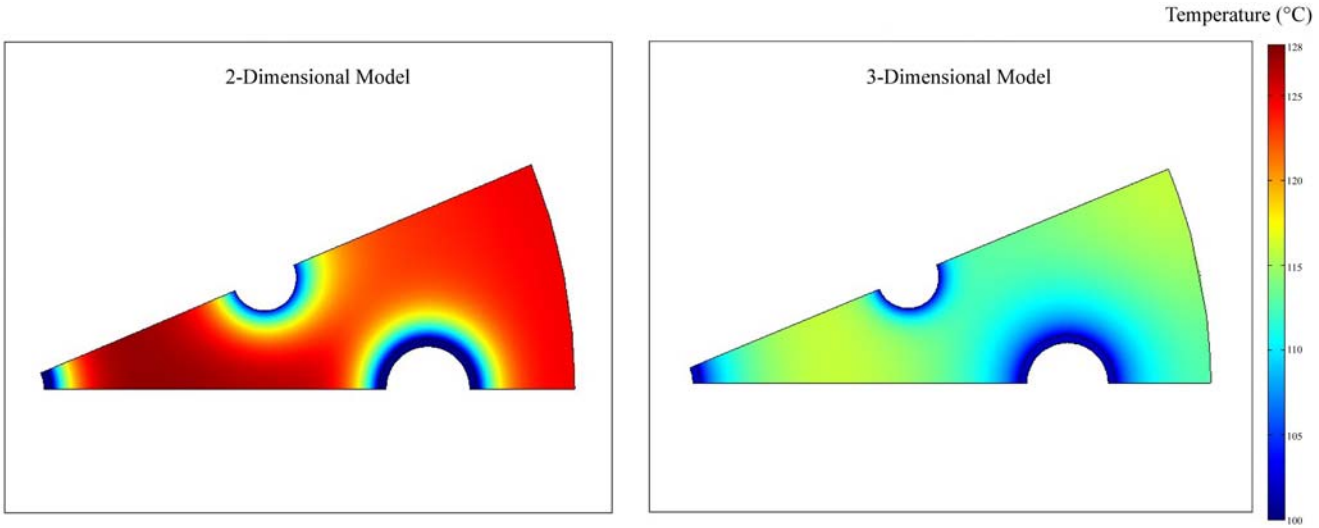

Figure 5.3-3 Comparison between 2-dimensional and 3-dimensional midplane temperature profiles at 60 seconds.

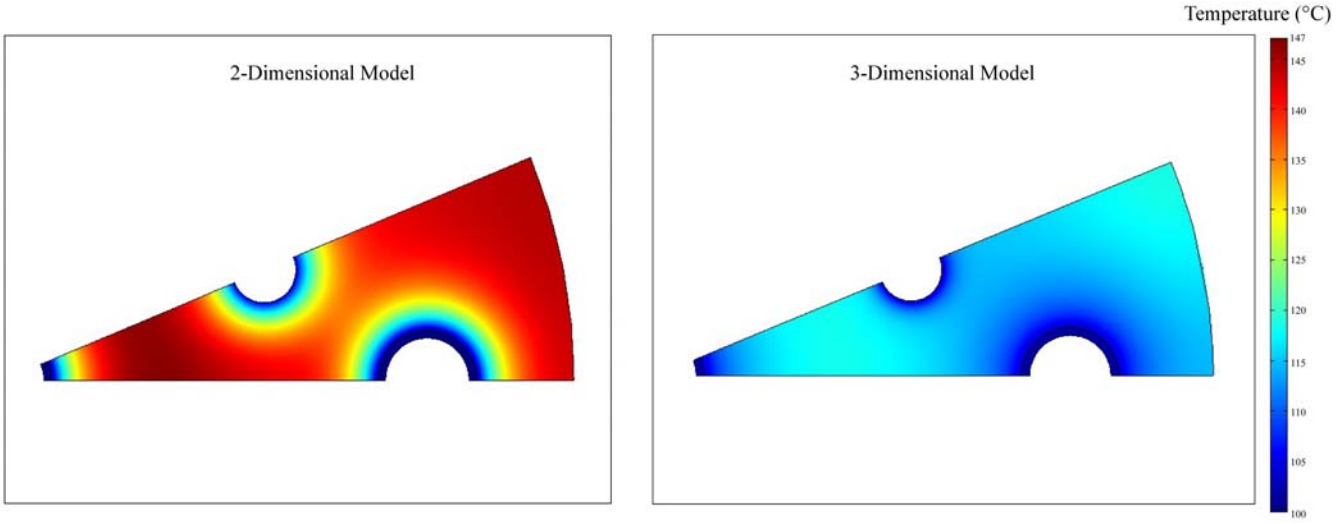

Figure 5.3-4 Comparison between 2-dimensional and 3-dimensional midplane temperature profiles at 120 seconds.

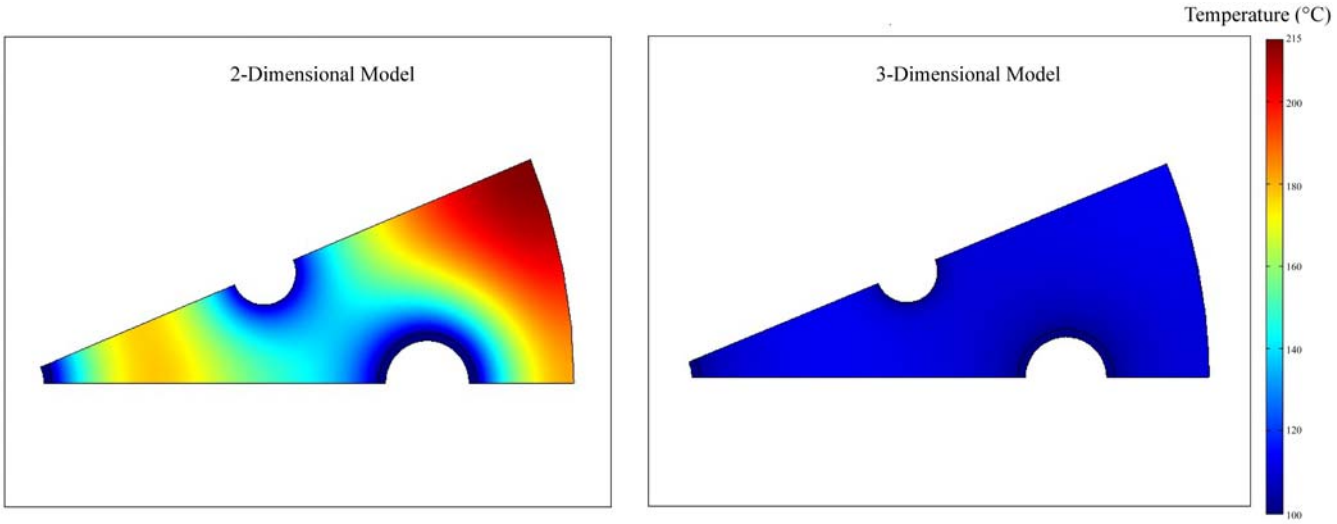

Figure 5.3-5 Comparison between 2-dimensional and 3-dimensional midplane temperature profiles at 720 seconds.

5.4 Bed Gas Flow

As the pressure in the hydrogen injection tube rises from its initial value of 1 bar to its final value of 50 bar, the resulting pressure gradient forces flow into the bed. For this system, the relation between the pressure gradient and the gas velocity is represented by the Blake-Kozeny equation. By this equation, the small effective diameter of the particles comprising the bed results in significant resistance to flow. As the local gas pressure in the bed increases, hydrogen is removed from the gas phase as the hydriding reactions take place, see Equation 4.4.5-1. Heating of the gas by the exothermic reactions, in turn, affects the gas pressure and the reaction rates. Expansion work performed as the gas flows in the direction of the pressure gradient also has an effect on the

gas temperature, see Equation 4.4.3-1. These complex, coupled phenomena are considered in the energy and mass balances.

Figures 5.4-1 and 5.4-2 show the magnitude and direction of the hydrogen velocity for the 2 and 3-dimensional finite element models at times of 10 and 40 seconds, respectively.

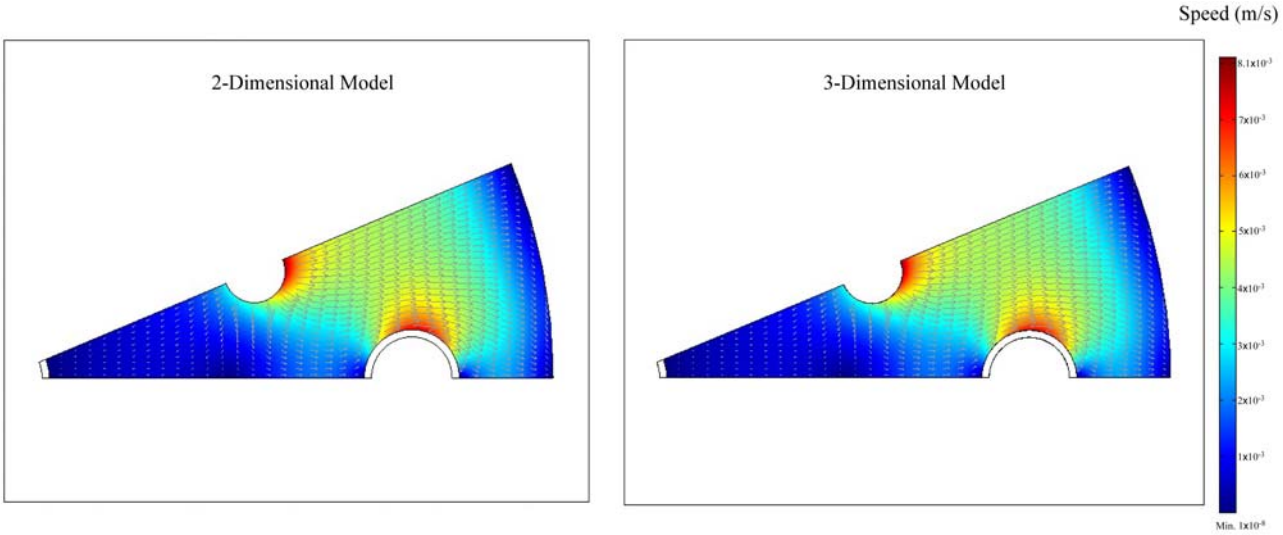

Figure 5.4-1 Hydrogen velocity profile at 10 seconds.

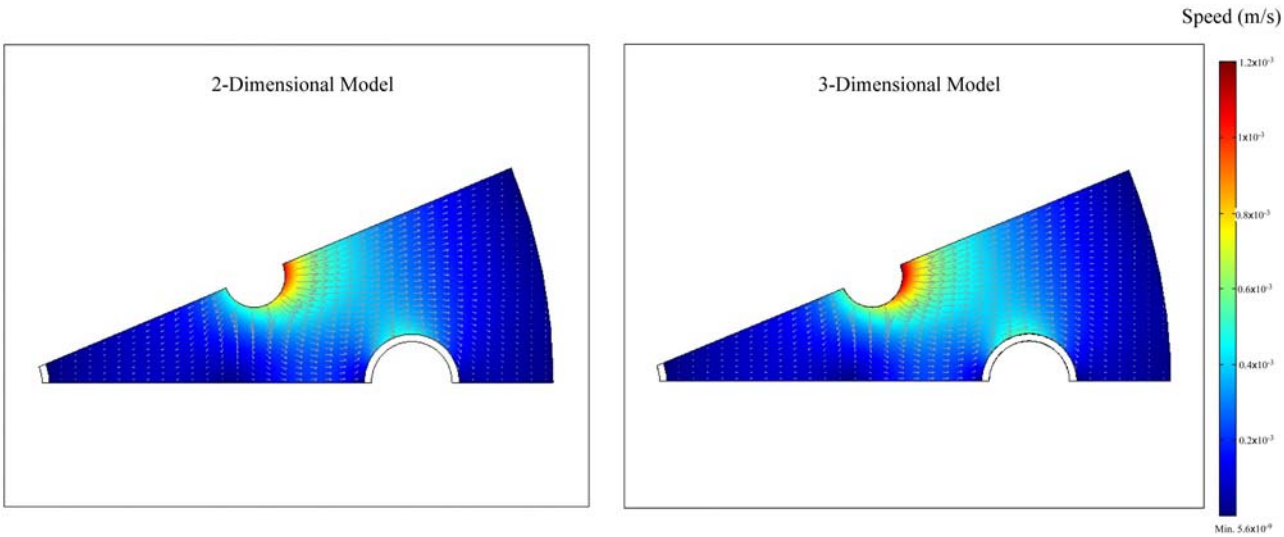

Figure 5.4-2 Hydrogen velocity profile at 40 seconds.

5.5 Hydride Concentration Profiles

Conversion of NaH to Na_3AlH_6 and then to $NaAlH_4$ occurrs as the bed is loaded with hydrogen. However, the hexa and tetra-hydrides first form in locations that have temperatures and pressures conducive to higher reaction rates. To use the bed efficiently, the concentration of tetra-hydride must be relatively uniform at the termination of the loading phase. Achieving full utilization of the bed requires design features that ensure proper heat transfer and flow within the bed.

Figures 5.5-1 through 5.5-4 compare the transient concentrations of Na_3AlH_6 and $NaAlH_4$ for the 2-dimensional model and at the midplane of the hydride for the 3-dimensional model.

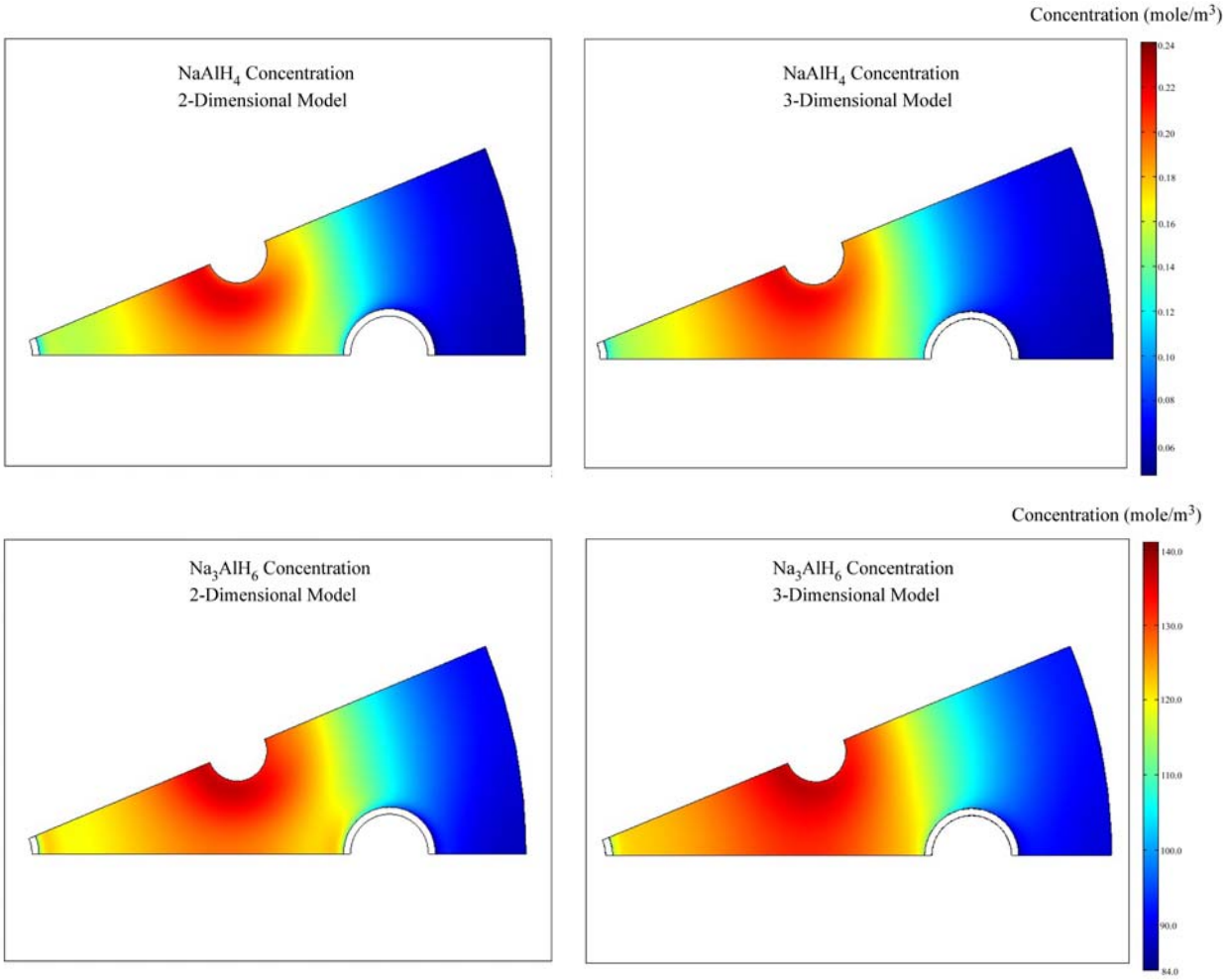

Figure 5.5-1 Comparison of 2-dimensional and 3-dimensional bed midplane hydride concentrations at 40 seconds.

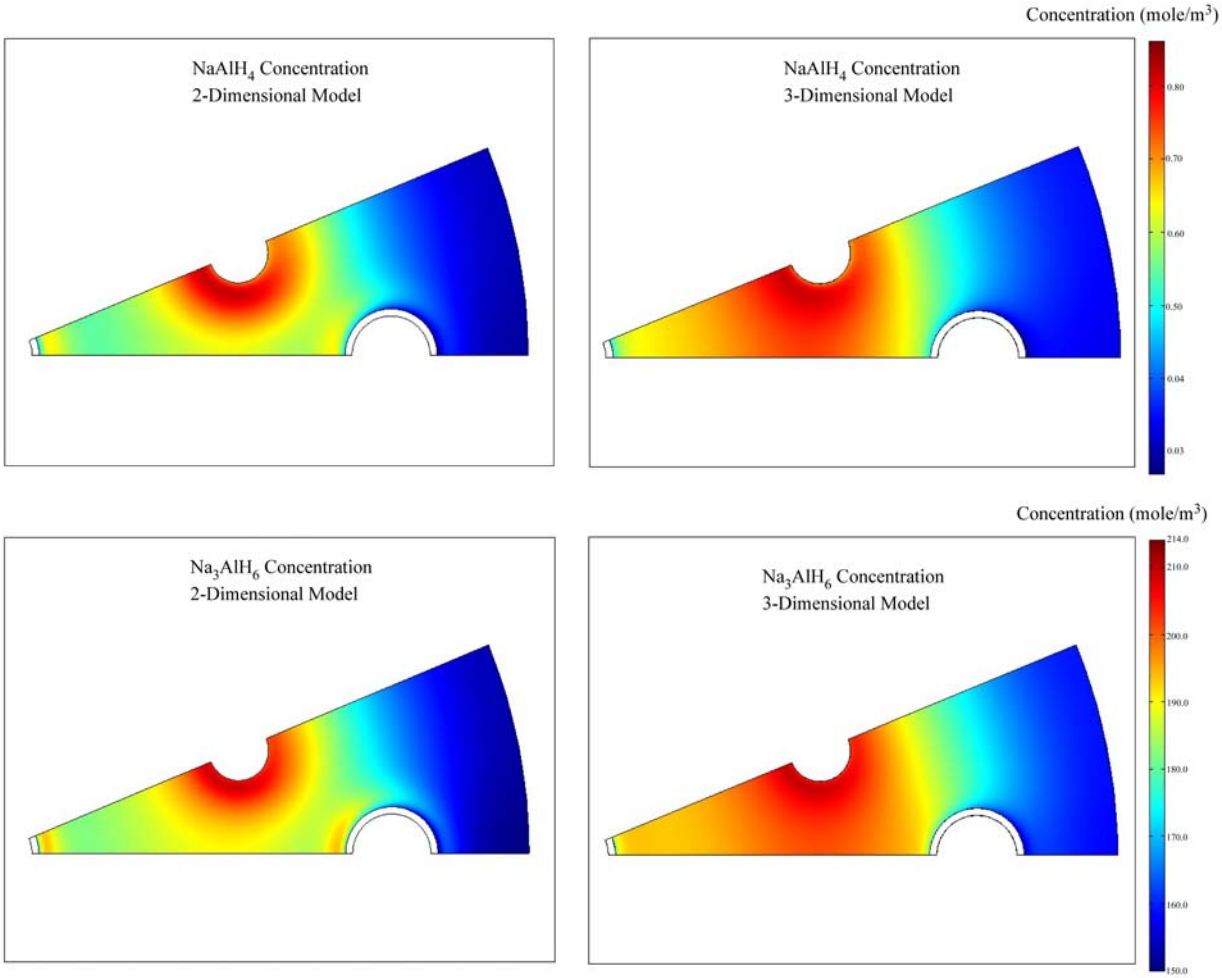

Figure 5.5-2 Comparison of 2-dimensional and 3-dimensional bed midplane hydride concentrations at 60 seconds.

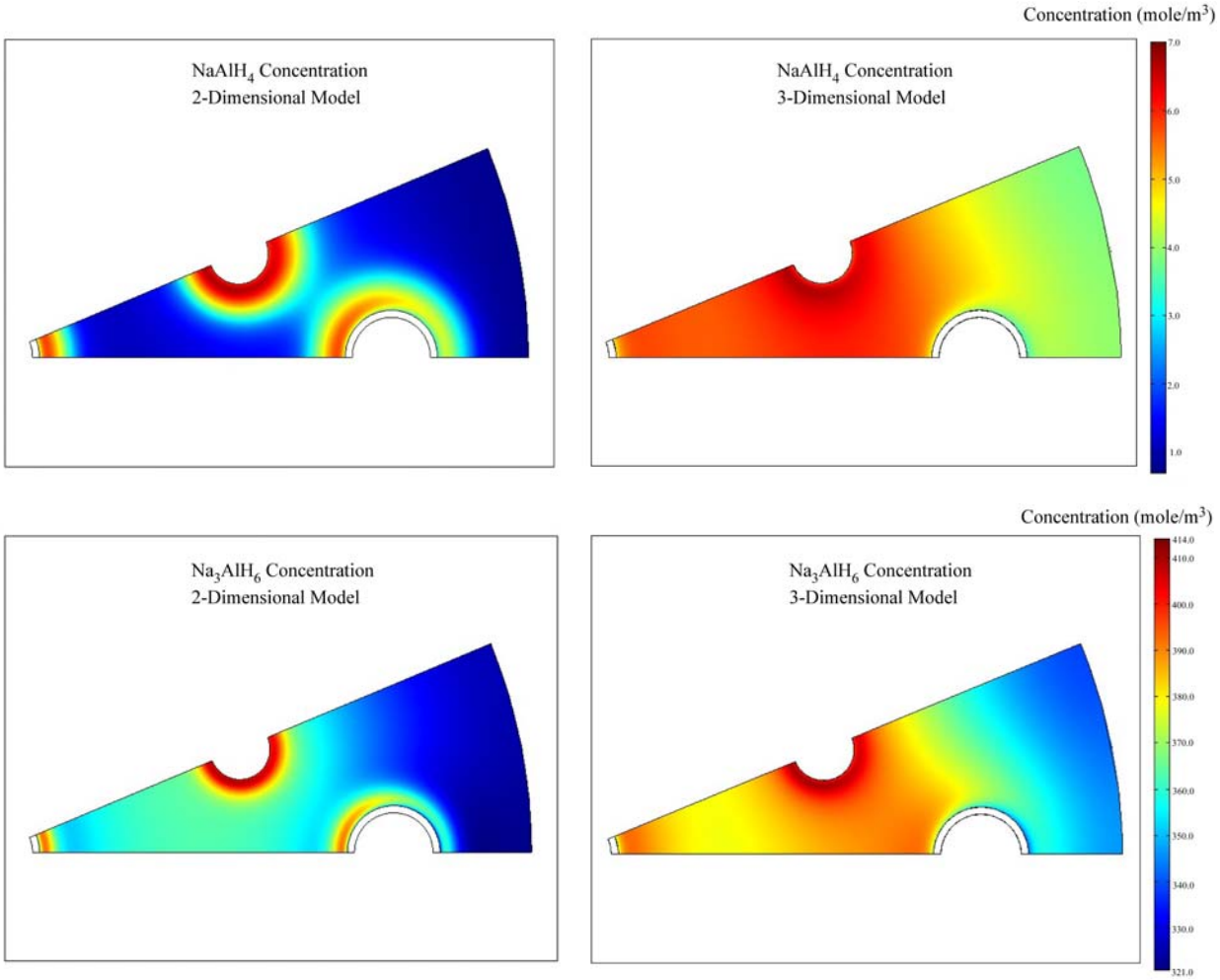

Figure 5.5-3 Comparison of 2-dimensional and 3-dimensional bed midplane hydride concentrations at 120 seconds.

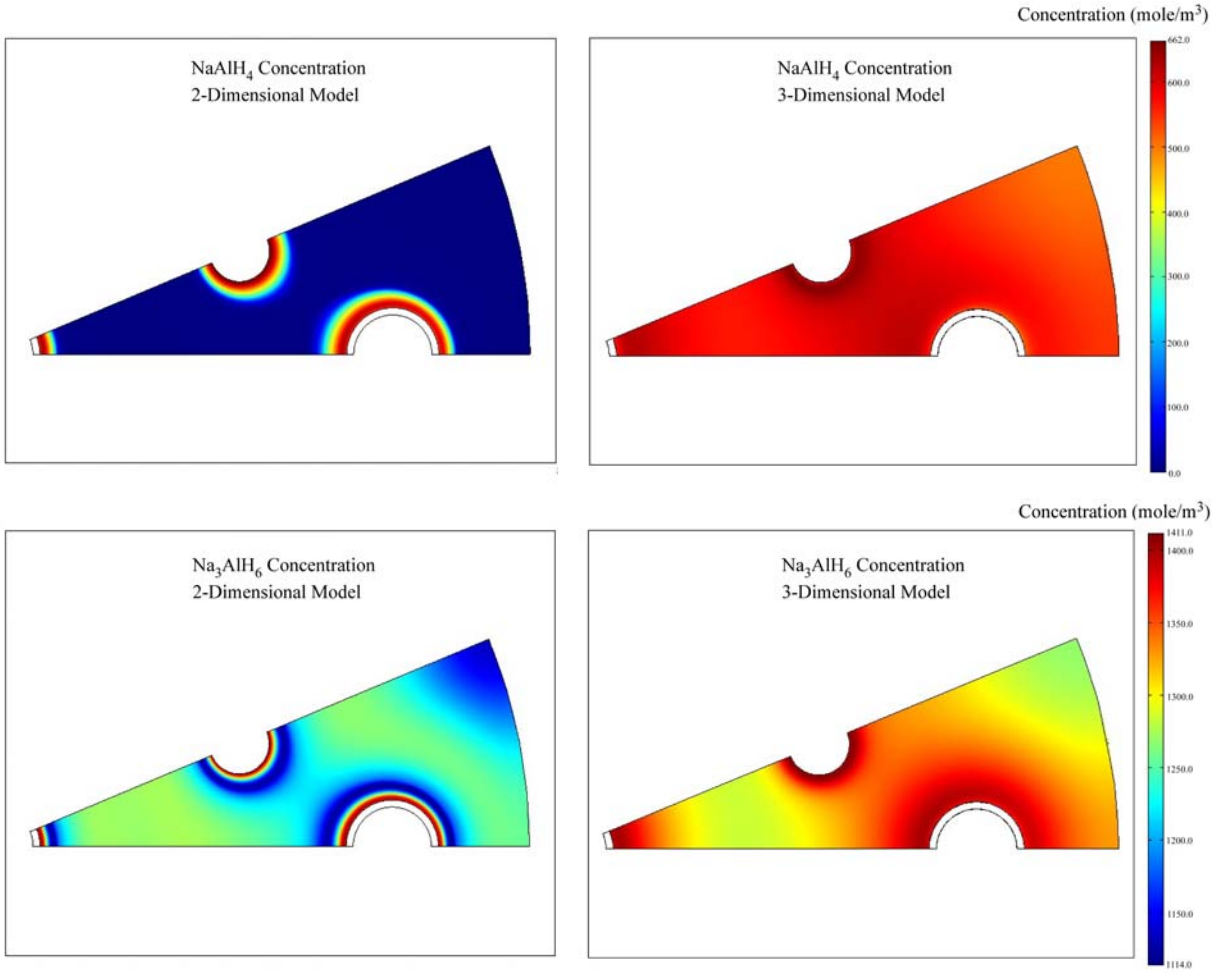

Figure 5.5-4 Comparison of 2-dimensional and 3-dimensional bed midplane hydride concentrations at 720 seconds.

6.0 CONCLUSIONS

The hydride bed model used in this document consists of four sub-models:

- A 0-dimensional Mathcad® based kinetics scoping model that evaluates loading and discharge kinetics, along with the maximum storage capacity, for a given hydride.
- A geometry scoping model, developed in a Microsoft Excel®, that determines system dimensions (length scales) required to store a given amount of hydrogen for a particular hydride and geometric configuration. The model also calculates placement of heat transfer elements, and the gravimetric and volumetric capacities for the system.
- A scoping model that estimates coolant flowrates, temperatures, pressure drops, etc., required to remove heat generated during hydrogen uptake. This model, developed in a Microsoft Excel® workbook, can also be used to identify suitable heat transfer fluids.
- Finite element models in 2 and 3-dimensions that couple mass, momentum and heat transfer, along with temperature dependent chemical kinetics. These models, developed using COMSOL Multiphysics®, are used to evaluate the detailed performance of the storage system.

The process of modeling a particular bed configuration and storage media is as follows:

1. The hydride kinetics are evaluated with the 0-dimensional Mathcad® kinetics scoping model. The model is used to determine the dependence of the reaction rates and hydrogen capacity on temperature and pressure. Pressures and temperatures that optimize loading and discharge rates are determined and possible errors in the kinetics model are identified. The bed gravimetric and volumetric capacities are calculated from the loading calculations and the bulk density of the storage material.
2. The hydrogen weight fraction from the kinetics scoping model, component densities, component dimensions and the required mass of hydrogen to be stored are input to the Excel® based geometry scoping model. The model calculates the size of the system, the location of heat transfer elements, as well as the gravimetric and volumetric capacities of the system.
3. System dimensions from the geometry scoping model, heat transfer fluid properties, thermal properties of the system components, heats of reaction, total amount of hydrogen to be stored and the time required to load the system are input to the heat removal scoping model. The model calculates the coolant flowrates, convection heat transfer coefficients and other parameters required to remove heat generated by the chemical reactions governing hydrogen uptake. The model is useful for determining if the operating parameters required for the cooling system are attainable and/or practical.
4. The storage vessel dimensions, geometry, heat transfer parameters and bed configuration are input to the 2 and/or 3-dimensional finite element COMSOL® based models. A number of other input parameters including material properties, flowrates, reaction kinetics, etc. are also required.
5. Detailed system behavior predicted by the finite element models is used to assess the ability of the system to meet technical requirements.
6. System design is refined by repeating steps 1 through 5 with modified parameters.

According to the UTRC™ kinetics correlations, the kinetics scoping model showed that at 50 bar, even at a near optimal temperature of 100°C, the weight fraction of hydrogen stored in $TiCl_3$ catalyzed $NaAlH_4$ over 3 minutes is 0.00238, more that 23 times lower than the theoretical value of 0.056. This implies a bed gravimetric capacity of 0.238% for the 2010 DOE technical target charging time of 3 minutes. The system gravimetric capacity would be lower. Based on these results, it is apparent that a more efficacious storage material must be found.

The detailed finite element models, however, indicated that the modified shell and tube heat exchanger, with fins normal to the axis, was very effective from the perspective of heat removal and temperature control. For identical states of the coolant and feed hydrogen, the modified shell and tube system permits far better control of the bed temperature than the system without fins. This was clearly demonstrated by comparing the temperatures predicted by the 3-dimensional and 2-dimensional models, which represented storage systems with and without fins, respectively, see Figures 5.3-2 through 5.3-5. Because the bed temperatures were maintained below 120°C, the hydrogen charging rate was significantly improved for the modified shell and tube system. The more uniform spatial temperatures in the modified storage system yielded smaller concentration gradients for the hexa and tetra-hydrides formed from NaH. This resulted in more efficient utilization of the bed. Figure 5.2-1 shows that the charging rate for the modified system is essentially the same as predicted by the 0-dimensional kinetics scoping model. This means that

charging in the modified system is limited by kinetics alone, which represents an upper bound to the charging rate at a given temperature and pressure.

7.0 FUTURE WORK

Recommended additions to the sodium alanate storage system model in this report are:

- Adjust bed dimensions to store 1000 kg of hydrogen during the allotted loading time.
- For the geometric configuration analyzed in this report, identify properties that the storage material must possess to meet the DOE technical targets listed in Attachment 3.
- Include pressure dependence in the thermal conductivity of hydrogen. Temperature dependence of the thermal conductivity is included in the current model.
- Apply the model to loading of partially discharged storage vessels.
- Investigate novel geometric configurations, other than shell and tube, for the storage system.

It is recommended that the systematic approach, employing the Mathcad® based kinetics model, the Microsoft Excel® based geometry model and the COMSOL Multiphysics® based finite element models be used in sensitivity studies to identify operating envelopes that hydrogen storage materials must meet to approach DOE technical targets. Since the system geometry, heat transfer characteristics, bed kinetics and heats of reaction are coupled, material operating envelopes will, of course, be related to the particular form of the bed.

8.0 REFERENCES

Aldas, K. and M. Mat. "Numerical Analysis of Hydrogen Storage in Metal- Hydride Beds." *Turk. J. Eng. Environ. Sci.*, **26**, 201-207, **2002**.

Aldas, K., M. Mat and Y.Kaplan. "A Three-Dimensional Model for Absorption of Hydrogen in a Metal Hydride Bed." *Int. J. Hydrogen Energy*, Vol. 27**, 10**, 1049-1056, **2002**.

Anton D. L. and D. A. Moser. "High Density Hydrogen Storage System Demonstration Using $NaAlH_4$ Complex Compound Hydride." Proceedings of the 2005 Hydrogen Program, 2005.

Askri, F. , A. Jemni and S. B. Nasrallah. "Prediction of Transient Heat and Mass Transfer in a Closed Metal-Hydrogen Reactor." *Intl. J. Hydrogen Energy*, Vol. 29, 195-208, **2004**.

Avallone, E. A., T. Baumeister III. "Mark's Standard Handbook for Mechanical Engineers." 9th Ed, *McGraw-Hill*, New York, NY, **1987**.

Bilgili, M. and Ö. E. Ataer. "Numerical Analysis of Hydrogen Absorption in a P/M Bed." *Powder Technology*, **160**, 141-148 **2005**.

Bird, R. B., W. E. Stewart, and E. N. Lightfoot. "Transport Phenomena." *John Wiley & Sons*, New York, **1960**.

COMSOL Multiphysics®, version 3.3.0.405. Copyright 1994-2006, COMSOL AB

El-Gammal, M. A., M. A El-Osairy, I. A. El-Osery, A. M. Metwally and M. A. Hassan. "A Study for he Major factors Affecting the Hydrogen Discharging in the Metal Hydrogen Storage Conduction Bed Model." *Modelling Measurement and Control*, Vol 46, **2**, 35-44, **1993**.

El-Osairy, M. A., I. A El-Osery, A. M. Metwally and M. M. Keshk. "Temperature and Composition Analysis of a Convective Model of Metal Hydride Hydrogen Storage Beds." *Int. J. Hydrogen Energy*, Vol 17, **2**, 125-128, **1992a**.

El-Osairy, M. A., I. A El-Osery, A. M. Metwally and M. M. Keshk. "On the Optimization of Convective Hydrogen Storage Bed Model Using $LaNi_5H_6$ or $FeTiH_{1.6}$." *Int. J. Hydrogen Energy*, Vol 17, **17**, 961-964, **1992b**.

El-Osairy, M. A., I. A El-Osery, A. M. Metwally and M. A. Hassan. "Temperature and Composition Distributions of $FeTiH_{1.6}$ and $MgNiH_4$ for Two-Dimensional Hydrogen Energy Conduction Bed Model." *J. Alloys and Compounds*, **202**, 125-128, **1993**.

El-Osairy, M. A., I. A El-Osery, A. M. Metwally and M. A. Hassan. "Temperature and Composition Distributions of $LaNi_5H_6$ metal Hydride for Different Geometries and Flow Regimes in Hydrogen Energy Conduction Bed Model." *Modelling Measurement and Control*, Vol 40, **1**, 53-63, **1994**.

El-Osery, I. A "A Comparative Study of "In-Out" and Out-In" Hydrogen Reaction Alternatives for Metal Hydride Beds Using RET1 Computer Code." *Int. Assoc. Hydrogen Energy*, Vol. 9, **5**, 421-444, **1984a**.

El-Osery, I. A "A Comparative Study of Different Designs for Metal Hydride Hydrogen Storage Beds Using TOBA Computer Code." *Hydrogen Energy Progress V*, *Proc. 5th World Hydrogen Conf., Toronto*, July 15-20 Vol. 3, Pergamon Press, Oxford, 1383-1392, **1984b**.

El-Osery, I. A "On Computer Calculations of Temperature-Composition Relations in Metal Hydride Hydrogen Storage Beds." *Surface and Coatings Tech.*, **28**, 397-404, **1986**.

El-Osery, I. A., M. A El-Osairy, A. M. Metwally, M. M. Keshk and M. A.El-Gammal,. "Dynamic Simulation of the Convective Model for Metal Hydride Hydrogen Storage Beds." *Energy Sources*, Vol 15, 523-530, **1993**.

Gadre, S.; A. Ebner, S. Al-Muhtaseb, J. Ritter. "Practical Modeling of Metal Hydride Hydrogen Storage Systems." *Ind. Eng. Chem. Res.*, Vol 42, 1713, **2003**.

Gopal, M. R. and S. S, Murthy. "Prediction of Heat and Mass transfer in Annular Cylindrical Metal Hydride Beds." *Int. J. Hydrogen Energy* Vol. 17, **10**, 795-805, **1992**.

Gopal, M. R. and S. S, Murthy. "Studies on Heat and Mass Transfer in Metal Hydride Beds." Int. J. Hydrogen Energy, Vol. 20, **11**, 911-917, **1995**.

Gross, K. J. "The Reversible Hydrides Solution for Hydrogen Storage." *Slide Presentation for G-CEP Hydrogen Workshop*, April 14 & 15, **2003**.

Gross, K. J., E. Majzoub, G. J. Thomas, and G. Sandrock "Hydride Development for Hydrogen Storage." *Proc. of the 2002 U.S. DOE Hydrogen Program Review*, NREL/CP-610-32405**,** April 14 & 15, **2002**.

Ha, M.Y.; I. K. Kim, H. D. Song; S. Sung; D. H. Lee. "A Numerical Study of Thermo-Fluid Phenomena in Metal Hydride Beds in the Hydriding Process." *Int. J. Heat and Mass Transfer*, Vol. 47, 2901, **2004**.

Hardy, B. J. "Geometry, Heat Removal and Kinetics Scoping Models for a Hydrogen Storage Systems." *Washington Savannah River Company Document*, WSRC-TR-20007-00439, Rev.1, **2007**.

Holman, J. P. "Heat Transfer." 4th Edition, *McGraw-Hill*, New York, NY, **1976**.

Jemni, A. and S.B.Nasrallah. "Study of Two-Dimensional Heat and Mass Transfer During Absorption in a Metal-Hydrogen Reactor." *Int. J. Hydrogen Energy*, Vol. 20, **1**, 43, **1995**.

Jemni, A.; Nasrallah, B.; Lamloumi, J. "Experimental and theoretical study of a metal-hydrogen reactor." *Int. J. Hydrogen Energy*, Vol. 24, 631, **1999**.

Kikkinides, E.S; M.C. Georgiadis and A.K. Stubos. "Dynamic Modeling and Optimization of Hydrogen Storage in Metal Hydride Beds." *Energy*, **31**, 2428, **2006**.

Lide, D. R., and H. V.Kehiaian. "CRC Handbook of Thermophysical and Thermochemical Data." CRC Press, Boca Raton, FL, **1994**.

Mat, M. and Y.Kaplan. "Numerical Study of Hydrogen Absorption in a $LaNi_5$ Hydride Reactor." I*nt. J. Hydrogen Energy*, Vol. 26, **9**, 957-963, **2001**.

Mathcad®, version 14.0.0.163. Copyright © 2007 Parametric Technology Corporation.

Mayer, U., M. Groll and W. Supper. "Heat and Mass Trasnfer in Metal Hydride Reaction Beds Experimental and Theoretical Results." *J. Less Common Met*., **131**, 235-244, **1987**.

Mazumdar, S.; M. R. Gopal and S. Bhattacharyya. "Thermodynamic Analysis and Optimization of Compressor-Driven metal Hydride Cooling Systems." *Int. J. Hydrogen Energy*, Vol. 30, 631, **2005**.

Microsoft® Excel **2002** (10.6834.6830) SP3. Microsoft Corporation.

Mosher, D, X. Tang, S. Arsenault, B. Laube, M. Cao, R. Brown and S. Saitta. "High Density Hydrogen Storage System Demonstration Using NaAlH4 Complex Compound Hydrides." *DOE Hydrogen Program Annual Peer Review*, Arlington, VA, **2007**.

Nasrallah, S.B. and A. Jemni. "Study of Two-Dimensional Heat and Mass Transfer During Desorption in a Metal-Hydrogen Reactor." *Int. J. Hydrogen Energy,* Vol. 22, **1**, 67, **1997**.

APPENDIX

A.1 GOVERNING EQUATIONS

The governing equations used in the hydride bed model are derived in this appendix. For clarity, expressions input to COMSOL® are enclosed in boxes.

A.1.1 Mass Balance

The mass transfer equation for the bed is derived from the integral mass balance as

$$\frac{\partial C}{\partial t} + \nabla \cdot \left(C\vec{v}\right) = \frac{S_{H_2}}{\varepsilon} \qquad \text{A.1.1-1}$$

where: S_{H_2} = Rate of H_2 generation per volume of bed [mole H_2/(m^3 - s)]

ε = Void fraction (porosity) of particle bed

$\vec{v}$ = Mean interstitial H_2 velocity [m/s]

C_{nd} = The non-dimensionalized concentration of H_2 = $\frac{C}{C_{ref}}$

C = Concentration of H_2 in the void space of the bed [mole/m^3].

C_{ref} = The reference H_2 concentration in the void space, C_{ref} [mole/m^3]

∇ = Gradient [1/m].

For a sodium alanate bed the H_2 uptake reaction consists of two steps following the chemical balance equation

$$\underbrace{NaAlH_4}_{\text{Species 1}} \underbrace{\leftrightarrow}_{\text{Reaction 1}} \underbrace{\frac{1}{3}Na_3AlH_6}_{\text{Species 2}} + \frac{2}{3}Al + H_2 \underbrace{\leftrightarrow}_{\text{Reaction 2}} \underbrace{NaH}_{\text{Species 3}} + Al + \frac{3}{2}H_2 \qquad \text{A.1.1-2}$$

For this case S_{H_2} takes the form

$$S_{H_2} = \left.\frac{\nu_{H_2}}{\nu_{NaH}}\right|_{Rxn2} \frac{\partial C_{NaH}}{\partial t} - \left.\frac{\nu_{H_2}}{\nu_{NaAlH_4}}\right|_{Rxn1} \frac{\partial C_{NaAlH_4}}{\partial t} \qquad \text{A.1.1-3}$$

where: $\left.\frac{\nu_{H_2}}{\nu_{NaH}}\right|_{Rxn2}$ = Ratio of the stoichiometric coefficient of H_2 to NaH in reaction 2 = 0.5

$\left.\frac{\nu_{H_2}}{\nu_{NaAlH_4}}\right|_{Rxn1}$ = Ratio of the stoichiometric coefficient of H_2 to $NaAlH_4$ in reaction 1 = 1

C_{NaH} = The bulk concentration of NaH [mole/m^3]

C_{NaAlH_4} = The bulk concentration of $NaAlH_4$ [mole/m^3].

Divide Eq. A.1.1-1 by the reference H_2 concentration, C_{ref} [mole/m^3]

$$\boxed{\frac{\partial C_{nd}}{\partial t} + \nabla \cdot \left(C_{nd} \vec{v} \right) = \frac{1}{C_{ref}} \left(\frac{S_{H_2}}{\varepsilon} \right)} \qquad \text{A.1.1-4}$$

where: C_{nd} = The non-dimensionalized concentration of $H_2 = \frac{C}{C_{ref}}$.

A.1.2 Momentum Balance

The momentum balance, which gives the components of the mean interstitial velocity, is simply the Blake-Kozeny equation, see Bird, Stewart and Lightfoot [1960]. Hence,

$$\begin{aligned} u &= -\frac{D_p^{\,2}}{150\mu} \left(\frac{\varepsilon}{1-\varepsilon} \right)^2 \frac{\partial P}{\partial x} \\ v &= -\frac{D_p^{\,2}}{150\mu} \left(\frac{\varepsilon}{1-\varepsilon} \right)^2 \frac{\partial P}{\partial y} \\ w &= -\frac{D_p^{\,2}}{150\mu} \left(\frac{\varepsilon}{1-\varepsilon} \right)^2 \frac{\partial P}{\partial z} \end{aligned} \qquad \text{A.1.2-1}$$

Divide by U_{ref} to non-dimensionalize the components of velocity in Eqs. A.1.2-1

$$\begin{aligned} u_{nd} &= -\frac{D_p^{\,2}}{150\mu} \left(\frac{\varepsilon}{1-\varepsilon} \right)^2 \frac{P_{ref}}{U_{ref}} \frac{\partial P_{nd}}{\partial x} \\ v_{nd} &= -\frac{D_p^{\,2}}{150\mu} \left(\frac{\varepsilon}{1-\varepsilon} \right)^2 \frac{P_{ref}}{U_{ref}} \frac{\partial P_{nd}}{\partial y} \\ w_{nd} &= -\frac{D_p^{\,2}}{150\mu} \left(\frac{\varepsilon}{1-\varepsilon} \right)^2 \frac{P_{ref}}{U_{ref}} \frac{\partial P_{nd}}{\partial z} \end{aligned} \qquad \text{A.1.2-2}$$

where: U_{ref} = Reference velocity [m/s]

$u_{nd} = \frac{u}{U_{ref}}$ = Non-dimensional x-component of velocity

$v_{nd} = \frac{v}{U_{ref}}$ = Non-dimensional y-component of velocity

$w_{nd} = \frac{w}{U_{ref}}$ = Non-dimensional z-component of velocity

P_{ref} = Reference pressure [Pa]

$P_{nd} = \frac{P}{P_{ref}}$ = Non-dimensional pressure

A.1.3 Energy Balance

In integral form, the energy balance for the bed is

$$\frac{\partial}{\partial t}\int_V \left[\varepsilon(\rho\iota)_{H_2} + (\rho\iota)_R + (\rho\iota)_P + (\rho\iota)_I\right]dV + \frac{\partial}{\partial t}\int_V \left[\varepsilon\rho_{H_2}\frac{\left(\vec{v}\cdot\vec{v}\right)}{2}\right]dV$$
$$= -\int_S \left[\varepsilon(\rho\iota)_{H_2}\vec{v}\cdot\hat{n}\right]dS - \int_S \left[\varepsilon\rho_{H_2}\frac{\left(\vec{v}\cdot\vec{v}\right)}{2}\vec{v}\cdot\hat{n}\right]dS + \int_S \left[\varepsilon\hat{n}\cdot\underline{\underline{\tau}}\cdot\vec{v}\right]dS + \int_V \varepsilon\left(\rho_{H_2}\vec{g}\cdot\vec{v}\right)dV \qquad \text{A.1.3-1}$$
$$-\int_S \left[\vec{q}''\cdot\hat{n}\right]dS - \int_S \left[\varepsilon P\vec{v}\cdot\hat{n}\right]dS$$

where:
- ι = Specific internal energy [J/kg]
- ρ = Mass density [kg/m^3]
- $(\ )_{H_2}$ = For H_2 gas
- $(\ )_R$ = For solid phase reactants
- $(\ )_P$ = For solid phase products
- $(\ )_I$ = For inert (non-reacting) material, such as metal foam
- $\hat{n}$ = Outward normal to surface
- S = Surface area [m^2]
- V = Volume [m^3]
- $\underline{\underline{\tau}}$ = Stress tensor, having components τ_{ij} [N/m^2]
- $\vec{g}$ = Gravitational acceleration vector [m/s^2]
- $\vec{q}''$ = Heat flux vector [W/m^2]
- P = Pressure [Pa]

In differential form, with constant ε, Eq. A.1.3-1 becomes

$$\varepsilon\frac{\partial(\rho\iota)_{H_2}}{\partial t} + \frac{\varepsilon}{2}\frac{\partial\left(\overrightarrow{\rho v}\cdot\vec{v}\right)_{H_2}}{\partial t} + \frac{\partial(\rho\iota)_R}{\partial t} + \frac{\partial(\rho\iota)_P}{\partial t} + \frac{\partial(\rho\iota)_I}{\partial t} \qquad \text{A.1.3-2}$$
$$= -\varepsilon\nabla\cdot\left[(\rho\iota)_{H_2}\vec{v}\right] - \frac{\varepsilon}{2}\nabla\cdot\left[\rho_{H_2}\left(\vec{v}\cdot\vec{v}\right)\vec{v}\right] + \varepsilon\nabla\cdot\left(\underline{\underline{\tau}}\cdot\vec{v}\right) + \varepsilon\rho_{H_2}\vec{g}\cdot\vec{v} - \nabla\cdot\vec{q}'' - \varepsilon\nabla\cdot\left(P\vec{v}\right)$$

The equation for H_2 continuity is

$$\varepsilon\frac{\partial\rho_{H_2}}{\partial t} = -\varepsilon\nabla\cdot\left(\rho_{H_2}\vec{v}\right) + S_{H_2} \qquad \text{A.1.3-3}$$

Substitute Eq. A.1.3-3 into Eq. A.1.3-2 and rearrange terms

By definition

$$h = \iota + \frac{P}{\rho} \qquad \text{A.1.3-4}$$

where: S_{H_2} = Source of H_2 from all chemical reactions,

$S_{H_2} > 0$ if H_2 is produced

$S_{H_2} < 0$ if H_2 is removed

h = Specific enthalpy [J/kg]

Substitute Eqs. A.1.3-3 and A.1.3-4 into Eq. A.1.3-2 to get

$$\begin{aligned}
&\varepsilon\frac{\partial(\rho h)_{H_2}}{\partial t}+\frac{\varepsilon}{2}\frac{\partial\left(\rho\vec{v}\cdot\vec{v}\right)_{H_2}}{\partial t}+\frac{\partial(\rho h)_R}{\partial t}+\frac{\partial(\rho h)_P}{\partial t}+\frac{\partial(\rho h)_I}{\partial t}-\frac{\partial P}{\partial t}\\
&=-\varepsilon\nabla\cdot\left[(\rho h)_{H_2}\vec{v}\right]-\frac{\varepsilon}{2}\nabla\cdot\left[\rho\left(\vec{v}\cdot\vec{v}\right)\vec{v}\right]+\varepsilon\nabla\cdot\left(\underline{\underline{\tau}}\cdot\vec{v}\right)+\varepsilon\rho_{H_2}\vec{g}\cdot\vec{v}-\nabla\cdot\vec{q}''\\
&=-\varepsilon h_{H_2}\nabla\cdot\left(\rho_{H_2}\vec{v}\right)-\varepsilon\left(\rho_{H_2}\vec{v}\right)\cdot\nabla h_{H_2}-\frac{\varepsilon}{2}\left(\vec{v}\cdot\vec{v}\right)\nabla\cdot\left[\rho_{H_2}\vec{v}\right]-\frac{\varepsilon}{2}\left(\rho_{H_2}\vec{v}\right)\cdot\nabla\left[\vec{v}\cdot\vec{v}\right]\\
&\quad+\varepsilon\nabla\cdot\left(\underline{\underline{\tau}}\cdot\vec{v}\right)+\varepsilon\rho_{H_2}\vec{g}\cdot\vec{v}-\nabla\cdot\vec{q}''\\
&=\varepsilon\left[h_{H_2}+\frac{\left(\vec{v}\cdot\vec{v}\right)}{2}\right]\frac{\partial\rho_{H_2}}{\partial t}-\varepsilon\left(\rho_{H_2}\vec{v}\right)\cdot\nabla h_{H_2}-\frac{\varepsilon}{2}\left(\rho_{H_2}\vec{v}\right)\cdot\nabla\left[\vec{v}\cdot\vec{v}\right]+\varepsilon\nabla\cdot\left(\underline{\underline{\tau}}\cdot\vec{v}\right)\\
&\quad+\varepsilon\rho_{H_2}\vec{g}\cdot\vec{v}-\nabla\cdot\vec{q}''-S_{H_2}\left(h_{H_2}+\frac{\left(\vec{v}\cdot\vec{v}\right)}{2}\right)
\end{aligned}\qquad \text{A.1.3-5}$$

Expand the right hand side of Eq. A.1.3-5, neglect inert, $(\ )_I$, components and rearrange terms

$$\begin{aligned}
&\varepsilon\rho_{H_2}\left(\frac{\partial h_{H_2}}{\partial t}+\frac{1}{2}\frac{\partial\left(\vec{v}\cdot\vec{v}\right)}{\partial t}\right)+\rho_R\frac{\partial h_R}{\partial t}+h_R\frac{\partial\rho_R}{\partial t}+\rho_P\frac{\partial h_P}{\partial t}+h_P\frac{\partial\rho_P}{\partial t}+S_{H_2}\left(h_{H_2}+\frac{\left(\vec{v}\cdot\vec{v}\right)}{2}\right)-\frac{\partial P}{\partial t}\\
&=-\varepsilon\left(\rho_{H_2}\vec{v}\right)\cdot\nabla h_{H_2}-\frac{\varepsilon}{2}\left(\rho_{H_2}\vec{v}\right)\cdot\nabla\left[\vec{v}\cdot\vec{v}\right]+\varepsilon\nabla\cdot\left(\underline{\underline{\tau}}\cdot\vec{v}\right)+\varepsilon\rho_{H_2}\vec{g}\cdot\vec{v}-\nabla\cdot\vec{q}''
\end{aligned}\qquad \text{A.1.3-6}$$

Now the reaction mass balance
[Rate of change in mass of reactants] = [Rate of change in mass of products]

is

$$\frac{\partial\rho_R}{\partial t}=-\left[\frac{\partial\rho_P}{\partial t}+S_{H_2}\right] \qquad \text{A.1.3-7}$$

So that

$$h_R\frac{\partial\rho_R}{\partial t}+h_P\frac{\partial\rho_P}{\partial t}+S_{H_2}h_{H_2}=\sum_i\left[\frac{1}{M_i}\frac{\partial\rho_i}{\partial t}\Delta H_i\right] \qquad \text{A.1.3-8}$$

where: M_i = Molecular weight of species i per mole [kg/g-mole]

ρ_i = Mass density of species i [kg/m^3]

ΔH_i = Enthalpy of reaction on a molar basis of species i [J/(mol of i)]

Substitute Eq. A.1.3-8 into Eq. A.1.3-6 to obtain the total energy balance as

$$\varepsilon\rho_{H_2}\left(\frac{Dh_{H_2}}{Dt}+\frac{1}{2}\frac{D\left(\vec{v}\cdot\vec{v}\right)}{Dt}\right)+S_{H_2}\frac{\left(\vec{v}\cdot\vec{v}\right)}{2}+\rho_R\frac{\partial h_R}{\partial t}++\rho_P\frac{\partial h_P}{\partial t}+\sum_i\left[\frac{1}{M_i}\frac{\partial\rho_i}{\partial t}\Delta H_i\right]-\frac{\partial P}{\partial t}$$
$$=\varepsilon\nabla\cdot\left(\underline{\underline{\tau}}\cdot\vec{v}\right)+\varepsilon\rho_{H_2}\vec{g}\cdot\vec{v}-\nabla\cdot\vec{q}'' \qquad \text{A.1.3-9}$$

Where $\frac{D(\ )}{Dt}$ is the substantial or material derivative, having the operator form $\frac{\partial(\ )}{\partial t}+\vec{v}\cdot\nabla(\ )$.

The momentum balance for the packed bed is

$$\varepsilon\frac{\partial\left(\rho_{H_2}\vec{v}\right)}{\partial t}=-\varepsilon\nabla P-\varepsilon\nabla\cdot\left[\vec{v}\left(\rho_{H_2}\vec{v}\right)\right]+\varepsilon\nabla\cdot\underline{\underline{\tau}}+\varepsilon\rho\vec{g}$$
$$=-\varepsilon\nabla P-\varepsilon\vec{v}\nabla\cdot\left(\rho_{H_2}\vec{v}\right)-\varepsilon\left(\rho_{H_2}\vec{v}\right)\cdot\nabla\vec{v}+\varepsilon\nabla\cdot\underline{\underline{\tau}}+\varepsilon\rho\vec{g} \qquad \text{A.1.3-10}$$

Apply the continuity equation, Eq. A.1.3-3, to Eq. A.1.3-10, and the momentum balance is

$$\varepsilon\rho_{H_2}\frac{D\vec{v}}{Dt}+\vec{v}S_{H_2}=-\varepsilon\nabla P+\varepsilon\nabla\cdot\underline{\underline{\tau}}+\varepsilon\rho\vec{g} \qquad \text{A.1.3-11}$$

Apply $\vec{v}\cdot\|$ to Eq. A.1.3-11 to obtain the mechanical energy balance as

$$\frac{\varepsilon\rho_{H_2}}{2}\frac{D\left(\vec{v}\cdot\vec{v}\right)}{Dt}+\left(\vec{v}\cdot\vec{v}\right)S_{H_2}=-\varepsilon\vec{v}\cdot\nabla P+\varepsilon\vec{v}\cdot\left(\nabla\cdot\underline{\underline{\tau}}\right)+\varepsilon\rho\vec{g}\cdot\vec{v} \qquad \text{A.1.3-12}$$

Where

$$\vec{v}\cdot\left(\nabla\cdot\underline{\underline{\tau}}\right)=v_j\frac{\partial\tau_{ij}}{\partial x_i}\quad\text{(summation convention)} \qquad \text{A.1.3-13}$$

Subtract the mechanical energy balance, Eq. A.1.3-12, from the energy balance, Eq. A.1.3-9, using Eq. A.1.3-13, to get the thermal energy balance

$$\varepsilon\rho_{H_2}\frac{Dh_{H_2}}{Dt}+\rho_R\frac{\partial h_R}{\partial t}+\rho_P\frac{\partial h_P}{\partial t}+\sum_i\left[\frac{1}{M_i}\frac{\partial\rho_i}{\partial t}\Delta H_i\right]-\frac{DP}{Dt}-\frac{\left(\vec{v}\cdot\vec{v}\right)}{2}S_{H_2}$$
$$=\varepsilon\underline{\underline{\tau}}:\nabla\vec{v}-\nabla\cdot\vec{q}''-(1-\varepsilon)\vec{v}\cdot\nabla P \qquad \text{A.1.3-14}$$

From

$$dh=\left.\frac{\partial h}{\partial T}\right|_P dT+\left.\frac{\partial h}{\partial P}\right|_T dP$$

The substantial derivative is

$$\frac{Dh}{Dt}=\left.\frac{\partial h}{\partial T}\right|_P\frac{DT}{Dt}+\left.\frac{\partial h}{\partial P}\right|_T\frac{DP}{Dt} \qquad \text{A.1.3-15}$$

For H_2 as an ideal gas $h_{H_2}=h_{H_2}(T)$

$$\frac{Dh_{H_2}}{Dt} = \left.\frac{\partial h_{H_2}}{\partial T}\right|_P \frac{DT}{Dt} = Cp_{H_2}\frac{DT}{Dt} \qquad \text{A.1.3-16}$$

For solids assume that $h_{H_2} \approx h_{H_2}(T)$, so that

$$\frac{Dh}{Dt} = \left.\frac{\partial h}{\partial T}\right|_P \frac{DT}{Dt} = Cp\frac{DT}{Dt} = Cp\left(\frac{\partial T}{\partial t} + \vec{v}_{solid}\cdot\nabla T\right) = Cp\frac{\partial T}{\partial t} = \frac{\partial h}{\partial t} \qquad \text{A.1.3-17}$$

Substitute Eqs. A.1.3-16 and A.1.3-17 into Eq. A.1.3-14 and neglect stress work, work done by gravitational forces and the contribution of kinetic energy terms. The thermal energy balance is then

$$\begin{aligned}\left(\varepsilon\rho_{H_2}Cp_{H_2} + \rho_R Cp_R + \rho_P Cp_P\right)\frac{\partial T}{\partial t} &= \frac{\partial P}{\partial t} + \varepsilon\vec{v}\cdot\nabla P + \nabla\cdot k\nabla T \\ &\quad - \sum_i\left[\frac{1}{M_i}\frac{\partial\rho_i}{\partial t}\Delta H_i\right] - \varepsilon\rho_{H_2}Cp_{H_2}\vec{v}\cdot\nabla T\end{aligned} \qquad \text{A.1.3-18}$$

where: k = Bed thermal conductivity.

Non-dimensionalize Eq. A.1.3-18 by dividing by the product o the reference temperature and the reference speed, T_{ref}. Also, rearrange terms to put the equation into the form used by COMSOL®.

$$\begin{aligned}\rho_{bed}Cp_{bed}\frac{\partial T_{nd}}{\partial t} - \nabla\cdot k\nabla T_{nd} &= -\varepsilon\rho_{H_2}Cp_{H_2}\left(\frac{\partial T_{nd}}{\partial t} + \vec{v}\cdot\nabla T_{nd}\right) + \frac{1}{T_{ref}}\left(\frac{\partial P}{\partial t} + \varepsilon\vec{v}\cdot\nabla P\right) \\ &\quad - \frac{1}{T_{ref}}\left(\sum_i\left[\frac{1}{M_i}\frac{\partial\rho_i}{\partial t}\Delta H_i\right]\right)\end{aligned} \qquad \text{A.1.3-19}$$

where: $\rho_{bed}Cp_{bed} = \rho_R Cp_R + \rho_P Cp_P$

T_{ref} = Reference temperature [K]

$T_{nd} = \dfrac{T}{T_{ref}}$ = Non-dimensional temperature

Rewrite the heat of reaction term as

$$Source = -\left(\sum_i\left[\frac{1}{M_i}\frac{\partial\rho_i}{\partial t}\Delta H_i\right]\right) \qquad \text{A.1.3-20}$$

Substitute Eq. A.1.3-20 into Eq. A.1.3-19

$$\begin{aligned}\rho_{bed}Cp_{bed}\frac{\partial T_{nd}}{\partial t} - \nabla\cdot k\nabla T_{nd} &= -\varepsilon\rho_{H_2}Cp_{H_2}\left(\frac{\partial T_{nd}}{\partial t} + \vec{v}\cdot\nabla T_{nd}\right) + \frac{1}{T_{ref}}\left(\frac{\partial P}{\partial t} + \varepsilon\vec{v}\cdot\nabla P\right) \\ &\quad + \frac{1}{T_{ref}}Source\end{aligned} \qquad \text{A.1.3-21}$$

A.1.4 Reaction Kinetics

A.1.4.1 United Technologies Sodium Alanate Model

The United Technologies Research Center™ (UTRC) developed an empirical kinetics model for $TiCl_3$ catalyzed $NaAlH_4$. For this material, the chemical reaction is

$$\underbrace{NaAlH_4}_{\text{Species 1}} \underbrace{\leftrightarrow}_{\text{Reaction 1}} \underbrace{\frac{1}{3}Na_3AlH_6}_{\text{Species 2}} + \frac{2}{3}Al + H_2 \underbrace{\leftrightarrow}_{\text{Reaction 2}} \underbrace{NaH}_{\text{Species 3}} + Al + \frac{3}{2}H_2 \qquad \text{A.1.4.1-1}$$

Define the expressions:

$$\begin{aligned}
r_{1F} &\equiv C_{eqv} A_{1F} \exp\left[-\frac{E_{1F}}{RT}\right]\left[\frac{P(C,T) - P_{eq1}(T)}{P_{eq1}(T)}\right] \\
r_{1B} &\equiv -C_{eqv} A_{1B} \exp\left[-\frac{E_{1B}}{RT}\right]\left[\frac{P_{eq1}(T) - P(C,T)}{P_{eq1}(T)}\right] \\
r_{2F} &\equiv -C_{eqv} A_{2F} \exp\left[-\frac{E_{2F}}{RT}\right]\left[\frac{P(C,T) - P_{eq2}(T)}{P_{eq2}(T)}\right] \\
r_{2B} &\equiv C_{eqv} A_{2B} \exp\left[-\frac{E_{2B}}{RT}\right]\left[\frac{P_{eq2}(T) - P(C,T)}{P_{eq2}(T)}\right]
\end{aligned} \qquad \text{A.1.4.1-2a-d}$$

where: C = Concentration of H_2 [moles/m^3]

C_{eqv} = Equivalent concentration of $NaAlH_4$ [moles/m^3] based on the initial concentrations of all metal species

$= C_{10} + 3C_{20} + C_{30}$

C_{10} = Initial concentration of $NaAlH_4$ [moles/m^3]

C_{20} = Initial concentration of Na_3AlH_6 [moles/m^3]

C_{30} = Initial concentration of NaH [moles/m^3]

$P_{eq1}(T)$ and $P_{eq2}(T)$ are the H_2 pressures, in Pa, in equilibrium with the $NaAlH_4$ and the Na_3AlH_6 metal hydrides, respectively, at temperature T, in [K]. These relations are given by the van't Hoff equations:

$$\begin{aligned}
P_{eq1}(T) &= 10^5 \exp\left[\frac{\Delta H_1}{RT} - \frac{\Delta S_1}{R}\right] \\
P_{eq2}(T) &= 10^5 \exp\left[\frac{\Delta H_2}{RT} - \frac{\Delta S_2}{R}\right]
\end{aligned} \qquad \text{A.1.4.1-3a-b}$$

Values for the constants used in Eqs. A.1.4.1-2a-d, and A.1.4.1-3a-b are listed in Table A.1.4.1-1

Table A.1.4.1-1
Constants for the Rate and Equilibrium Expressions

Constant	Value
A_{1F}	10^8
A_{1B}	4×10^5
A_{2F}	1.5×10^5
A_{2B}	6×10^{12}
E_{1F}	80.0 kJ/mol
E_{1B}	110.0 kJ/mol
E_{2F}	70.0 kJ/mol
E_{2B}	110.0 kJ/mol
χ_{1F}	2.0
χ_{1B}	2.0
χ_{2F}	1.0
χ_{2B}	1.0
$\frac{\Delta H_1}{R}$	-4475
$\frac{\Delta S_1}{R}$	-14.83
$\frac{\Delta H_2}{R}$	-6150
$\frac{\Delta S_2}{R}$	-16.22

The reference for this model, contained in Attachment A.2, proposes the kinetics equations

$$\frac{dC_1}{dt}=\begin{cases} r_{1F}\left[\frac{3C_2(t)}{C_{eqv}}-C_{2sat}(T)\right]^{\chi_{1F}} & \text{if} \quad P\ge P_{eq1}(T) \\ r_{1B}\left[\frac{C_1(t)}{C_{eqv}}\right]^{\chi_{1B}} & \text{if} \quad P<P_{eq1}(T) \text{ and } C_1(t)\ge 0 \end{cases} \qquad \text{A.1.4.1-4a}$$

and

$$\frac{dC_3}{dt}=\begin{cases} r_{2F}\left[\frac{C_3(t)}{C_{eqv}}-C_{3sat}(T)\right]^{\chi_{2F}} & \text{if} \quad P\ge P_{eq2}(T) \\ r_{2B}\left[\frac{3C_2(t)}{C_{eqv}}\right]^{\chi_{2B}} & \text{if} \quad P<P_{eq2}(T) \text{ and } C_2(t)\ge 0 \end{cases} \qquad \text{A.1.4.1-4b}$$

By Eq. A.1.4.1-1

$$\frac{dC_2}{dt}=-\frac{1}{3}\left(\frac{dC_1}{dt}+\frac{dC_3}{dt}\right) \quad \text{or} \quad C_2=C_{20}-\frac{1}{3}\left[\left(C_1-C_{10}\right)+\left(C_3-C_{30}\right)\right] \qquad \text{A.1.4.1-4c}$$

where: C_1 = Concentration of $NaAlH_4$ [moles/m^3]
C_2 = Concentration of Na_3AlH_6 [moles/m^3]
C_3 = Concentration of NaH [moles/m^3]

Based on data for the loading of NaH, expressions for $C_{2\,sat}(T)$ and $C_{3\,sat}(T)$, in [moles/m^3], were estimated by UTRC in Attachment 1 as

$$C_{2\,sat}(T) = 0$$

$$C_{3\,sat}(T) = r_{sat}\left(1 - \frac{wf_{iso}^{sat}(T)}{0.056}\right) \qquad \text{A.1.4.1-5}$$

where: $$r_{sat} = \text{Max}\left[1, \left(1 - \frac{0.0373}{0.056 - wf_{iso}^{sat}(T)}\right)\right] \qquad \text{A.1.4.1-6}$$

The values for $wf_{iso}^{sat}(T)$, the saturation hydrogen weight fraction for loading at a fixed temperature T, are listed in Table A.1.4.1-2. Both the Mathcad® kinetics model, and the COMSOL® two and three-dimensional system models, use a spline fit to this data with extrapolated values fixed at the endpoints.

Table A.1.4.1-2
Values for $wf_{iso}^{sat}(T)$

T (K)	$wf_{iso}^{sat}(T)$
353.15	0.021
363.15	0.023
373.15	0.029
393.15	0.022
413.15	0.018

The weight fraction of H_2 contained in the sodium alanate metal, based on Eq. 1.4.1-1, is defined as

$$wf = \frac{\text{Mass of } H_2 \text{ in Metal}}{\text{Equivalent Mass of } NaAlH_4}$$
$$= \frac{\left(1.5n_{NaAlH_4} + 0.5n_{Na_3AlH_6}\right)M_{H_2}}{\left(n_{NaAlH_4} + 3n_{Na_3AlH_6} + n_{NaH}\right)M_{NaALH_4}} \qquad \text{A.1.4.1-7}$$
$$= \frac{1.5C_1 + 0.5C_2}{C_{eqv}}\frac{M_{H_2}}{M_{NaALH_4}}$$

where: n_{NaAlH_4} = Number of moles of $NaAlH_4$
$n_{Na_3AlH_6}$ = Number of moles of Na_3AlH_6

n_{NaH} = Number of moles of NaH

M_{NaALH_4} = Gram molecular weight of $NaAlH_4$ [kg/g-mol]

$M_{Na_3AlH_6}$ = Gram molecular weight of Na_3AlH_6 [kg/g-mol]

M_{NaH} = Gram molecular weight of NaH [kg/g-mol]

M_{H_2} = Gram molecular weight of H_2 [kg/g-mol]

For sodium alanate, the reaction heat term for the energy balance in Eq. A.1.3-19 is

$$\text{Source} = \frac{dC_1}{dt}\Delta H_{rxn\ 1} - 0.5\frac{dC_3}{dt}\Delta H_{rxn\ 2} \qquad \text{A.1.4.1-8}$$

where by Gross [2003]:

$\Delta H_{rxn\ 1}$ = Heat of per mole of H_2 consumed going to left for reaction 1

= -37 kJ/(mol H_2)

$\Delta H_{rxn\ 2}$ = Heat of per mole of H_2 consumed going to left for reaction 2

= -47 kJ/(mol H_2)

A.2 SYSTEM SCALING AND KINETICS

A.2.1 System Dimensions

The dimensions for the $NaAlH_4$ system modeled in this document were based on the parameters input to the Microsoft Excel® scaling tool shown in Figure A.2.1, see Hardy [2007].

Dimensions of Hydride Bed

6/25/2007

Chemical balance equations

$$\underbrace{NaAlH_4}_{\text{Species 1}} \overset{\text{Rx extent 1}}{\leftrightarrow} \underbrace{\frac{1}{3}Na_3AlH_6}_{\text{Species 2}} + \frac{2}{3}Al + H_2 \overset{\text{Rx extent 2}}{\leftrightarrow} \underbrace{NaH}_{\text{Species 3}} + Al + \frac{3}{2}H_2$$

Input Parameters											
M_{H2}	2.016 g/mol	Gram-Molecular Weight of H_2									
M_{NaAlH4}	54.000 g/mol	Gram-Molecular Weight of $NaAlH_4$									
m_{H2}	1000.00 g	Mass of recoverable H_2 to be stored in vessel			n_{H2}	496.03 mols	Moles of H_2 to be stored in vessel				
n_{H2}/n_{NaAlH4}	1.500	Practical ratio of moles H_2 to moles $NaAlH_4$ that can be stored			n_{NaAlH4}	330.69 mols	Moles of $NaAlH_4$ required for vessel				
ρ_{NaAlH4}	0.72 g/cm^3	Bulk density of NaAlH4 powder			m_{NaAlH4}	17857.28 g	Mass of $NaAlH_4$ required for vessel				
D	23.00 cm	Hydride bed diameter, no walls		9.06 in	V_{NaAlH4}	24801.77 cm^3	Volume of NaAlH4 required to store hydrogen				
D_{tool}	1.91 cm	Diameter of coolant tubes									
$D_{H2\ inject}$	1.27 cm	Diameter of H_2 injection tubes									
n_{tool}	9	Number of coolant tubes			A_{tool}	27.36 cm^2	Total area of coolant tube holes				
$n_{H2\ inject}$	8	Number of H_2 injection tubes			A_{H2}	10.13 cm^2	Total area of H_2 injection tube holes				
t	0.0313 cm	Thickness of fin plates	0.0123 in			0.015625					
s	0.64 cm	Approximate spacing between fin plates		0.2500 in		0.333125					
tw	0.12 cm	Tube wall thickness									
ρ_{tube}	2.70 g/cm^3	Density of tube material (6061-T6 Al from table onpg 6-11 of Mark's 9th Ed)									
ρ_{fin}	2.70 g/cm^3	Density of fin material (6061-T6 Al from table onpg 6-11 of Mark's 9th Ed)									
$\rho_{H2\ inject}$	2.70 g/cm^3	Material density of porous insert for H_2 delivery (6061-T6 Al from table onpg 6-11 of Mark's 9th Ed)									
$\epsilon_{H2\ inject}$	0.70	Void fraction of porous insert for H_2 delivery									
ρ_{Tank}	1.50 g/cm^3	Density of tank material (Composite @ 0.05419lbm/in^3 from spreadsheet W:\u_hydrogen_storage_size_calculation_composite_vessel.xls)									
ρ_{Liner}	2.70 g/cm^3	Density of liner material (6061-T6 Al from table onpg 6-11 of Mark's 9th Ed)									
Gap thickness	0.159 cm	Guess 1/16 in gap									
Liner Thickness	0.079 cm	Guess 1/32 in thick liner									
Tank Wall Thickness	0.132 cm	At 50 bar w/ safety factor-Wu				COMSOL Extrusion					
						1.5625E-04 m					
Calculated Parameters						3.3109E-03 m					
L_{NaAlH4}	65.62 cm	Required length of hydride only									
n_{Plate}	105	Total number of fin plates, including ends									
L_{Total}	68.90 cm	Total length of bed, no vessel	27.13 in	6.89E-01 m	V_{tube}	431.70 cm^3	Total volume of coolant tubes	m_{tube}	1165.59 g	Total mass of coolant tubes	
$s_{Plate\ Act}$	0.63 cm	Actual spacing of plates	0.25 in	6.31E-03 m	V_{fin}	1358.11 cm^3	Total volume of plate fins, including part of fin extruded over the outside of the coolant tubes	m_{fin}	3666.91 g	Total mass of plate fins, including part of fin extruded over the outside of the coolant tubes	
m_{bed}	24642.84 g	Mass of bed; including fins, tubes & $NaAlH_4$			V_{gap}	6899.97 cm^3	Total volume of gap including semi-spherical ends	m_{gap}	0.00 g	Total mass of gap including semi-spherical ends	
V_{bed}	36237.36 cm^3	Volume of bed with vessel & liner			V_{Liner}	266.38 cm^3	Total volume of liner	m_{Liner}	719.23 g	Total mass of liner	
L_{Vessel}	92.64 cm	Overall length of vessel	36.472 in		V_{Tank}	445.52 cm^3	Total volume of tank material	m_{Tank}	668.27 g	Total mass of tank material	
					$V_{H2\ inject}$	698.22 cm^3	Total volume of H_2 injection tubes	$m_{H2\ inject}$	565.56 g	Total mass of H_2 injection tubes	
Bed Characteristics											
Gravimetric Capacity	0.041 kg H2/Kg Total	With Outer Vessel & Liner			Hydride Grav Capacity	0.056 kg H2/Kg Total	Grav density of $NaAlH_4$ only				
Volumetric Capacity	0.028 kg H2/L Total	With Outer Vessel & Liner			Hydride Vol Capacity	0.040 kg H2/L Total	Vol density of $NaAlH_4$ only				
Radial Distance to Center of Outer Coolant Tubes (Maintains same Area to Cooling Surface Ratio)											
r	8.55 cm	9.50 cm	Radial location of center of coolant tube. Initially guessed, then optimized for hydride area to cooling surface ratio.								
θ	3.04 radians	174.45 °	Angle at center of coolant tube formed by intersection of tube center radius and tube inner wall								
S	2.52 cm		Arc length along inner wall of coolant tube from intersections of tube celer radius and tube inner wall								
A_1	209.13 cm^2		Cross-sectional area of bed, inside the radius to the center of the coolant tubes, less interior of coolant tubes								
A_2	176.82 cm^2		Cross-sectional area of bed, outside the radius to the center of the coolant tubes, less interior of coolant tubes								
S_1	25.37 cm		Sum of arc lengths of inner wall of all coolnat tubes inside the radius to the center of the cooling tubes								
S_2	21.45 cm		Sum of arc lengths of inner wall of all coolnat tubes outside the radius to the center of the cooling tubes								
Obj Funct	-1.0330E-11		Adjust variable r (the radial location of the center of the coolant tube) to make the objective function zero								

Figure A.2.1 System dimensions calculated with the scaling tool.

A.2.2 Heat Transfer Requirements For the $NaAlH_4$ System

Heat transfer requirements for the $NaAlH_4$ system modeled in this document were based on calculations with the Microsoft Excel® scaling tool shown in Figure A.2.2, see Hardy [2007].

Heat Generation on Uptake

6/26/2007

This worksheet calculates the heat generation occurring during hydration of $NaAlH_4$. The total moles of hydrogen taken up by the reaction are from the worksheet "Bed Dimensions."

Chemical balance equations

$$\underbrace{NaAlH_4}_{\text{Species 1}} \underset{\text{Reaction 1}}{\leftrightarrow} \underbrace{\frac{1}{3}Na_3AlH_6}_{\text{Species 2}} + \frac{2}{3}Al + H_2 \underset{\text{Reaction 2}}{\leftrightarrow} \underbrace{NaH}_{\text{Species 3}} + Al + \frac{3}{2}H_2$$

Input Parameters								
ΔH_{Rxn1}	37.00 kJ/mol H2	Heat of reaction from species 2 to species 1(from Karl Gross, Sandia Slides)						
ΔH_{Rxn2}	47.00 kJ/mol H2	Heat of reaction from species 3 to species 2 (from Karl Gross, Sandia Slides)						
Charging Time	180.00 sec							
Wall Temp	90.00 °C							
2ϕ Coolant Liquid Density	1.58 g/cm^3	1.58 g/cm^3	DuPont Vertrel-XF	2ϕ Coolant Sat Temp	55.00 °C			
2ϕ Coolant Vapor Density	0.0101 g/cm^3	0.0101 g/cm^3	DuPont Vertrel-XF	Approximate, from DiMarco Paper				
2ϕ Coolant Liquid Themal Cond	0.060 Btu/(hr ft °F)	1.04E-03 W/(cm °C)	DuPont Vertrel-XF	Guessed from Dowtherm T				
2ϕ Coolant Liquid Viscosity	0.67 cps	0.01 g/(cm s)	DuPont Vertrel-XF					
2ϕ Coolant Liquid Specific Heat	0.27 Btu/(lbm °F)	1.13 J/(g °C)	DuPont Vertrel-XF					
2ϕ Coolant Phase Change Enthalpy	31.00 cal/g	129.80 J/g	DuPont Vertrel-XF					
2ϕ Coolant Liquid Prandtl No.		7.29	DuPont Vertrel-XF					
Void Fraction (ε)	0.01							
Quality (x)	6.45656E-05							
1ϕ Coolant Liquid Density	51.00 lbm/ft^3	0.82 g/cm^3	Dowtherm T	1ϕ Coolant Inlet Temp	20.00 °C			
1ϕ Coolant Liquid Themal Cond	0.060 Btu/(hr ft °F)	1.04E-03 W/(cm °C)	Dowtherm T					
1ϕ Coolant Viscosity	3.00 cps	3.00E-02 g/(cm s)	Dowtherm T					
1ϕ Coolant Specific Heat	0.55 Btu/(lbm °F)	2.30 J/(g °C)	Dowtherm T					
1ϕ Coolant Prandtl No.		66.52	Dowtherm T					
Calculated Parameters								
$\Delta H_{overall}$	40.33 kJ/mol H2	Overall heat of reaction to form $NaAlH_4$ per mole of H_2						
Total Heat Released								
δQ	20006.61 kJ	Total heat removal requirement						
δQ/δt	111147.85 W	Required rate of heat removal		δQ/(δtδV)	4.4814E+06 W/m^3	Volumetric Rate of Heat Generation		
q"	3.51E+01 W/cm^2	Heat flux to coolant inside tubes						
Coolant Mass Flux								
Single Phase Coolant				***Two Phase Coolant***				
Dowtherm T				**DuPont Vertrel-XF**				
$G_{1\phi}$	1054.94 g/(cm^2 s)	From Dittus-Boelter correlation		$G_{2\phi}$	1670.39 g/(cm^2 s)	From Gungor-Winterton (1987) correlation		
v	1291.20 cm/s	h_{DB}	0.5017 W/(cm^2 °C)	v_{mix}	1067.82 cm/s	h_{GW}	0.9929 W/(cm^2 °C)	
Re_D	58235.51			Re_L	412853.11	$q"_{GW}$-q"	-3.04E-10 W/cm^2	Correlation is OK
ΔP	1.23E+01 psi			ΔP		Fr_L	687.8815	
ΔT	2.41E+00 °C			Δx	0.02695			
				Δε	0.80288			

By Dittus Boelter, Ref Holman, 4th Ed

$$Nu_D = 0.023 Re_D^{0.8} Pr^{0.4}, \quad Nu_D = \frac{hD}{k}, \quad Re_D = \frac{GD}{\mu}, \quad Pr = \frac{v}{\alpha} = \frac{\mu C_p}{k}$$

$$q" = h(T_w - T_{liq}) = 0.023 \frac{k}{D}\left(\frac{GD}{\mu}\right)^{0.8} Pr^{0.4}(T_w - T_{liq})$$

$$G = \left[\frac{q"}{0.023 \frac{k}{D}\left(\frac{D}{\mu}\right)^{0.8} Pr^{0.4}(T_w - T_{liq})}\right]^{1/0.8}$$

Figure A.2.2 System heat transfer parameters estimated with the scaling tool.

A.2.3 $NaAlH_4$ Reaction Kinetics

Chemical kinetics and bed utilization for $NaAlH_4$ were evaluated with the model developed in Mathcad®, shown below, see Hardy [2007].

Evaluation of Kinetics Model for NaH

Reaction

$NaAlH_4 \leftrightarrow 1/3Na_3AlH_6 + 2/3Al + H_2 \leftrightarrow NaH + Al + 3/2H_2$

Species 1 Rxn 1 Species 2 Rxn 2 Species 3

Nomenclature

C_1=Concentration of $NaAlH_4$ (mol/m^3)

C_2=Concentration of Na_3AlH_6 (mol/m^3)

C_3=Concentration of NaH (mol/m^3)

n_{H2}=Moles of H2 taken in to the metal hydride (mol/m^3)

r_{1F}=Rate of formation of $NaAlH_4$ from Na_3AlH_6 (mol/m^3-sec)

r_{1B}=Rate of dissociation of $NaAlH_4$ to Na_3AlH_6 (mol/m^3-sec)

r_{2F}=Rate of formation of Na_3AlH_6 from NaH (mol/m^3-sec)

r_{2B}=Rate of dissociation of Na_3AlH_6 to NaH (mol/m^3-sec)

Note that

$\partial C_2/\partial t = -1/3(\partial C_1/\partial t + \partial C_3/\partial t)$

$\partial n_{H2}/\partial t = \partial C_1/\partial t - 1/2\partial C_3/\partial t$

and

$\partial C_1/\partial t = r_{1F}$ If P>Peq1(T)

$\partial C_1/\partial t = -r_{1B}$ If P<Peq1(T)

$\partial C_3/\partial t = r_{2B}$ If P<Peq1(T)

$\partial C_3/\partial t = -r_{2F}$ If P>Peq1(T)

Tchg := 100

Tdisch := 120

Pchg := 50 Pressure (bar)

Pdisch := 1 Pressure (bar)

General Parameter Values

RR := 8.314 Ideal gas constant (J/mol-K)

Create step function that is 0 or -1 over period 2h

h := 40000 Half Period (sec)

$k(tx) := ceil\left(\frac{tx}{h}\right)$

$test(tx) := 2 \cdot floor\left(\frac{k(tx)}{2}\right) - k(tx)$

$P(tx) := \text{if}(\text{test}(tx) < 0, Pchg, Pdisch)$ Pressure (bar)

Parameter Values (From Fit to Data)

Reaction 1

$A1F := 10^{8}$ $A1B := 4 \cdot 10^{12}$ $\chi 1F := 2.0$ $\chi 1B := 2.0$

$E1F := 80000$ Activation Energy (KJ/mol) $E1B := 110000$ Activation Energy (KJ/mol)

$\Delta H\_R1 := -4475$ $\Delta S\_R1 := -14.83$

Reaction 2

$A2F := 1.5 \cdot 10^{5}$ $A2B := 6 \times 10^{12}$ $\chi 2F := 1.0$ $\chi 2B := 1.0$

$E2F := 70000$ Activation Energy (J/mol) $E2B := 110000$ Activation Energy (J/mol)

$\Delta H\_R2 := -6150$ $\Delta S\_R2 := -16.22$

Equilibrium Pressure (in bar?)

Reaction 1

$$P\_eq1(TT) := \exp\left(\frac{\Delta H\_R1}{TT + 273} - \Delta S\_R1\right)$$ TT is Temperature in (C)

Reaction 2

$$P\_eq2(TT) := \exp\left(\frac{\Delta H\_R2}{TT + 273} - \Delta S\_R2\right)$$ TT is Temperature in (C)

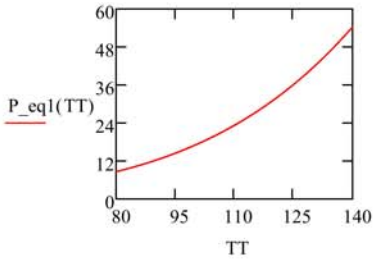

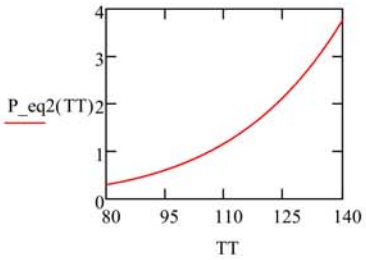

Initial Conditions

$C10 := 0$ $C20 := 0$ $C30 := 330.69$ $nH20 := 0$

$Temp(tx) := \text{if}(\text{test}(tx) < 0, Tchg, Tdisch)$ Temperature (C)

Saturation Concentrations

$Ceqv := C10 + 3 \cdot C20 + C30$ Equivalent Concentration, Needed to relate species concentrations (mol/m^3) to the non-dimensional concenrations used in calculations

Fit the saturation weight fraction to temperature TT is in C

:=

wfdata :=

	0	1
0	300	0.021
1	353	0.021
2	353.15	0.021
3	359	0.022
4	363.15	0.023
5	373.15	0.029
6	393.15	0.022
7	405	0.019
8	413.15	0.018
9	413.5	0.018
10	600	0.018

$wfdata := csort(wfdata, 0)$ TT is in C

$vTT := wfdata^{\langle 0 \rangle} - 273.15$

$vy := wfdata^{\langle 1 \rangle}$

$vs := lspline(vTT, vy)$

$wf\_sat(TT) := interp(vs, vTT, vy, TT)$

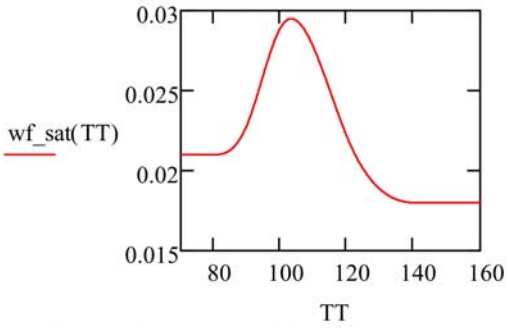

Compute the non-dimensional "saturation" concentrations from fit

$$rsat(TT) := \max\left(1, 1 - \frac{0.056 - 0.0187}{0.056 - wf\_sat(TT)}\right)$$ TT is in C

$$C3sat(TT) := \left(1 - \frac{wf\_sat(TT)}{0.056}\right) \cdot rsat(TT)$$ TT is in C

$$C2sat(TT) := \frac{(1 - rsat(TT)) \cdot (0.056 - wf\_sat(TT))}{(0.056 - 0.0187)}$$ TT is in C

Forward and Backward Reaction Rates

$$r1F(TT,tx) := \text{if}\left[(P(tx) \geq P\_eq1(TT)), Ceqv \cdot A1F \cdot \exp\left[\frac{-E1F}{RR\cdot(TT+273.15)}\right]\cdot\frac{P(tx)-P\_eq1(TT)}{P\_eq1(TT)}, 0\right]$$ TT is in C

$$r1B(TT,tx) := \text{if}\left[(P(tx) < P\_eq1(TT)), Ceqv \cdot A1B \cdot \exp\left[\frac{-E1B}{RR\cdot(TT+273.15)}\right]\cdot\left[\frac{(P\_eq1(TT)-P(tx))}{P\_eq1(TT)}\right], 0\right]$$

$$r2F(TT,tx) := \text{if}\left[(P(tx) \geq P\_eq2(TT)), Ceqv \cdot A2F \cdot \exp\left[\frac{-E2F}{RR\cdot(TT+273.15)}\right]\cdot\left[\frac{(P(tx)-P\_eq2(TT))}{P\_eq2(TT)}\right], 0\right]$$

$$r2B(TT,tx) := \text{if}\left[(P(tx) < P\_eq2(TT)), Ceqv \cdot A2B \cdot \exp\left[\frac{-E2B}{RR\cdot(TT+273.15)}\right]\cdot\left(\frac{P\_eq2(TT)-P(tx)}{P\_eq2(TT)}\right), 0\right]$$

Hydrogen Concentration From Kinetics Equations

Given

$$\frac{d}{dt}C1(t) = r1F(Temp(t),t)\cdot\left(\left(\frac{3\,C2(t)}{Ceqv} - C2sat(Temp(t))\right)\right)^{\chi 1F} - r1B(Temp(t),t)\cdot\left(\frac{C1(t)}{Ceqv}\right)^{\chi 1B}$$

$$\frac{d}{dt}C2(t) = -\left[\frac{1}{3}\cdot\left(\frac{d}{dt}C1(t) + \frac{d}{dt}C3(t)\right)\right]$$

$$\frac{d}{dt}C3(t) = -r2F(Temp(t),t)\cdot\left(\frac{C3(t)}{Ceqv} - C3sat(Temp(t))\right)^{\chi 2F} + r2B(Temp(t),t)\cdot\left(\frac{3\,C2(t)}{Ceqv}\right)^{\chi 2B}$$

$$\frac{d}{dt}nH2(t) = \frac{d}{dt}C1(t) - \frac{1}{2}\cdot\left(\frac{d}{dt}C3(t)\right)$$ nH2 is the number of moles of H2 per volume of hydride that are contained for release in the metal hydride

$$C1(0) = C10 \quad C2(0) = C20 \quad C3(0) = C30 \quad nH2(0) = nH20$$

$$\begin{pmatrix} C1 \\ C2 \\ C3 \\ nH2 \end{pmatrix} := Odesolve\left[\begin{pmatrix} C1 \\ C2 \\ C3 \\ nH2 \end{pmatrix}, t, 240000, 20000\right]$$ t is time in seconds

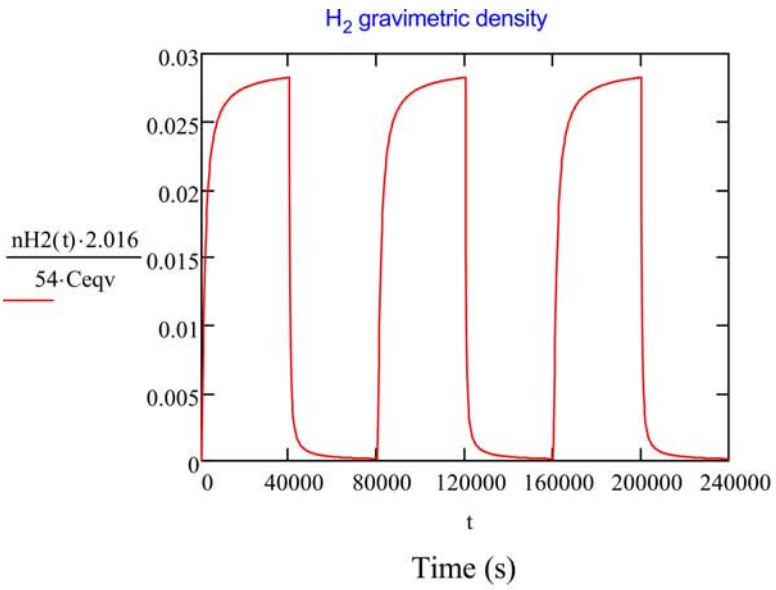

$$\frac{nH2(720)\cdot 2.016}{54\cdot Ceqv} = 0.007940$$

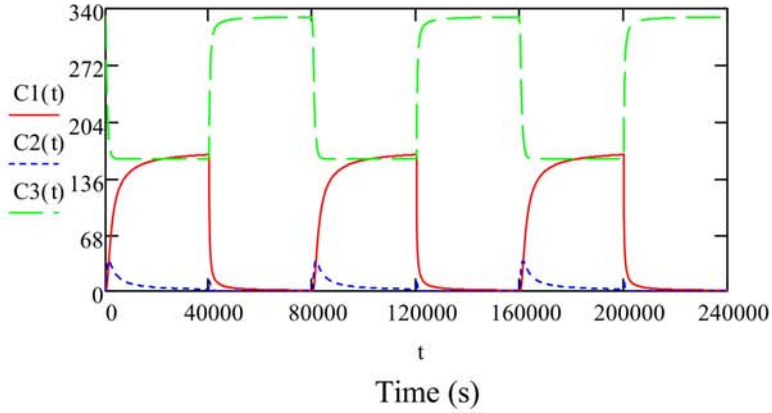

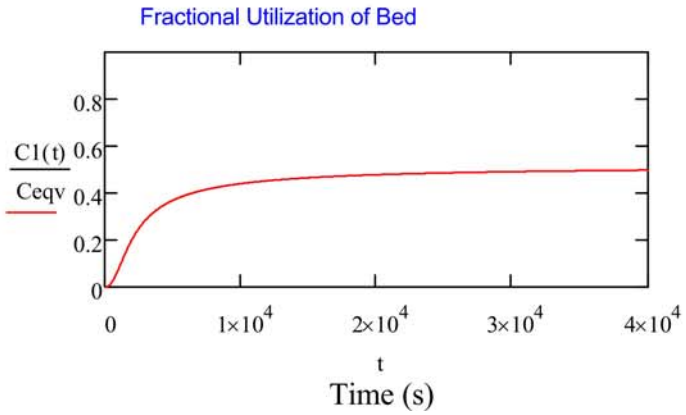

ATTACHMENTS

Attachment 1

Practical Sorption Kinetics of $TiCl_3$ Catalyzed $NaAlH_4$

Xia Tang, Daniel A Mosher and Donald L Anton

United Technologies Research Center

411 Silver Lane

East Hartford, CT 06108

Abstract

Sodium alanate has been studied as a promising candidate material for reversible hydrogen storage due to its intermediate temperature range and relatively high storage capacity. Its rates of desorption and absorption of hydrogen have been shown to be enhanced by the addition of Ti in various compounds. To date, the sorption kinetics, especially absorption kinetics, is not well understood. In this study, a practical sorption kinetics model for $TiCl_3$ catalyzed $NaAlH_4$ has been developed to assist in the engineering design and evaluation of a prototype hydrogen storage system.

Introduction

The design of a hydrogen storage system using any exothermic hydriding compound, such as $NaAlH_4$, requires detailed consideration of local heat management. This is especially important in the critical hydrogen absorption stage, where high kinetics are required and heat flow is at its maximum. Thermal transport architectures such as cooling tubes and metal foam structures need to be designed to meet the optimum operational characteristics of the hydrogen storage media. In order to design and model these architectures and obtain a gravimetrically and volumetrically optimized storage system, absorption and desorption kinetic models need to be identified and validated. Many current models, such as the well-known Arrhenius model, are insufficient to characterize materials behavior under transient or partially discharged conditions. Previous kinetics studies of $NaAlH_4$ mainly focused on the desorption reaction [1-4]. Aborption and desorption kinetics models were developed by Luo and Cross [5] to simulate NaH+Al $\leftrightarrow$$NaAlH_4$ reactions using NaH and Al as starting materials. No kinetics model was reported to simulate transient hydriding rate and hydrogen absorption capacity of NaH+Al derived from $NaAlH_4$. In this study, a solid/gas chemical kinetics model originally developed by El-Osery [6-9] to design conventional metal hydride systems was utilized. This model was adapted for use in the multi-step hydrogen absorption mechanisms of NaH+Al$\rightarrow$$NaAlH_4$.

Basic Kinetics Model

The dehydrogenation and hydrogenation of sodium alanate involve the following well-known reactions:

$NaAlH_4 \leftrightarrow 1/3\ Na_3AlH_6 + 2/3\ Al + H_2 \leftrightarrow\ NaH + Al + 3/2\ H_2$

For compactness, the compositional state can be tracked by a single variable for each product/reactant, C_1, C_2 and C_3 as:

C_1: $NaH + Al + 3/2\ H_2$

C_2: $1/3\ Na_3AlH_6 + 2/3\ Al + H_2$

C_3: $NaAlH_4$

The nomenclatures for all reactions are listed in Table 1.

Table 1 Nomenclature for All Reactions

Label	Action	Reactant	Product
r_1	Dehydriding of Na_3AlH_6	C_2	C_1
r_2	Hydriding of NaH	C_1	C_2
r_3	Dehydriding of $NaAlH_4$	C_3	C_2
r_4	Hydriding of Na_3AlH_6	C_2	C_3

Reaction rates can be represented by equation (1) based on the metal hydride model developed by El-Osery [6-7]:

$$\left(\frac{dC_j}{dt}\right)_{r_i} = f_T(T) * f_P(P) * f_C(C_k) \quad (1)$$

i for reaction r_i
j for composition product C_j
k for composition reactant C_k.

The temperature dependant term is that of the typical Arrhenius equation given as:

$$f_T = A_i \exp\left(-\frac{E_i}{RT}\right) \quad (1a)$$

The pressure dependant term can be expressed simply as a first order expression:

$$f_P = (-1)^i * \left(\frac{P - P_{e,i}}{P_{e,i}}\right) \quad (1b)$$

where $P_{e,i}$ is the equilibrium pressure for the reaction and is valid for both hydriding and dehydriding. Equilibrium pressure $P_{e,i}$ is temperature dependant and obeys the van't Hoff equation:

$$\ln(P_{e,i}) = \frac{\Delta H}{RT} - \frac{\Delta S}{R} \quad (1c)$$

In El-Osery's description, a first order function of hydrogen/metal atomic ratio was used in a concentration factor for hydriding. In hydriding reactions of the NaH+Al system, however, two solid reactants are involved in each reaction respectively. They may have higher reaction orders. The concentration factor is thus represented as being proportional to the reactant concentration to some power, χ_i as:

$$f_C = (C_k)^{\chi_i} \quad (1d)$$

Combining these factors results in the rate equation:

$$\frac{dC_j}{dt} = A_i \exp\left(-\frac{E_i}{RT}\right) * (-1)^i * \left(\frac{P - P_{e,i}}{P_{e,i}}\right) * (C_k)^{\chi_i} \quad (2)$$

Applying equation (2) to r_2 and r_4, one obtains the following equations for high pressure hydriding (r_2 and r_4 are active).

$$\left(\frac{dC_2}{dt}\right)_{r2} = A_2 \exp\left(-\frac{E_2}{RT}\right) * \left(\frac{P - P_{e,2}}{P_{e,2}}\right) * (C_1)^{\chi_2} \quad \text{and} \quad \left(\frac{dC_1}{dt}\right)_{r2} = -\left(\frac{dC_2}{dt}\right)_{r2}$$

$$\left(\frac{dC_3}{dt}\right)_{r4} = A_4 \exp\left(-\frac{E_4}{RT}\right)*\left(\frac{P-P_{e,4}}{P_{e,4}}\right)*(C_2)^{\chi_4} \quad \text{and} \quad \left(\frac{dC_2}{dt}\right)_{r4} = -\left(\frac{dC_3}{dt}\right)_{r4}$$

The reaction rate of each composition can be represented as:

$$\frac{dC_1}{dt} = -A_2 \exp\left(-\frac{E_2}{RT}\right)*\left(\frac{P-P_{e,2}}{P_{e,2}}\right)*(C_1)^{\chi_2} \tag{5}$$

$$\frac{dC_2}{dt} = A_2 \exp\left(-\frac{E_2}{RT}\right)*\left(\frac{P-P_{e,2}}{P_{e,2}}\right)*(C_1)^{\chi_2} - A_4 \exp\left(-\frac{E_4}{RT}\right)*\left(\frac{P-P_{e,4}}{P_{e,4}}\right)*(C_2)^{\chi_4} \tag{6}$$

$$\frac{dC_3}{dt} = A_4 \exp\left(-\frac{E_4}{RT}\right)*\left(\frac{P-P_{e,4}}{P_{e,4}}\right)*(C_2)^{\chi_4} \tag{7}$$

$$0 \le C_i \le 1$$

with the initial reaction conditions: $C_1^{t=0} = 1$, $C_2^{t=0} = 0$, $C_3^{t=0} = 0$,

Experimental Procedure

To validate the applicability of this kinetic model, a well-known alanate composition was chosen for empirical assessment. Commercial grade $NaAlH_4$ was purchased from Albemarle Co. (Baton Rouge, LA) with a chemical certification analysis of 86.3% $NaAlH_4$, 4.7%Na_3AlH_6, 7.5% free Al and 10.1% insoluble Al (with all analyses given in wt%). The catalyst, $TiCl_3$ (99.99%), was obtained from Aldrich Corp. All materials were used in the as-received condition.

The $NaAlH_4$ was catalyzed with 4 mol % $TiCl_3$ by high energy SPEX ball milling for three hours under nitrogen. Immediately after ball milling, approximately 1 g of the sample was transferred into the sample holder of a modified Sievert's apparatus. All the storage and transferring of $NaAlH_4$ and $TiCl_3$ were performed under a high purity nitrogen environment inside a glove box with an oxygen concentration $<10^{-5}$ ppm.

$TiCl_3$ catalyzed $NaAlH_4$ was first desorbed at 150°C in vacuum for more than 7 hours to ensure maximum desorption. Absorption was conducted with the hydrogen pressure ranging from 6.8-6.0 MPa. Extent of reaction versus time was measured by monitoring hydrogen pressure change using a gas reaction controller made by Advanced Materials Co. (Pittsburg, PA).

Results and Discussion

Rate equations (5) to (7) represent an ideal kinetics model, where the total charging capacity over long periods approaches the ideal capacity of 5.6 wt%. However, in reality, the total capacity is usually less than the theoretical value. Saturation compositions, $C_k^{Sat}(T)$, are introduced into the rate equations to reflect this non-ideal capacity. They represent the residual reactant compositions at the hydriding saturation point fordifferent temperature values.

The concentration factors in equation (1d) are thus changed to:

$$f_C = \left(C_k - C_k^{sat}(t)\right)^{\chi_i} \text{ if } C_k - C_k^{sat}(T) \ge 0 \tag{1e}$$

$$f_C = 0 \text{ if } C_k - C_k^{sat}(T) < 0 \tag{1f}$$

The rate equations are represented accordingly by:

$$\frac{dC_1}{dt} = -A_2 \exp\left(-\frac{E_2}{RT}\right) * \left(\frac{P - P_{e,2}}{P_{e,2}}\right) * \left[C_1 - C_1^{sat}(T)\right]^{\chi_2} \quad (8)$$

$$\frac{dC_2}{dt} = A_2 \exp\left(-\frac{E_2}{RT}\right) * \left(\frac{P - P_{e,2}}{P_{e,2}}\right) * \left[C_1 - C_1^{sat}(T)\right]^{\chi_2} - A_4 \exp\left(-\frac{E_4}{RT}\right) * \left(\frac{P - P_{e,4}}{P_{e,4}}\right) * \left[C_2 - C_2^{sat}(T)\right]^{\chi_4} \quad (9)$$

$$\frac{dC_3}{dt} = A_4 \exp\left(-\frac{E_4}{RT}\right) * \left(\frac{P - P_{e,4}}{P_{e,4}}\right) * \left[C_2 - C_2^{sat}(T)\right]^{\chi_4} \quad (10)$$

The modified compositions and total hydriding capacity at saturation are:

$$C_1 = C_1^{sat}(T), \quad C_2 = C_2^{sat}(T), \quad C_3 = 1 - C_1^{sat}(T) - C_2^{sat}(T)$$

The total H_2 absorption capacity $w_{iso}^{sat}(T)$:

$$w_{iso}^{sat}(T) = 0.0187 * C_2^{sat}(T) + 0.056 * \left(1 - C_1^{sat}(T) - C_2^{sat}(T)\right) \quad (11)$$

Curve fitting with experimental data using equations (8) to (13) is shown in Figure 1. The parameters used for fitting are listed in Table 2. The slope and intercept in the van't Hoff plot were derived from data published by Cross *et al.* [10].

Table 2 Fitting Parameters in Figure 1

$(\Delta H/R)r_2$	-6150	Slope in van't Hoff plot
$-(\Delta S/R)r_2$	16.22	Intercept in van't Hoff plot
A_2	1.50E+05	Pre-exponent coefficient for r_2
E_2	70	Activation energy for r_2, KJ/mol of H_2 for r_2
χ_2	1	Reaction order for r_2
$(\Delta H/R)r_4$	-4475	Slope in van't Hoff plot, r_4
$-(\Delta S/R)r_4$	14.83	Intercept in van't Hoff plot, r_4
A_4	1.00E+08	Pre-exponent coefficient for r_4
E_4	80	Activation energy for r_2, kJ/mol of H_2 for r_4
χ_4	2	Reaction order for r_4

The activation energies, E_i, for r_2 and r_4 are 70 and 80 KJ/mol of H_2 and the pre-exponent coefficients, A_i, 1.50E+05 and 1.00E+08 respectively. The hydriding reaction, r_4 (Na_3AlH_6 to $NaAlH_4$) has a higher activation energy than the reaction, r_2, NaH to Na_3AlH_6. However, the pre-exponential coefficient of r_4 is much higher than r_2. This could be due to catalyst placement preferentially at positions favorable to r_4 reaction. The reaction orders of the two hydriding steps appear to be different, with r_2 being nominally a first order reaction, and r_4 a second order reaction. The reaction orders are consistent with those reported by Luo and Gross [5]. During the formation of Na_3AlH_6, NaH is the limiting reactant and Al is in access. Al concentration can be considered as constant and the reaction becomes a pseudo first order. In r_4, the reactants, Na_3AlH_6 and Al, are in stichometric ratio. Both concentrations can affect reaction rate. The formation of $NaAlH_4$, therefore, is a second order reaction.

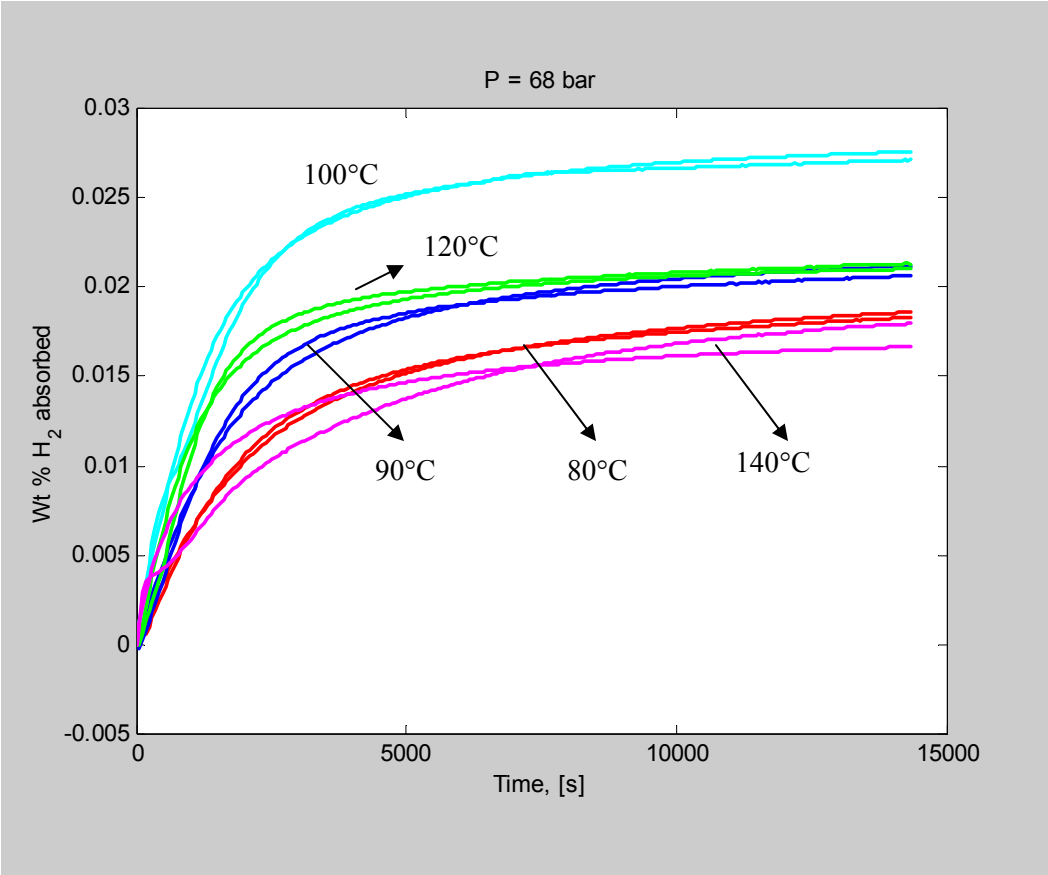

Figure 1 H_2 absorption curves at 80-140°C with H_2 pressure ranging from 6.0-6.8MPa. The dashed lines are model results, with red=80°C; blue=90°C; cyan=100°C; green=120°C; and magenta=140°C.

As shown in Figure 1, the model fits experimental data well in absorption temperature range of 80°C-120°C. However, the fit is not as accurate for absorption at 140°C. As the temperature increases, the hydriding reaction of Na_3AlH_6 to $NaAlH_4$ approaches its thermodynamic equilibrium at 6.0-6.8 MPa hydrogen pressure. The P_e for 2 mol.% $Ti(OBu^n)_4$ catalyzed materials is 5.4 MPa [9]. Although the reaction rate increases with temperature, the capacity decreases as a result of decreasing thermodynamic driving force. Absorption at this temperature is not recommended at this hydriding pressure.

By close inspection. it can be seen in Figure 1 that inflection regions are present during the initial rapid hydriding. Similar inflections were also observed in previous absorption data published by Sandrock *et al.* [11]. There are two possibilities for this observation; (i) a temperature rise in the sample upon exothermic hydriding of NaH to form Na_3AlH_6 or (ii) the combination of slowing down of the first hydriding reaction, r_2, and starting of the second reaction, r_4. To resolve this question, accurate sample temperature measurement is required. This non-isothermal factor can be included in future models when accurate *in-situ* measurement of the sample temperature becomes available. In addition, the current model is fit to isothermal hydriding data, with the assumption that the hydriding rate is not affected by thermal histories except that captured by the variables C_k. Reactions involving solid reactants and products usually involve product nucleation and growth periods, and reaction rates are closely related to the characteristics of these periods. Previous thermal histories could affect particle sizes, packing and reactant/catalyst distribution. These changes will have an effect on the characteristics of nucleation and growth, therefore altering reaction rates. Future kinetics models should take these factors into consideration.

Conclusion

A practical kinetics model has been developed to simulate hydrogen absorption of NaH + Al obtained from $TiCl_3$ catalyzed $NaAlH_4$. Physical meaning of the basic model is discussed. Modification of the model has been made with additional parameters for non-stoichiometric saturation compositions. The modified model fits well with experimental data at temperatures ranging from 80°C to120°C in the pressures range 6.0-6.8MPa. This model has provided kinetic information needed in the design of 1 kg hydrogen storage system using $NaAlH_4$ as storage media. Although this model needs further refinement to include non-isothermal factors and solid state reaction mechanisms, it has given valuable insights in optimizing thermal management and operational conditions for the 1 kg prototype system.

Acknowledgements

The funding for this study is provided by U.S. Department of Energy, under the contract DE-FC36-02AL67610 and the input of Dr. C. Read. The authors also acknowledge Mr. R. Brown for his valuable contribution in performing experimental work.

References

1. T. Kiyobayashi, S.S. Srinivasan, D. Sun and C.M. Jensen, J. Phys. Chem.A 107, 7671-7674 (2003).
2. G. Sandrock, K. Gross and G. Thomas, J. Alloys Comp. **339** 299-308 (2002).
3. K.J. Gross, E.H. Majzoub and S.W. Spangler, J. Alloys Comp. **356-357**, 423-428 (2003).
4. D.L. Anton, J. Alloys Comp. **356-357**, 400-404 (2003).
5. W. Luo and K.J. Gross, J. Alloys Comp. **385** 224-231 (2002).
6. I.A. El-Osery, Int. J. Hydrogen Energy, **8**, 191-198 (1983).
7. M.A. El-Osairy, I.A. El-Osery, A.M. Metwally and M.A. Hassan, J. Alloys Comp. **202**, 125-128(1993)
8. M.A. El-Gammal, I.A. El-Osery, A.M. Metwally and M.A. Hassan, Modeling, Measurement and Control, **46,** 35-44 (1994).
9. M.A. El-Osairy, I.A. El-Osery, A.M. Metwally and M.A. Hassan, Int. J. Hydrogen Energy, **18,** 517-524 (1993)
10. K.J. Gross, G.J. Thomas and C.M. Jensen, J. Alloys Comp. **330-332** 683-690 (2002).
11. G. Sandrock, K. Gross and G. Thomas, J. Alloys Comp. **339** 299-308 (2002).

Attachment 2

DLA

Kinetics Model Refinements

Dan Mosher
6/26/03

$NaAlH_4 \underset{r_5}{\overset{r_1}{\rightleftharpoons}} \frac{1}{3}Na_3AlH_6 + \frac{2}{3}Al + H_2 \underset{r_4}{\overset{r_3}{\rightleftharpoons}} NaH + Al + \frac{3}{2}H_2$

A number of refinements have been added to the kinetics model framework:

1. Check to make sure the composition variables are not outside the bounds of
$$0 \le C_i \le 1$$
2. Modify the reaction rate forms to allow different saturation hydrogen weight percentages at different temperatures.

1 Maintaining consistent values of the compositions, C_i ← Mole fractions?

1.1 Comment on Model Aspect which Keeps Consistent values of C_i

What is it in the modeling framework that maintains consistent values for the compositions? The consistency requirements are

$$0 \le C_i \le 1$$

and

Equation 1
$$\sum_{i=1}^{3} C_i = 1.$$

$C_1 \rightarrow NaH + Al + \frac{3}{2}H_2$
$C_2 \rightarrow \frac{1}{3}Na_3AlH_6 + \frac{2}{3}Al + H_2$
$C_3 \rightarrow NaAlH_4$

$dC_1 = dC_{NaH}$
$dC_2 = 3\,dC_{Na_3AlH_6}$
$dC_3 = dC_{NaAlH_4}$

For reaction 2 involving the hydriding of NaH (in the original model form with no saturation levels), we have

Equation 2
$$\left(\frac{dC_2}{dt}\right)_{r2} \propto (C_1)^{\chi_2}$$

Mol eqv of $NaAlH_4$ $= C_{eqv} = C_{NaAlH_4} + 3C_{Na_3AlH_6}$
$C_i = \frac{C_{NaH}}{C_{eqv}}$ + C_{NaAlH_4}
$C_{Na_3AlH_6} = \frac{C_{Na_3AlH_6}}{C_{eqv}}$
$C_3 = \frac{C_{NaH}}{C_{eqv}}$

This produces a C_2 that will reach a limit as $C_1 \rightarrow 0$, but it does not ensure that $0 \le C_2 \le 1$. However, the relationship which balances the product formation rate with the reactant consumption rate,

Equation 3
$$\left(\frac{dC_1}{dt}\right)_{r2} = -\left(\frac{dC_2}{dt}\right)_{r2}$$

when integrated over a small time step, will produce

$$(\Delta C_1)_{r2} = -(\Delta C_2)_{r2}$$

In this case,

$$(\Delta C_1 + \Delta C_2)_{r2} = (-\Delta C_2 + \Delta C_2)_{r2} = 0$$

If we consider pressure regime three where both reactions 2 and 4 are active, we will also have

$$(\Delta C_2 + \Delta C_3)_{r4} = 0$$

If we add these two equations,

Equation 4
$$(\Delta C_1 + \Delta C_2)_{r2} + (\Delta C_2 + \Delta C_3)_{r4} = 0$$

Since the model framework specifies that for pressure regime 3,

$$(\Delta C_1)_{total} = (\Delta C_1)_{r2}$$
$$(\Delta C_2)_{total} = (\Delta C_2)_{r2} + (\Delta C_2)_{r4}$$
$$(\Delta C_3)_{total} = (\Delta C_3)_{r4}$$

Equation 4 becomes

$$(\Delta C_1 + \Delta C_2 + \Delta C_3)_{total} = 0$$

or

$$C_1 + C_2 + C_3 = \text{constant}$$

If we start with values which sum to 1, then Equation 1 will be satisfied for all time.

Figure 1 demonstrates that this indeed does occur during the simultations even with the potential errors associated with numerical integration. The sum of C's is 1.000000 +/- 8e-7.

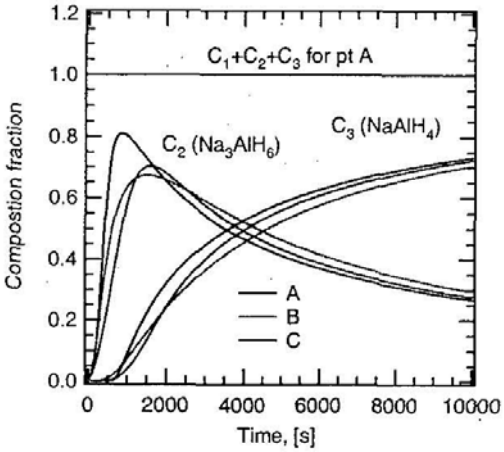

Figure 1: Composition results for four hole configuration.

1.2 Potential Issue with Numerical Integration which Should Be Corrected

With numerical integration, finite time steps are used. In this case, it is conceivable that the value of a reactant would not hit exactly 0 but could overshoot and become negative. An important influence of this is the value of the exponent χ on the composition variable. For the specific reaction of Equation 2 with $\chi_2 = 1$, if $C_1 < 0$ then $dC_2/dt < 0$ and by Equation 3, $dC_1/dt > 0$ which will self correct the value of C_1 toward 0. However, if $\chi_2 = 2$, the square of a negative number is a positive number, so that C_1 will become more negative in a run away numerical effect where C_1 becomes substantially less than 0 and C_2 becomes substantially greater than 1. As discussed above,

$$(\Delta C_1 + \Delta C_2)_{r2} = 0$$

would still apply but the individual values of C_1 and C_2 will diverge and be meaningless. Even though a value of $\chi = 2$ has been used in ABAQUS simulations, this problem has not been observed probably because the reaction rates slow down adequately as $C_1 \rightarrow 0$ so that the finite time steps do not produce an overshoot.

Nevertheless, modifications should be added to the coding to make sure that all of the compositions stay within the physical bounds of 0 and 1. One approach is to simply check the values of the compositions and if they are starting to deviate, to set them equal to 0 or 1 as appropriate. For the particular reaction, it also might be necessary to adjust the conjugate variable in the reaction to avoid any drifting of the composition sum. Another approach is to modify the coding used to represent Equation 2 as

$$\left(\frac{dC_2}{dt}\right)_{r2} \propto sign(C_1)*[abs(C_1)]^{\chi_2}$$

This has two advantages. First, the self correcting nature is preserved even if $\chi = 2$. Second, there will not be computation errors if C_1 is negative and the exponent is non-integer. Another, perhaps perferrable approach is to have

$$\left(\frac{dC_2}{dt}\right)_{r2} \propto [C_1]^{\chi_2} \text{ if } C_1 \geq 0$$

$$\left(\frac{dC_2}{dt}\right)_{r2} = 0 \text{ if } C_1 < 0$$

This essentially stops the hydriding reaction when the reactant concentration become slightly negative.

2 Modeling of Saturation Weight Percentages Which Vary with Temperature

2.1 Introduction

As shown in Figure 2, the saturation weight fraction absorbed can vary significantly with temperature. The value of 90 C is 0.02 and that for 100 C is 0.027. In the present modeling structure, the hydrogen weight fraction stored in the material is calculated from the composition variables as

Equation 5 $$w = \nu*(0.0187*C_2 + 0.056*C_3)$$

The variable ν represents the nonideal capacity. As a first attempt to fit the data in Figure 2, this variable was made temperature dependent,

Equation 6 $$w = \nu(T)*(0.0187*C_2 + 0.056*C_3)$$

and the comparison with data in Figure 2 is reasonably good at longer times. The complexities of the incubation period where not modeled and therefore the short time comparison is not good.

This approach is adequate to match the constant temperature data, but it will have unrealistic behavior when temperature is changing. As an example, if at 10,000 s, the temperature is changed from 90 to 100 C, the weight fraction will jump instantaneously from 0.02 to 0.027 which would not occur physically. Additional experiments in which the temperature is changed will be conducted to examine this effect.

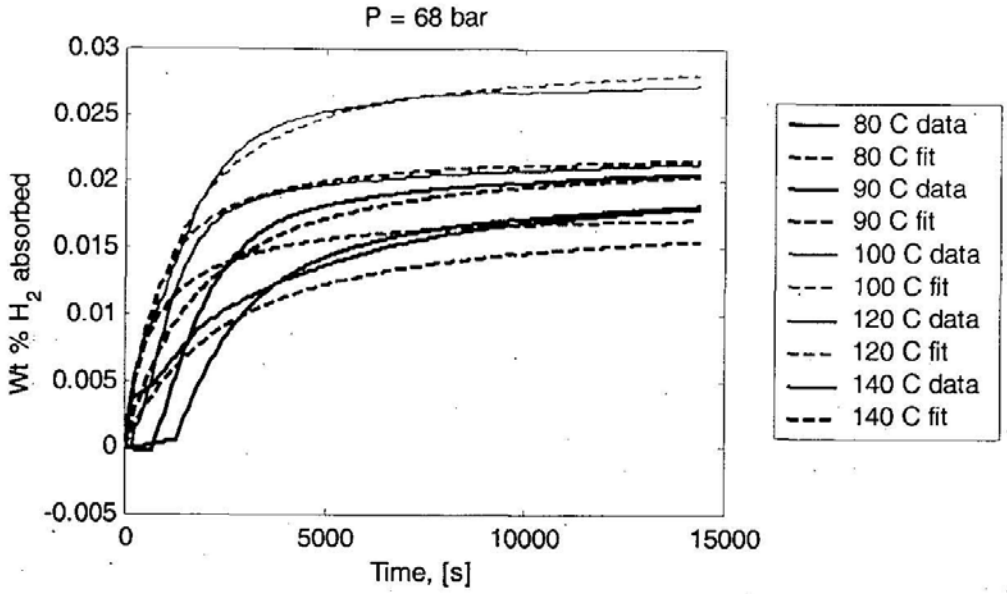

Figure 2: Absorption data for 6% TiCl3 with fit to constant temperature model.

2.2 Saturation Form for Single Composition, C_1

The framework modifications to allow for saturation weight fraction differences for arbitrary temperature histories are discussed next. One modeling approach is to have

$$\left(\frac{dC_2}{dt}\right)_{r2} \propto \left(C_1 - C_1^{sat}(T)\right)^{\chi_2}$$

which should be represented in the coding as

Equation 7
$$\left(\frac{dC_2}{dt}\right)_{r2} \propto \left[C_1 - C_1^{sat}(T)\right]^{\chi_2} \text{ if } C_1 - C_1^{sat}(T) \geq 0$$

Equation 8
$$\left(\frac{dC_2}{dt}\right)_{r2} = 0 \text{ if } C_1 - C_1^{sat}(T) < 0$$

The value of this saturation C_1 is calcuated by considering the resulting long-time composition,

$$C_1 = C_1^{sat}, \quad C_2 = 0, \quad C_3 = 1 - C_1^{sat}$$

and substituting these values into a modified version of Equation 5 where the obsolete factor of ν has been removed,

Equation 9
$$w = 0.0187 * C_2 + 0.056 * C_3$$

This results in a saturation value for the weight fraction under an isothermal temperature history of

$$w_{iso}^{sat} = 0.056 * \left(1 - C_1^{sat}\right)$$

or

Equation 10
$$C_1^{sat}(T) = 1 - \frac{w_{iso}^{sat}(T)}{0.056}$$

The parameter $w_{iso}^{sat}(T)$ represents the saturation level at long times for the absorbed weight fraction of hydrogen under an isothermal temperature history.

Because reaction 2 is a hydriding reaction, it can only proceed in the direction where C_2 is being produced and therefore we must have $C_1 > C_1^{sat}$. If not, then Equation 8 applies.

The equation for the second hydriding reaction would not necessarily need to be altered with a saturation level for the reactant,

$$\left(\frac{dC_3}{dt}\right)_{r4} \propto (C_2)^{\chi_4}.$$

To illustrate this with an example, consider if $w_{iso}^{sat} = 0.020$ and so $C_1^{sat} = 0.643$. If we start off with $C_1 = 1, \quad C_2 = 0, \quad C_3 = 0$, then after a long amount of hydriding, we would obtain $C_1 = 0.643, \quad C_2 = 0, \quad C_3 = 0.357$.
then we will obtain the desired value of

$$w = 0.0187 * 0 + 0.056 * 0.357 = 0.020$$

This approach appears to give reasonble physical behavior when changing temperatures for C_1^{sat} increasing with time. If for example, we hydride at 90 C for 10,000 s and then increase the temperature to 100 C, the value of C_1^{sat} will decrease and reaction 2 will become active again. This will produce a gradual change in w rather than the step change of Equation 6. Whether this rate of change matches experiment is another question which needs to be addressed with additional experiments.

2.3 Saturation Form for Two Compositions, C_1 and C_2

If we are not able to match experiments (or if we just prefer the approach below with more adjustable parameters), a possible modification is to have a saturation level of C_2^{sat} for reaction 4

Equation 11
$$\left(\frac{dC_3}{dt}\right)_{r4} \propto \left[C_2 - C_2^{sat}(T)\right]^{\chi_4} \text{ if } C_2 - C_2^{sat}(T) \geq 0$$

Equation 12
$$\left(\frac{dC_3}{dt}\right)_{r4} = 0 \text{ if } C_2 - C_2^{sat}(T) < 0$$

and to choose values of C_1^{sat} and C_2^{sat} from w_{iso}^{sat} so that they are consistent with the final capacity. For this, after long times of hydriding in pressure regime 3 at a certain temperature T,

$$C_1 = C_1^{sat}(T), \quad C_2 = C_2^{sat}(T), \quad C_3 = 1 - C_1^{sat}(T) - C_2^{sat}(T)$$

Applying Equation 9,

Equation 13
$$w_{iso}^{sat}(T) = 0.0187 * C_2^{sat}(T) + 0.056 * \left(1 - C_1^{sat}(T) - C_2^{sat}(T)\right)$$

There are two unknowns and one equation, so we cannot uniquely determine C_1^{sat} and C_2^{sat}. An assumption on their relationship to each other or additional data is required to proceed. If we relate the two saturation values by (an alternate relation given in Equation 17 below was used ultimately in the coding implementation)

$$R^{sat} = \frac{C_2^{sat}(T)}{C_1^{sat}(T)},$$

assuming that R^{sat} does not depend on temperature, then

Equation 14 $$C_2^{sat}(T) = R^{sat} * C_1^{sat}(T)$$

and from Equation 13,

$$w_{iso}^{sat}(T) = 0.0187 * R^{sat} * C_1^{sat}(T) + 0.056 * \left(1 - C_1^{sat}(T) - R^{sat} * C_1^{sat}(T)\right)$$

Solving for C_1^{sat},

$$w_{iso}^{sat} = C_1^{sat} * \left(0.0187 * R^{sat} + 0.056 * (-1 - R^{sat})\right) + 0.056$$
$$w_{iso}^{sat} - 0.056 = C_1^{sat} * \left(R^{sat} * (0.0187 - 0.056) - 0.056\right)$$

$$C_1^{sat} = \frac{w_{iso}^{sat} - 0.056}{R^{sat} * (0.0187 - 0.056) - 0.056}$$

and multiplying numerator and denominator by –1,

Equation 15 $$C_1^{sat} = \frac{0.056 - w_{iso}^{sat}}{0.056 + R^{sat} * (0.056 - 0.0187)}$$

And putting the temperature dependencies back in,

Equation 16 $$C_1^{sat}(T) = \frac{0.056 - w_{iso}^{sat}(T)}{0.056 + R^{sat} * (0.056 - 0.0187)}$$

As a check, if we only have C_1^{sat}, so that $R^{sat} = 0$, then

$$C_1^{sat} = \frac{0.056 - w_{iso}^{sat}}{0.056} = 1 - \frac{w_{iso}^{sat}}{0.056}$$

which agrees with Equation 10.

The parameter R^{sat} is an additional model parameter that can be adjusted to give the best match of all the data. In particular, it is expected that the data from temperature change tests will be the most useful in determining a representative value of R^{sat}. Also, it was noted in parameter fits that the value of R^{sat} produced an inflection of the curve in some circumstances.

Returning to Equation 13 and solving for $C_2^{sat}(T)$,

$$w_{iso}^{sat}(T) = (0.0187 - 0.056) * C_2^{sat}(T) + 0.056 * \left(1 - C_1^{sat}(T)\right)$$
$$(0.0187 - 0.056) * C_2^{sat}(T) = w_{iso}^{sat}(T) - 0.056 * \left(1 - C_1^{sat}(T)\right)$$

$$C_2^{sat}(T) = \frac{w_{iso}^{sat}(T) - 0.056*\left(1 - C_1^{sat}(T)\right)}{(0.0187 - 0.056)}$$

$$C_2^{sat}(T) = \frac{0.056*\left(1 - C_1^{sat}(T)\right) - w_{iso}^{sat}(T)}{(0.056 - 0.0187)}$$

If we hydride at 100 C to achieve the greatest capacity and then increase to 120 C, we would not expect the saturation weight fraction to drop to the lower level of a constant 120 C history. Experiments need to examine this. If experiments do find that the saturation weight fraction does not change after the temperature change from 100 to 120 C, then this will be consistent with the model described above. To step through examination of the model, when the temperature is increased from 100 to 120 C, the value of $w_{iso}^{sat}(T)$ will drop. The values of $C_1^{sat}(T)$ and $C_2^{sat}(T)$ determined from Equation 16 and Equation 14 will increase so that the arguments $\left(C_1 - C_1^{sat}\right)$ and $\left(C_2 - C_2^{sat}\right)$ will be less than zero and according to Equation 8 and Equation 12, the reaction rates will be zero as desired.

Physically, if $C_1^{sat}(T) = 1$, then both reactions r2 and r4 will be eliminated and the saturated weight fraction can be set as low as 0. However, setting $C_2^{sat}(T) = 1$ by itself will only restrict reaction r4. If $C_1^{sat}(T) \approx 0$ associated with large values of R^{sat}, then the minimum weight fraction stored will be 0.0187 and this will all occur during reaction r2 giving little opportunity for an inflected curve. Because of this, restrictions on valid values of R^{sat} and $w_{iso}^{sat}(T)$ would be needed.

Rather than attempt such restrictions, an alternate form relating $C_1^{sat}(T)$ and $C_2^{sat}(T)$ was developed. In order for $C_1^{sat}(T) \geq 0$,

$$0.056*\left(1 - C_1^{sat}(T)\right) \geq w_{iso}^{sat}(T)$$

$$C_1^{sat}(T) \leq 1 - \frac{w_{iso}^{sat}(T)}{0.056}$$

A convenient way to impose this restriction is to define

$$C_1^{sat,\max}(T) = 1 - \frac{w_{iso}^{sat}(T)}{0.056}$$

Then define a new independent parameter, r^{sat},

Equation 17

$$r^{sat} = \frac{C_1^{sat}(T)}{C_1^{sat,\max}(T)}$$

such that

$$C_1^{sat}(T) = r^{sat} * C_1^{sat,\max}(T)$$

or

Equation 18

$$C_1^{sat}(T) = r^{sat} * \left(1 - \frac{w_{iso}^{sat}(T)}{0.056}\right)$$

In this way, the restriction is easier to remember and enforce as $0 \le r^{sat} \le 1$. Note that the right hand factor in Equation 18 will also be between 0 and 1 for reasonable values of $w_{iso}^{sat}(T)$ so that after multiplying these two factors, we will have $0 \le C_1^{sat}(T) \le 1$. Once r^{sat} is chosen, compute $C_1^{sat}(T)$ from Equation 18 and compute $C_2^{sat}(T)$ from

$$C_2^{sat}(T) = \frac{0.056 * \left(1 - r^{sat} * \left(1 - \frac{w_{iso}^{sat}(T)}{0.056}\right)\right) - w_{iso}^{sat}(T)}{(0.056 - 0.0187)}$$

$$= \frac{\left(0.056 - r^{sat} * \left(0.056 - w_{iso}^{sat}(T)\right)\right) - w_{iso}^{sat}(T)}{(0.056 - 0.0187)}$$

$$= \frac{\left(1 - r^{sat}\right) * \left(0.056 - w_{iso}^{sat}(T)\right)}{(0.056 - 0.0187)}$$

or

Equation 19

$$C_2^{sat}(T) = \frac{\left(1 - r^{sat}\right) * \left(0.056 - w_{iso}^{sat}(T)\right)}{(0.056 - 0.0187)}$$

The form of Equation 19 shows that $C_2^{sat}(T)$ must go to zero as r^{sat} approaches 1 or $w_{iso}^{sat}(T)$ approaches 0.056. This is intuitive since the first condition is if all of the nonideal capacity is accounted for in $C_1^{sat}(T)$ and the latter is that the actual capacity equals the ideal level, i.e. no need for saturation compositions. An additional restriction is needed however, because it is possible for $C_2^{sat}(T)$ to become greater than 1 if $w_{iso}^{sat}(T)$ is less than 0.0187 and r^{sat} is 0 or nearly 0. To examine this second restriction,

$$C_2^{sat}(T) \le 1$$

$$\frac{\left(1 - r^{sat}\right) * \left(0.056 - w_{iso}^{sat}(T)\right)}{(0.056 - 0.0187)} \le 1$$

$$\left(1 - r^{sat}\right) * \left(0.056 - w_{iso}^{sat}(T)\right) \le (0.056 - 0.0187)$$

$$1 - r^{sat} \le \frac{(0.056 - 0.0187)}{\left(0.056 - w_{iso}^{sat}(T)\right)}$$

$$r^{sat} \ge 1 - \frac{0.056 - 0.0187}{0.056 - w_{iso}^{sat}(T)}$$

One characteristic of the model with both $C_1^{sat}(T)$ and $C_2^{sat}(T)$ is if we start out with an initial composition of $C_2 = 0$, the first hydriding reaction will need to proceed to the point were $C_2 > C_2^{sat}$ before reaction 4 will begin. Thus there will be a time lag between when some C_2 reactant is available and when reaction 4 becomes active. This may produce an inflection in the curve.

2.4 *Modified Form for All Pressure Regimes*

The previous examination has focused just on pressure regime 3 for which both reactions are proceeding in the hydriding direction. For reversible reactions, we would anticipate that the amount stored would need to equal the amount released, at least after steady state has been reached. Because the amount stored was limited by introducing saturation levels for C_1 and C_2, the amount released will already be limited and we do not need to change the form for the dehydriding reactions (although the parameters will need to be modified from previous estimates). Another way to consider whether to have saturation levels on the dehydriding reactions is to think that in the dehydriding direction, we want all of the reactants to be consumed so the compositions can return to the initial state of $C_1 = 1, \quad C_2 = 0, \quad C_3 = 0$. If we have saturation levels for C_2 or C_3, then the dehydriding rate will go to zero before the compositions drop to zero. Therefore, we do not want saturation values on the reactants for the dehydriding reactions.

In the current model framework, the composition at the start of hydriding test after complete dehydriding would be

$$C_1 = 1, \quad C_2 = 0, \quad C_3 = 0$$

and the composition at the start of dehydriding after complete hydriding at temperature T would be

$$C_1 = C_1^{sat}(T), \quad C_2 = C_2^{sat}(T), \quad C_3 = 1 - C_1^{sat}(T) - C_2^{sat}(T)$$

A sketch of the three pressure regimes is shown in Figure 3.

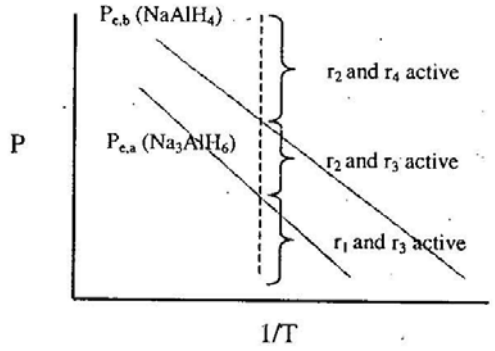

Figure 3: Reaction pressure regimes.

The complete model for all three pressure regimes will be,

Table 1: Complete listing of reaction rate equations.

Pressure regime 1 r1 and r3 active	If $C_2 \geq 0$, $\left(\frac{dC_1}{dt}\right)_{r1} = A_1 \exp\left(-\frac{E_1}{RT}\right) * \left(\frac{P_{e,1} - P}{P_{e,1}}\right) * (C_2)^{\chi_1}$ $\left(\frac{dC_2}{dt}\right)_{r1} = -\left(\frac{dC_1}{dt}\right)_{r1}$ If $C_3 \geq 0$, $\left(\frac{dC_2}{dt}\right)_{r3} = A_3 \exp\left(-\frac{E_3}{RT}\right) * \left(\frac{P_{e,3} - P}{P_{e,3}}\right) * (C_3)^{\chi_3}$ $\left(\frac{dC_3}{dt}\right)_{r3} = -\left(\frac{dC_2}{dt}\right)_{r3}$
Pressure regime 2 r2 and r3 active	If $C_1 - C_1^{sat}(T) \geq 0$, $\left(\frac{dC_2}{dt}\right)_{r2} = A_2 \exp\left(-\frac{E_2}{RT}\right) * \left(\frac{P - P_{e,2}}{P_{e,2}}\right) * \left(C_1 - C_1^{sat}(T)\right)^{\chi_2}$ $\left(\frac{dC_1}{dt}\right)_{r2} = -\left(\frac{dC_2}{dt}\right)_{r2}$ If $C_3 \geq 0$, $\left(\frac{dC_2}{dt}\right)_{r3} = A_3 \exp\left(-\frac{E_3}{RT}\right) * \left(\frac{P_{e,3} - P}{P_{e,3}}\right) * (C_3)^{\chi_3}$ $\left(\frac{dC_3}{dt}\right)_{r3} = -\left(\frac{dC_2}{dt}\right)_{r3}$
Pressure regime 3 r2 and r4 active	If $C_1 - C_1^{sat}(T) \geq 0$, $\left(\frac{dC_2}{dt}\right)_{r2} = A_2 \exp\left(-\frac{E_2}{RT}\right) * \left(\frac{P - P_{e,2}}{P_{e,2}}\right) * \left(C_1 - C_1^{sat}(T)\right)^{\chi_2}$ $\left(\frac{dC_1}{dt}\right)_{r2} = -\left(\frac{dC_2}{dt}\right)_{r2}$ If $C_2 - C_2^{sat}(T) \geq 0$, $\left(\frac{dC_3}{dt}\right)_{r4} = A_4 \exp\left(-\frac{E_4}{RT}\right) * \left(\frac{P - P_{e,4}}{P_{e,4}}\right) * \left(C_2 - C_2^{sat}(T)\right)^{\chi_4}$ $\left(\frac{dC_2}{dt}\right)_{r4} = -\left(\frac{dC_3}{dt}\right)_{r4}$

If the quantities stated in Table 1 which need to be ≥ 0 are actually < 0, then the associated reaction rate is set to 0.

For all three pressure regimes, the total rate of change for C_2 will be the sum for each of the two active reactions,

$$\left(\frac{dC_2}{dt}\right)_{total} = \left(\frac{dC_2}{dt}\right)_{\text{r1 or r2}} + \left(\frac{dC_2}{dt}\right)_{\text{r3 or r4}}$$

As present previously, the equilibrium pressure is

$$\ln(P_e) = \frac{\Delta H}{RT} - \frac{\Delta S}{R}$$

or

Equation 20

$$P_e(T) = \exp\left(\frac{\Delta H}{RT} - \frac{\Delta S}{R}\right).$$

3 Effect of Parameters on Curve Characteristics

Some parameter fitting and sensitivity studies were conducted with the initial relation of Equation 14 using R^{sat} for the saturation compositions. The value of R^{sat} influences the weight fraction level at which the inflection point occurs for the transition between the reactions. This is shown in Figure 4 through Figure 7 for the 100 C data. A slightly different set of parameters was used to fit the 120 C data shown in Figure 8 through Figure 11.

Using Equation 17 to choose different values of the saturation compositions, it seemed more difficult to produce the inflection point in the curves during parameter estimatation trials using MATLAB. There is no restriction in the new form that should make this happen, and it is likely that this was caused by having different values of the other model parameters that affect the relative rates etc. of the two hydriding reactions. A small amount of thought was invested into what conditions would lead to a more prominent inflection region, but this was shelved in the interest of completing the model and its application. For an inflection region to occur, one needs reaction 2 to slow down, to have reaction 4 become active, to have reaction 2 still proceed to produce more reactant for reaction 4 but to have reaction 4 accelerate in hydrogen production. It is still unclear what values of the parameters (or dependencies between them) will produce a pronounced inflection region.

The fit to experimental data using Equation 17 is shown in Figure 12 using the parameter values of Table 2. The value of r^{sat} was set equal to 1 for all temperatures, which in effect sets $C_2^{sat} = 0$ and would appear to eliminate the possibility of an inflection region. Other parameter combination are still possible to give a better match. Nevertheless, the results are reasonably good. The fit at 140 C is the poorest due to the large inflection region. The model was also fit to the desorption data shown in Figure 13. A different value for $C_1^{sat} = 0.5$ was used to best match the resulting capacities. We could argue that such flexibility in choosing C_1^{sat} is acceptable since we do not known the actual composition of the as received / milled material.

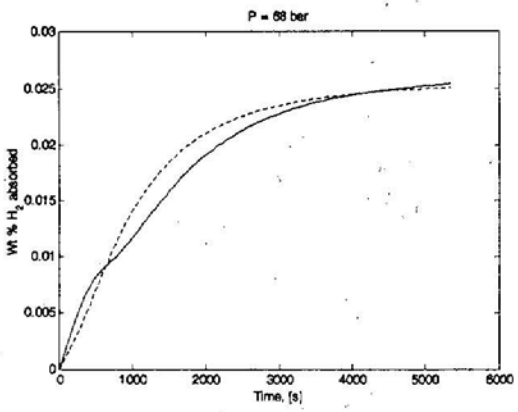

Figure 4: Data (solid) and model (dashed) for absoption at 100 C with $R^{sat} = 0$.

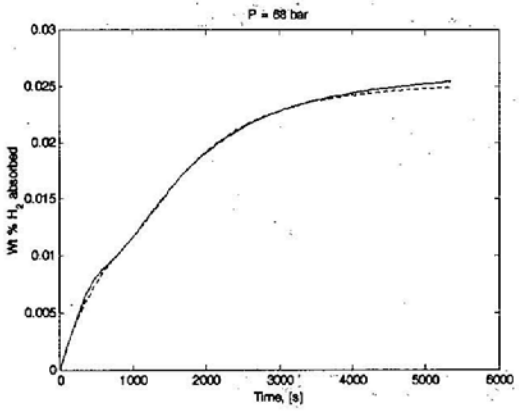

Figure 5: Data (solid) and model (dashed) for absoption at 100 C with $R^{sat} = 3$.

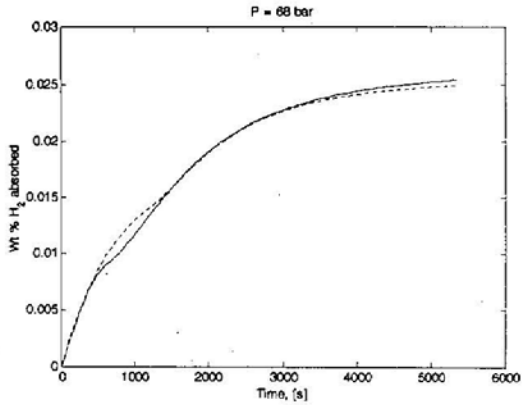

Figure 6: Data (solid) and model (dashed) for absoption at 100 C with $R^{sat} = 10$.

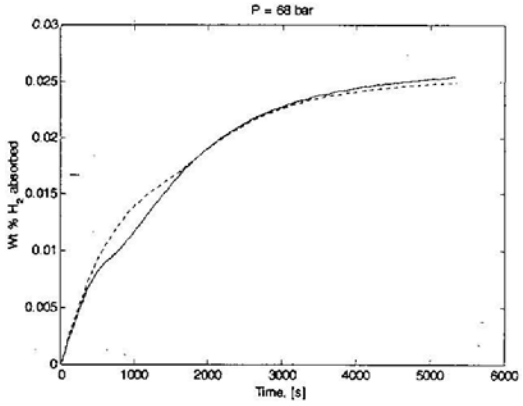

Figure 7: Data (solid) and model (dashed) for absoption at 100 C with $R^{sat} = 1000$.

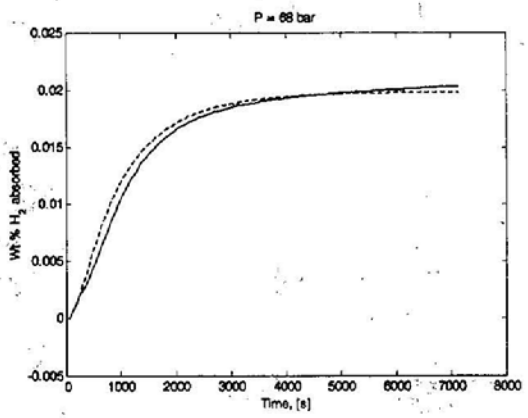

Figure 8: Data (solid) and model (dashed) for absoption at 120 C with $R^{sat} = 0$.

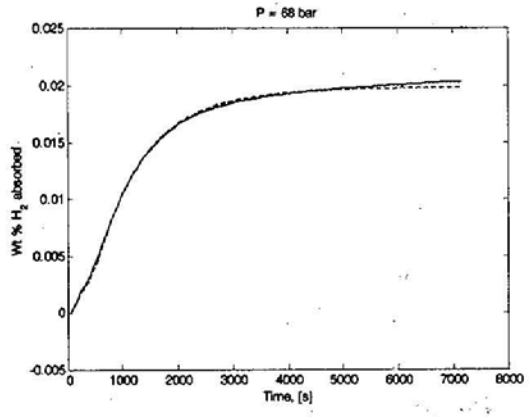

Figure 9: Data (solid) and model (dashed) for absoption at 120 C with $R^{sat} = 0.2$.

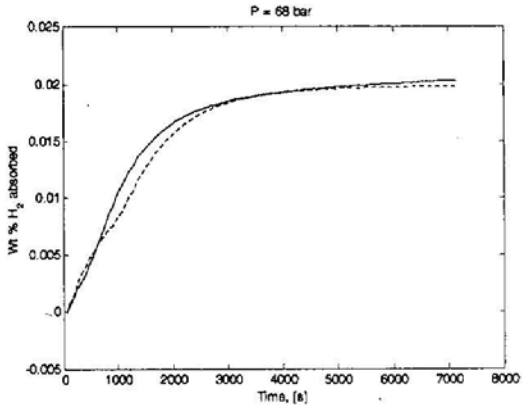

Figure 10: Data (solid) and model (dashed) for absoption at 120 C with $R^{sat} = 1$.

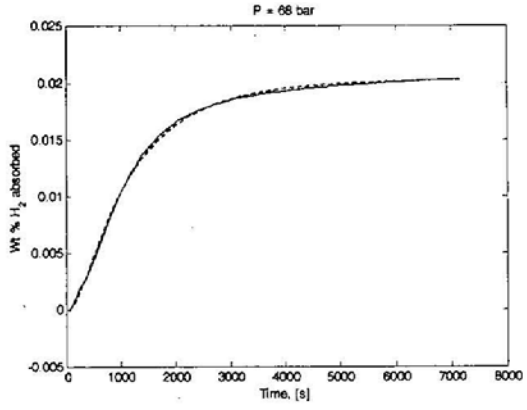

Figure 11: Data (solid) and model (dashed) for absoption at 120 C with $R^{sat} = 0$ with other parameter optimized (A_T reduced from 7.0e4 to 5.5e4, w_sat increased from 0.020 to 0.0205).

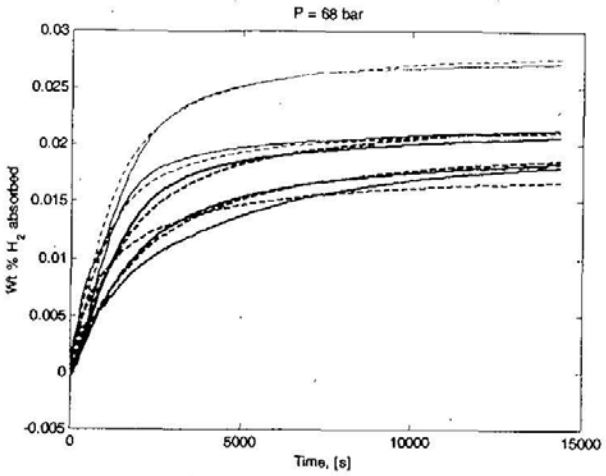

Figure 12: Absorption with starting C_1 = 1 and T dependent C_1_sat (r_sat(T) = 1 so C_2_sat = 0). The dashed lines are the model with red=80C; blue=90C; cyan=100C; green=120C; and magenta=140C.

Table 2: MATLAB coding giving model parameter values.

```
T_sat_C = [0   80   90   100   120   140   300 ];    % temperatures associated with w_iso
w_sat =  [0.021 0.021 0.023 0.029 0.022 0.018 0.018];   % saturation weight fractions at tempertures T_iso_C
r_sat =  [1    1    1    1.0   1    1    1   ];      % ratio of C_1_sat / C_1_sat_max
r_sat_threshold = 1 - (0.056 - 0.0187) ./ (0.056 - w_sat);  % restriction level for r_sat, 1 - (0.056 - 0.0187) / 0.056 = 0.333
r_sat = max(r_sat, r_sat_threshold);        % check for values of r_sat that will maintain C_2_sat < 1.
T_sat_K = T_sat_C + 273;

i_r = 1;  % directional reaction 1, dehydriding of Na3AlH6 to NaH
      param(i_r,1) = -6150;      % A or delta H / R, slope in van't Hoff plot
      param(i_r,2) = 16.22;      % B or -delta S / R, intercept in van't Hoff plot
      param(i_r,3) = 6.0e12;     % A_T, leading coefficient in temperature factor, time unit of seconds
      param(i_r,4) = 110000;     % E, thermal activation energy, J / mol of H_2
      param(i_r,5) = 1.0;        % chi, exponent on reactant weight fraction
i_r = 2;  % directional reaction 2, hydriding of NaH to Na3AlH6
      param(i_r,1) = -6150;      % A, not used, value for i_r = 1 used
      param(i_r,2) = 16.22;      % B, not used, value for i_r = 1 used
      param(i_r,3) = 1.5e5;      % A_T
      param(i_r,4) = 70000;      % E
      param(i_r,5) = 1.0;        % chi
i_r = 3;  % directional reaction 3, dehydriding of NaAlH4 to Na3AlH6
      param(i_r,1) = -4475;      % A, used for r3 and r4
      param(i_r,2) = 14.83;      % B, used for r3 and r4 (14.83)
      param(i_r,3) = 4.0e12;     % A_T
      param(i_r,4) = 110000;     % E
      param(i_r,5) = 2.0;        % chi
i_r = 4;  % directional reaction 4, hydriding of Na3AlH6 to NaAlH4
      param(i_r,1) = -4475;      % A, not used, value for i_r = 3 used
      param(i_r,2) = 14.83;      % B, not used, value for i_r = 3 used (14.83)
      param(i_r,3) = 1.0e8;      % A_T
      param(i_r,4) = 80000;      % E
      param(i_r,5) = 2;          % chi
```

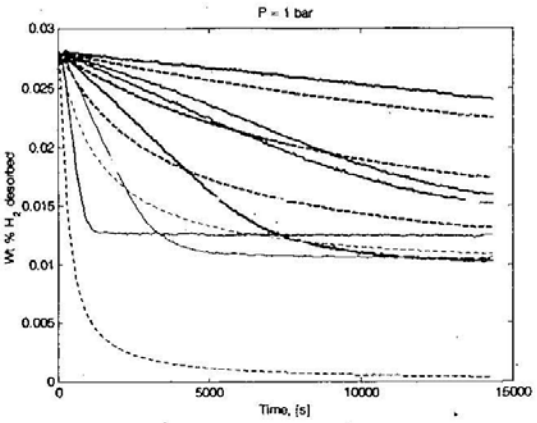

Figure 13: Desorption from as milled condition (assume C_1_sat = 0.5). Dashed lines are model. Temperatures are black=70C; red = 80 C (two experiments); blue=90C; cyan=100C; yellow=110C; green=120C;

Note that the equilibrium pressure for the lower van't Hoff line using a modified Equation 20 and parameters in Table 2 is

$$P_e(T) = \exp\left(\frac{A}{T} + B\right) = \exp\left(\frac{-6150}{T} + 16.22\right)$$

Solving for the transition temperature for the desorption pressure of 1 atm,

$$T = \frac{-6150}{\ln(P_e(T)) - 16.22} = \frac{-6150}{\ln(1\,\text{atm}) - 16.22} = 379\,\text{K} = 106\,\text{C}$$

Thus, we would expect significant differences in capacity for temperatures above 106 C versus those below it. This is reflected in the model predictions of Figure 13 (yellow and green lines) but not in the experimental data. In fact, after 8,000 s, the desorbed capacity at 90 C is greater than at 120 C. Additional experimentation and modeling is required to understand this effect.

The modifications to the kinetics model were made to the ABAQUS subroutines and check with a simple isothermal test problem. The user subroutine "powder_user2.for" was developed from the previous "powder_user.for" file based on additional modeling and parameter estimation in MATLAB. The implementation of changes required adding parameters to calculate saturation compositions and also the addition of these saturation levels to the hydriding reaction rate equations. Simple simulations were conducted in ABAQUS to verify that the implementation was accurate. These were nearly isothermal simulations of a cube 0.1m in size. A slight temperature difference was produced by imposing a convective boundary condition which was 1 degree C higher than the initial temperature to avoid numerical problems of taking to small of a time step in transient thermal analyses. Such a small time (100 s) is needed to integrate the reaction equations.

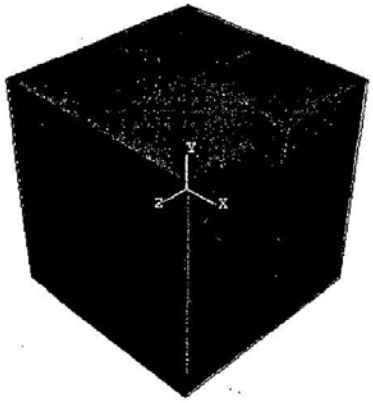

Figure 14: 0.1 meter cube used to test implementation of model in ABAQUS.

The results below are very similar to the comparison of data with the MATLAB implementation as expected. After these simulations were run, code was added to the user subroutine HETVAL to check whether the composition factors were positive. A simulation at 140 C was then rerun and the results did not changed at all. This is expected since the value of r_sat was 1 for all temperatures so that C_2_sat = 0 and therefore there would not be any negative composition factors for an isothermal history starting with C_1 = 1. Note that the checks for negative composition factors were in the MATLAB code used to fit the parameters. Therefore, though the code was modified, it is expected that the results for the other temperatures besides 140 C will also agree as in the figure.

The results in Figure 15 show good agreement with Figure 12 indicating the coding of equations including their integration is accurate, at least for these conditions.

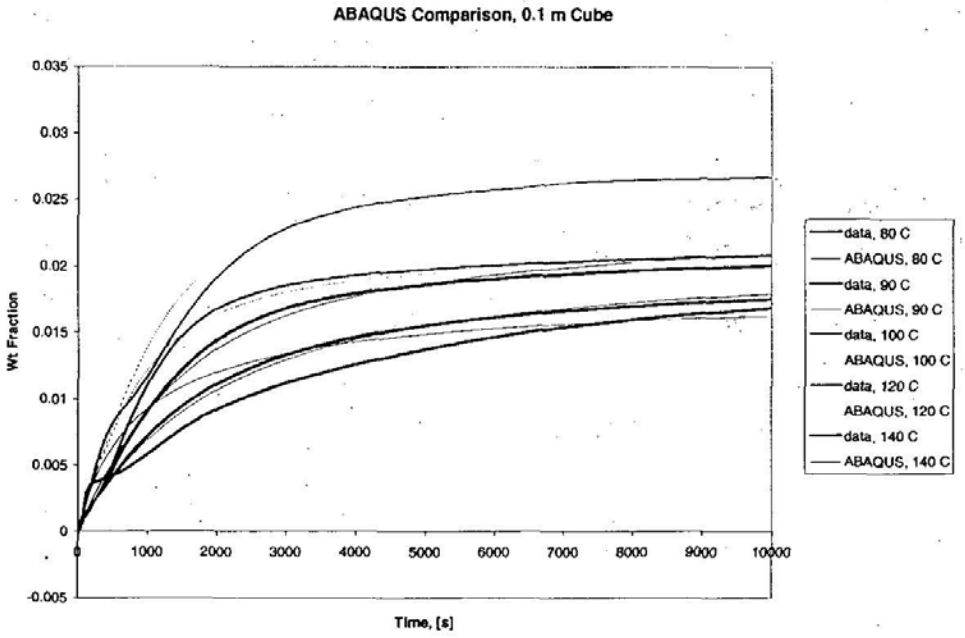

Figure 15: Results for absorption conditions.

Attachment 3

DOE Technical Targets for On-Board Hydrogen Storage Systems

Storage Parameter	Units	2007	2010	2015
System Gravimetric Capacity: Usable, specific-energy from H_2 (net useful energy/max system mass)[a]	kWh/kg (kg H_2/kg system)	1.5 (0.045)	2 (0.06)	3 (0.09)
System Volumetric Capacity: Usable energy density from H_2 (net useful energy/max system volume)	kWh/L (kg H_2/L system)	1.2 (0.036)	1.5 (0.045)	2.7 (0.081)
Storage system cost[b] (& fuel cost)[c]	$/kWh net ($/kg H_2) $/gge at pump	6 (200) ---	4 (133) 2-3	2 (67) 2-3
Durability/Operability • Operating ambient temperature[d] • Min/max delivery temperature • Cycle life (1/4 tank to full)[e] • Cycle life variation[f] • Min delivery pressure from tank; FC= fuel cell, I=ICE • Max delivery pressure from tank[g]	 ºC ºC Cycles % of mean (min) at % confidence Atm (abs) Atm (abs)	 -20/50 (sun) -30/85 500 N/A 8FC / 10 ICE 100	 -30/50 (sun) -40/85 1000 90/90 4FC / 35 ICE 100	 -40/60 (sun) -40/85 1500 99/90 3FC / 35 ICE 100
Charging/discharging Rates • System fill time (for 5 kg) • Minimum full flow rate • Start time to full flow (20 ºC) • Start time to full flow (- 20 ºC) • Transient response 10%-90% and 90% - 0%	 min (g/s)/kW s s s	 10 0.02 15 30 1.75	 3 0.02 5 15 0.75	 2.5 0.02 5 15 0.75
Fuel Purity (H_2 from storage)[j]	% H_2	99.99 (dry basis)		
Environmental Health & Safety • Permeation & leakage[k] • Toxicity • Safety • Loss of useable H_2	Scc/h - (g/h)/kg H_2 stored	- (g/h)/kg H_2 stored Meets or exceeds applicable standards 1	0.1	0.05